

# **Leg 204 Preliminary Report**

Drilling Gas Hydrates on Hydrate Ridge,  
Cascadia Continental Margin

7 July–2 September 2002

Shipboard Scientific Party

Ocean Drilling Program  
Texas A&M University  
1000 Discovery Drive  
College Station TX 77845-9547  
USA

December 2002

## PUBLISHER'S NOTES

This report was prepared from shipboard files by scientists who participated in the cruise. The report was assembled under time constraints and does not contain all works and findings that will appear in the *Initial Reports* of the ODP *Proceedings*. Reference to the whole or to part of this report should be made as follows:

Shipboard Scientific Party, 2002. Leg 204 Preliminary Report. *ODP Prelim. Rpt.*, 104 [Online]. Available from World Wide Web: <[http://www-odp.tamu.edu/publications/prelim/204\\_prel/204PREL.PDF](http://www-odp.tamu.edu/publications/prelim/204_prel/204PREL.PDF)>. [Cited YYYY-MM-DD]

Distribution: Electronic copies of this series may be obtained from the Ocean Drilling Program's World Wide Web site at <http://www-odp.tamu.edu/publications>.

This publication was prepared by the Ocean Drilling Program, Texas A&M University, as an account of work performed under the international Ocean Drilling Program, which is managed by Joint Oceanographic Institutions, Inc., under contract with the National Science Foundation. Funding for the program is provided by the following agencies:

Australia/Canada/Chinese Taipei/Korea Consortium for Ocean Drilling  
Deutsche Forschungsgemeinschaft (Federal Republic of Germany)  
Institut National des Sciences de l'Univers—Centre National de la Recherche Scientifique (INSU-CNRS; France)  
Ocean Research Institute of the University of Tokyo (Japan)  
National Science Foundation (United States)  
Natural Environment Research Council (United Kingdom)  
European Science Foundation Consortium for Ocean Drilling (Belgium, Denmark, Finland, Iceland, Ireland, Italy, The Netherlands, Norway, Portugal, Spain, Sweden, and Switzerland)  
Marine High-Technology Bureau of the State Science and Technology Commission of the People's Republic of China

## DISCLAIMER

Any opinions, findings, and conclusions or recommendations expressed in this publication are those of the author(s) and do not necessarily reflect the views of the National Science Foundation, the participating agencies, Joint Oceanographic Institutions, Inc., Texas A&M University, or Texas A&M Research Foundation.

The following scientists and personnel were aboard the *JOIDES Resolution* for Leg 204 of the Ocean Drilling Program:

**SHIPBOARD SCIENTIFIC PARTY**

**Gerhard Bohrmann**  
**Co-Chief Scientist**

GEOMAR  
Christian-Albrechts-Universität zu Kiel  
Wischofstrasse 1-3  
24148 Kiel  
Germany  
Work: (49) 431-600-2319  
Fax: (49) 431-600-2928  
[gbohrmann@geomar.de](mailto:gbohrmann@geomar.de)

**Anne M. Tréhu**

**Co-Chief Scientist**

College of Oceanic and Atmospheric Sciences  
Oregon State University  
104 Oceanography Administration Building  
Corvallis OR 97331-5503  
USA  
Work: (541) 737-2655  
Fax: (541) 737-2064  
[trehu@coas.oregonstate.edu](mailto:trehu@coas.oregonstate.edu)

**Frank R. Rack**

**Staff Scientist**

Joint Oceanographic Institutions Inc.  
1755 Massachusetts Avenue Northwest, Suite 700  
Washington DC 20036  
USA  
Work: (202) 232-3900, ext. 216  
Fax: (202) 462-8754  
[frack@joiscience.org](mailto:frack@joiscience.org)

**Nathan L. Bangs**

**Logging Scientist**

Institute for Geophysics  
University of Texas at Austin  
4412 Spicewood Springs Road, Building 600  
Austin TX 78759-8500  
USA  
Work: (512) 471-0424  
Fax: (512) 471-0348  
[nathan@utig.ig.utexas.edu](mailto:nathan@utig.ig.utexas.edu)

**Samantha R. Barr**

**Logging Staff Scientist**

Department of Geology  
University of Leicester  
University Road  
Leicester LE1 7RH  
United Kingdom  
Work: (44) 116-252-3608  
Fax: (44) 116-252-3918  
[srb7@leicester.ac.uk](mailto:srb7@leicester.ac.uk)

**Walter S. Borowski**

**Inorganic Geochemist**

Department of Earth Sciences  
Eastern Kentucky University  
512 Lancaster Avenue  
Roark 103  
Richmond KY 40475-3102  
USA  
Work: (859) 622-1277  
Fax: (859) 622-1451  
[w.borowski@eku.edu](mailto:w.borowski@eku.edu)

**George E. Claypool**

**Organic Geochemist**

8910 West 2nd Avenue  
Lakewood CO 80226  
USA  
Work: (303) 237-8273  
Fax: (303) 237-8273  
[geclaypool@aol.com](mailto:geclaypool@aol.com)

**Timothy S. Collett**

**Logging Scientist**

Energy Resources Program  
U.S. Geological Survey  
Denver Federal Center  
Box 25046, MS 939  
Denver CO 80225  
USA  
Work: (303) 236-5731  
Fax: (303) 236-0459  
[tcollett@usgs.gov](mailto:tcollett@usgs.gov)

**Mark E. Delwiche**

**Microbiologist**

Biotechnologies  
Idaho National Engineering and Environmental  
Laboratory  
2525 North Fremont Street  
Idaho Falls ID 83415-2203  
USA  
Work: (208) 526-1870  
Fax: (208) 525-0828  
[mde1@inel.gov](mailto:mde1@inel.gov)

**Gerald R. Dickens**

**Pressure Core Sampler Scientist**

Department of Earth Science  
Rice University  
6100 Main Street  
Houston TX 77005  
Work: (713) 348-5130  
Fax: (713) 3485214  
[jerry@rice.edu](mailto:jerry@rice.edu)

**David S. Goldberg**  
**Logging Staff Scientist**  
Borehole Research Group  
Lamont-Doherty Earth Observatory  
of Columbia University  
PO Box 1000, 61 Route 9W  
Palisades NY 10964  
USA  
Work: (914) 365-8674  
Fax: (914) 365-3182  
[goldberg@ldeo.columbia.edu](mailto:goldberg@ldeo.columbia.edu)

**Eulàlia Gràcia**  
**Sedimentologist**  
Centre Mediterrani d'Investigacions Marines  
i Ambientals (CMIMA)  
Unitat de Tecnologia Marina  
CSIC  
Pg. Marítim de la Barceloneta, 37-49  
08003 Barcelona  
Spain  
Work: (34) 93 230 9536  
Fax: (34) 93 230 9555  
[egracia@utm.csic.es](mailto:egracia@utm.csic.es)

**Gilles Guérin**  
**Logging Staff Scientist**  
Borehole Research Group  
Lamont-Doherty Earth Observatory  
of Columbia University  
PO Box 1000, 61 Route 9W  
Palisades NY 10964  
USA  
Work: (845) 365-8671  
Fax: (845) 365-3182  
[guerin@ldeo.columbia.edu](mailto:guerin@ldeo.columbia.edu)

**Melanie Holland**  
**Microbiologist**  
Department of Geological Sciences  
Box 871404  
Arizona State University  
Tempe AZ 85287  
USA  
Work: (480) 965-9142  
Fax: (480) 965-8102  
[melanie.holland@asu.edu](mailto:melanie.holland@asu.edu)

**Joel E. Johnson**  
**Sedimentologist**  
College of Oceanic and Atmospheric Sciences  
Oregon State University  
104 Ocean Administration Building  
Corvallis OR 97331  
USA  
Work: (541) 737-9002  
Fax: (541) 737-2064  
[jjohnson@coas.oregonstate.edu](mailto:jjohnson@coas.oregonstate.edu)

**Young-Joo Lee**  
**Organic Geochemist**  
Petroleum and Marine Resources Research Division  
Korea Institute of Geoscience and Mineral Resources  
(KIGAM)  
30 Kajung-Dong, Yusong-Gu  
Daejeon 305-350  
South Korea  
Work: (82) 42-868-3209  
Fax: (82) 42-862-7275  
[yjl@rock25t.kigam.re.kr](mailto:yjl@rock25t.kigam.re.kr)

**Char-Shine Liu**  
**Physical Properties Specialist**  
Institute of Oceanography  
National Taiwan University  
PO Box 23-13  
Taipei 106  
Taiwan  
Work: (886) 2-2366-0881  
Fax: (886) 2-2366-0881  
[cslu@ccms.ntu.edu.tw](mailto:cslu@ccms.ntu.edu.tw)

**Philip E. Long**  
**Physical Properties Specialist**  
Environmental Technology Division  
Pacific Northwest National Laboratory  
PO Box 999, Mail Stop K9-33  
Richland WA 99352  
USA  
Work: (509) 372-6090  
Fax: (509) 372-6089  
[philip.long@pnl.gov](mailto:philip.long@pnl.gov)

**Alexei V. Milkov**  
**Sedimentologist**  
Geology and Geophysics  
Woods Hole Oceanographic Institution  
300 Woods Hole Road, MS 22  
Woods Hole MA 02543  
USA  
Work: (508) 289-2841  
Fax: (508) 289-2187  
[amilkov@whoi.edu](mailto:amilkov@whoi.edu)

**Michael Riedel**  
**Physical Properties Specialist**  
Geological Survey of Canada  
Pacific Geoscience Centre  
9860 West Saanich Road  
Sidney BC V8L 4B2  
Canada  
Work: (250) 363-6589  
Fax: (250) 363-6565  
[mriedel@pgc-gsc.nrcan.gc.ca](mailto:mriedel@pgc-gsc.nrcan.gc.ca)

**Peter Schultheiss**  
**Physical Properties Specialist**

GEOTEK Ltd.  
3, Faraday Close  
Drayton Fields  
Daventry  
Northants NN11 5RD  
United Kingdom  
Work: (44) 1327-311666  
Fax: (44) 1327-311555  
[peter@geotek.co.uk](mailto:peter@geotek.co.uk)

**Xin Su**  
**Sedimentologist/Paleontologist**

Center of Marine Geology  
China University of Geosciences  
Xueyuan Road 29  
Beijing 100083  
People's Republic of China  
Work: (86)10-82320065  
Fax: (86)10-82321540  
[xsu@cugb.edu.cn](mailto:xsu@cugb.edu.cn)

**Barbara Teichert**  
**Sedimentologist**

GEOMAR  
Christian-Albrechts-Universität zu Kiel  
Wischhofstrasse 1-3  
24148 Kiel  
Germany  
Work: (49) 431-600-1405  
Fax: (49) 431-600-1400  
[bteichert@geomar.de](mailto:bteichert@geomar.de)

**Hitoshi Tomaru**  
**Inorganic Geochemist**

Graduate School of Science  
University of Tokyo  
Science Building 5  
7-3-1 Hong, Bunkyo-ku  
Tokyo 113-0033  
Japan  
Work: (81) 3-5841-7590  
Fax: (81) 3-5841-4569  
[tomaru@gbs.eps.s.u-tokyo.ac.jp](mailto:tomaru@gbs.eps.s.u-tokyo.ac.jp)

**Marta E. Torres**  
**Inorganic Geochemist**

College of Oceanic and Atmospheric Sciences  
Oregon State University  
104 Oceanography Administration Building  
Corvallis OR 97331-5503  
USA  
Work: (541) 737-2902  
Fax: (541) 737-2064  
[mtorres@coas.oregonstate.edu](mailto:mtorres@coas.oregonstate.edu)

**Maarten Vanneste**  
**Geophysicist**

Department of Geology  
Universitetet i Tromsø  
Dramsveien 201  
9037 Tromsø  
Norway  
Work: (47) 77646505  
Fax: (47) 77645600  
[maarten@ibg.uit.no](mailto:maarten@ibg.uit.no)

**Mahito Watanabe**  
**Paleontologist (diatoms)**

Geoscience Institute  
Geological Survey of Japan, AIST  
1-1-1 Central 7 Higashi  
Tsukuba 305-8567  
Japan  
Work: (81) 298-61-2471  
Fax: (81) 298-61-3742  
[mht.watanabe@aist.go.jp](mailto:mht.watanabe@aist.go.jp)

**Jill L. Weinberger**  
**Sedimentologist/Structural Geologist**

Scripps Institution of Oceanography  
University of California, San Diego  
9500 Gilman Drive  
Mail Code 0244  
San Diego CA 92093-0244  
USA  
Work: (858) 822-0591  
Fax: (858) 534-0784  
[jlweinbe@ucsd.edu](mailto:jlweinbe@ucsd.edu)

**TRANSOCEAN OFFICIALS**

**Peter Mowat**  
**Master of the Drilling Vessel**  
Overseas Drilling Ltd.  
707 Texas Avenue South, Suite 213D  
College Station TX 77840-1917  
USA

**Tim McCown**  
**Drilling Superintendent**  
Overseas Drilling Ltd.  
707 Texas Avenue South, Suite 213D  
College Station TX 77840-1917  
USA

**ODP SHIPBOARD PERSONNEL**  
**AND TECHNICAL REPRESENTATIVES**

**Roeland Baas**  
Fugro Engineer

**John W. Beck**  
Marine Laboratory Specialist (Photographer)

**James Benjamin Bloys**  
Chevron/Texaco Visiting Engineer

**Timothy Bronk**

Assistant Laboratory Officer

**Jason Deardorff**

Marine Laboratory Specialist (Temporary)

**Sandy Dillard**

Marine Laboratory Specialist  
(Downhole Tools/Thin Sections)

**Dennis Graham**

Marine Laboratory Specialist (Chemistry)

**Kevin Grigar**

Design Engineer

**Jessica Huckemeyer**

Marine Laboratory Specialist (Curator)

**W. Brian Jones**

Marine Laboratory Specialist (Chemistry)

**Bradley Julson**

Laboratory Officer

**Peter Kannberg**

Marine Laboratory Specialist (Temporary)

**Jan Jurie Kotzé**

Marine Electronics Specialist

**Terry Langsdorf**

Fugro-McClelland Engineer

**Herbert Leyton**

Schlumberger Vertical Seismic Profile Specialist/  
Engineer

**Angeline Miller**

Marine Laboratory Specialist (Yeoperson)

**Erik Moortgat**

Marine Computer Specialist

**Khaled Moudjeber**

Schlumberger Engineer/Logging-While-Drilling  
Specialist

**Stefan Mrozewski**

Schlumberger Engineer/Logging-While-Drilling  
Specialist

**Pieter Pretorius**

Marine Electronics Specialist

**John W.P. Riley**

Marine Laboratory Specialist (Physical Properties)

**Derryl Schroeder**

Development Engineer

**Michael A. Storms**

Operations Manager

**Johanna M. Suhonen**

Marine Laboratory Specialist (Underway Geophysics)

**Kerry Swain**

Schlumberger Engineer

**Paul Ténrière**

Marine Laboratory Specialist (Temporary)

**Thjunjoto**

Maritime Technik HYACE/HYACINTH Engineer

**Ko-Min Tjok**

Fugro-McClelland Engineer

**Floris Tuynder**

Fugro Engineer

**Felix Weise**

Institute of Petroleum Engineering HYACE/HYACINTH  
Engineer

**Robert M. Wheatley**

Marine Laboratory Specialist (X-Ray)

**MEDIA REPRESENTATIVES**

**Stephan Braun**

Context TV  
Elssholzstrasse 11  
10823 Berlin  
Germany

**Jan Hartmann**

Context TV  
Lützowstrasse 92  
10785 Berlin  
Germany

**Randy Lee Showstack**

Eos, the newspaper of the American Geophysical  
Union  
Washington DC  
USA

**Alexandra Witze**

Media Representative  
Dallas Morning News  
508 Young Street  
Dallas TX 75202  
USA

## **ABSTRACT**

During Leg 204, we cored and logged nine sites on the Oregon continental margin to determine the distribution and concentration of gas hydrates in an accretionary ridge and adjacent slope basin, investigate the mechanisms that transport methane and other gases into the gas hydrate stability zone (GHSZ), and obtain constraints on physical properties of gas hydrates in situ. A three-dimensional seismic survey conducted from 19 June through 3 July 2000 provided images of potential subsurface fluid conduits and indicated the depth of the GHSZ throughout the survey region. After coring at the first site, we acquired logging-while-drilling (LWD) data at all but one site to provide an overview of downhole physical properties prior to coring. The LWD data confirmed the general position of key seismic stratigraphic horizons and yielded an initial estimate of gas hydrate concentration through the proxy of in situ electrical resistivity. These records proved to be of great value in planning subsequent coring. We also tested the use of infrared thermal imaging of cores as a new and effective tool to identify gas hydrates while the cores were on the catwalk as rapidly as possible after core retrieval. The thermal images were used to estimate the distribution and texture of hydrate within the cores. Geochemical analyses of interstitial waters and of headspace and void gases provided additional information on the distribution and concentration of hydrate within the stability zone, the origin and pathway of fluids into and through the GHSZ, and the rates at which the process of gas hydrate formation is occurring. Biostratigraphic and lithostratigraphic descriptions of cores, measurement of physical properties, and in situ pressure core sampling and thermal measurements complement the data set, providing ground-truth tests of inferred physical and sedimentological properties.

Among the most interesting preliminary results are the following:

1. Gas hydrates are distributed within a broad depth range within the GHSZ.
2. Within this broad range, lithology is an important factor influencing hydrate concentration.
3. Different physical and chemical proxies for hydrate distribution and concentration give generally consistent results.
4. The gas hydrate system at Hydrate Ridge contains significant concentrations of higher-order hydrocarbons.
5. Fractionation and mixing signals provide important constraints on gas hydrate dynamics.
6. Very high chloride concentration values extend to a depth of 20–30 meters below seafloor near the summit, indicating that hydrate formation here must be very recent and rapid.
7. Gas hydrate concentration is significantly greater beneath the ridge than beneath the adjacent slope basin.
8. In the slope basin, hydrates are concentrated just above the bottom-simulating reflector (BSR).
9. The BSR represents a discontinuity in several chemical constituents of pore waters and gas voids, indicating that hydrate formation has profound geochemical effects.

## **INTRODUCTION**

Gas hydrate is an icelike mineral that contains methane or other low molecular weight gases in a lattice of water molecules. Methane hydrates are stable under the temperature and pressure conditions generally found in the Arctic and near the seafloor at water depths >300 m. They are quite common beneath the slope of both active and passive continental margins where methane originates from the decomposition of organic matter by biogenic and/or thermogenic processes. International interest in this material has

increased considerably in the past several years because of increasing recognition that the large volumes of gas stored in these structures represent a significant fraction of the global methane budget (see review by Kvenvolden and Lorenson, 2001) and may, therefore, be a potential energy resource for the future (e.g., Milvov and Sassen, 2002). Several authors have also suggested that sudden widespread dissociation of subseafloor gas hydrates in response to changing environmental conditions may have had a significant effect on past climate (e.g., Revelle, 1983; Nisbet, 1990; Paull et al., 1991; Katz et al., 1999; Dickens, 2001). These effects remain speculative, as the volume of gas stored in the gas hydrate reservoir and its behavior during changing environmental conditions are currently poorly constrained.

In order to evaluate the economic potential of hydrates, their role as a natural hazard, and their impact on climate, we need to know the following:

How are hydrates and underlying free gas distributed vertically and horizontally in the sediment?

What is the gas hydrate inventory on Hydrate Ridge?

What controls their distribution (i.e., lithologic controls on fluid migration and on hydrate nucleation and growth)?

What are the effects of this distribution on the mechanical properties of the seafloor?

How can hydrate and gas distribution be regionally mapped using remote sensing geophysical techniques?

How does hydrate respond to changes in pressure and temperature resulting from tectonic and oceanographic perturbation?

How can we use the isotopic record as a proxy for past tectonic and climate changes?

Does the hydrate system harbor a rich biosphere? This question is of broad interest, particularly given the recent recognition that the biosphere extends deeper into the earth and that it has a larger impact on the geologic record than previously thought.

These questions were the focus of Ocean Drilling Program (ODP) Leg 204, which was dedicated to understanding the biogeochemical factors controlling the distribution and concentration of gas hydrates in an accretionary margin setting. Coring was guided by a three-dimensional (3-D) seismic site survey (Trehu and Bangs, 2001; Trehu et al., 2002) and by logging-while-drilling (LWD) data acquired at the beginning of the leg. These two data sets provided a "road map" to guide coring and sampling, enabling us to anticipate the depths at which gas hydrates should be expected and better focus special sampling tools. Accurate quantification of in situ hydrate and gas concentrations is difficult because of hydrate dissociation and gas loss during core retrieval (Paull and Ussler, 2001). A major focus of Leg 204 was, therefore, to acquire samples under pressure using the ODP pressure core sampler (PCS) system and the recently developed Hydrate Autoclave Coring Equipment (HYACE) system, which includes a laboratory transfer chamber for maintaining pressure while making physical property measurements. Extensive use was made of infrared (IR) cameras on the catwalk to rapidly identify potential hydrate-bearing samples and preserve them for careful study. Extra attention was also given to making high-resolution measurements of the chemistry of interstitial waters, resulting in a large number of interstitial water samples from this cruise. We also had frequent deployments of tools to measure in situ temperature and pressure, especially in zones where LWD data indicated rapid changes in the physical properties of the sediments, and conducted an extensive suite of downhole and two-ship seismic experiments.



## GEOLOGIC AND BIOGEOCHEMICAL SETTING

Hydrate Ridge is a 25-km-long and 15-km-wide ridge in the Cascadia accretionary complex, formed as the Juan de Fuca plate subducts obliquely beneath North America at a rate of ~4.5 cm/yr (Fig. F1A). Sediment on the subducting plate contains large volumes of sandy and silty turbidites. At present, most of this sediment is accreted to the continental margin either by offscraping at the deformation front or by underplating beneath the accretionary complex some 10 km east of the deformation front (MacKay et al., 1992; MacKay, 1995) (Fig. F2).

Hydrate Ridge has been the site of many geological and geophysical cruises since cold seeps were first discovered on this part of the margin nearly 20 yr ago (Kulm et al., 1986). It is characterized by a northern peak having a minimum depth of ~600 m and a southern peak with a depth of ~800 m (Fig. F1B). Hydrate Ridge appears to be capped by hydrate, as indicated by a nearly ubiquitous and strong bottom-simulating reflector (BSR) (Trehu et al., 1999).

A regional two-dimensional multichannel seismic survey was acquired in 1989 as a site survey for ODP Leg 146, which was designed primarily to study dynamics of fluid flow in accretionary complexes. The location where an upward deflection of the BSR is cut by a fault on the northern summit of Hydrate Ridge was selected for ODP Site 892 (Scientific Party, 1993). At this site, massive H<sub>2</sub>S-rich hydrates were recovered from 2 to 19 meters below seafloor (mbsf) (Kastner et al., 1995). No hydrate was recovered near the BSR, but geochemical pore water and temperature anomalies suggested the presence of disseminated hydrate in the pore space to 68 mbsf (Kastner et al., 1995; Hovland et al., 1995). Vertical seismic profiles (VSPs) indicated the presence of free gas for at least 20 m beneath the gas hydrate stability zone (GHSZ) (MacKay et al., 1994). Methane at Site 892 is primarily of biogenic origin (Kvenvolden, 1995), but higher-order hydrocarbons of thermogenic origin are also present (Hovland et al., 1995; Schluter et al., 1998).

Since 1996, there have been several cruises per year to this area, which have generated a comprehensive swath bathymetry and deep-towed side-scan database as well as extensive seafloor observations and sample collections by submersible and remotely operated vehicle (ROV) (Suess and Bohrmann, 1997; Clague et al., 2001; Johnson and Goldfinger, pers. comm., 2002; Torres et al., 1998, 1999; Bohrmann et al., 2000; Linke and Suess, 2001). In addition, a high-resolution 3-D seismic survey was conducted from 19 June to 3 July 2000 as a site survey for Leg 204 (Trehu and Bangs, 2001; Trehu et al., 2002).

### Seafloor Observations of Southern Hydrate Ridge

Side-scan data, seafloor camera tows, and diving with manned and the deep sea vessel *Alvin* and various ROVs demonstrated the presence of extensive massive carbonate pavement on the northern summit of Hydrate Ridge (Carson et al., 1994; Clague et al., 2001; Sample and Kopf, 1995; Bohrmann et al., 1988; Greinert et al., 2001). Until recently, massive authigenic carbonate pavement was thought to be absent on the southern summit of Hydrate Ridge. During *Alvin* dives in 1999, however, a 50-m-high carbonate pinnacle (Fig. F4A) was discovered 250 m southwest of the summit (Torres et al., 1999). Deep-towed side-scan data indicate that the Pinnacle is located in the center of a buried carbonate apron with a diameter of ~250 m (Johnson and Goldfinger, pers. comm., 2002). Authigenic carbonates on the Cascadia margin form as a result of methane oxidation within the sediments and discharge of isotopically light dissolved inorganic carbon at seafloor. The relative absence of carbonate on the southern summit of Hydrate Ridge was interpreted to indicate that this gas system is younger than that on the northern summit, providing a spatial proxy for temporal evolution of hydrate-bearing accretionary ridges (Trehu et al., 1999). This interpretation is supported by U-Th dating of recovered carbonates (Teichert et al., in press), which

indicates that the Pinnacle is <12,000 yr old, whereas the carbonate carapace on northern Hydrate Ridge is >100,000 yr old.

One especially interesting feature of southern Hydrate Ridge is the abundance of massive hydrate at the seafloor near its summit. This was first discovered in 1996, when >50 kg of massive hydrate was recovered with a television-guided grab sample (Bohrmann et al., 1998). The samples show dense interfingering of gas hydrate with soft sediment (Fig. F4B). In most cases, pure white hydrate is present in layers several millimeters to several centimeters thick. Host sediment is often present as small clasts within the pure gas hydrate matrix. On a macroscopic scale, the fabric varies from highly porous (with pores of up to 5 cm in diameter) to massive (Suess et al., 2001). Thin sections show a structure in which gas bubbles have been filled with hydrate. Wet bulk densities of 80 hydrate samples measured on board the *Sonne* range from 0.35 to 7.5 g/cm<sup>3</sup>. Pore space was estimated from the change in sample volume before and after compression to ~160 kb (Suess et al., 2002). The samples show high variability in pore volumes ranging from 10% to 70%, and the values are negatively correlated with sample density. From this correlation, the end-member density at zero porosity was estimated to be ~0.81 g/cm<sup>3</sup>. This value is lower than the theoretical density of pure methane hydrate (0.91 g/cm<sup>3</sup>). Field-emission scanning electron microscopy indicates that this is a result of submicrometer porosity of the massive hydrate (Suess et al., 2002). The low bulk density of the natural methane hydrates from Hydrate Ridge results in a strong positive buoyancy force, implying that the hydrate remains on the seafloor only because of the shear strength of the host sediment. Unusual seafloor topography observed on southern Hydrate Ridge during *Alvin* and *ROPOS* surveys, which is characterized by mounds and depressions with a wavelength of a few meters (Fig. F4C), may result from spontaneous breaking off of hydrate from the seafloor. This may be an important mechanism for transporting methane from the seafloor to the atmosphere (Suess et al., 2001). An important objective of Leg 204 was to determine the depth to which gas hydrate is present.

Vigorous streams of methane bubbles have been observed emanating from vents on the seafloor on the northern and southern peaks of Hydrate Ridge (Suess and Bohrmann, 1997; Suess et al., 1999; Torres et al., 1998, 1999, 2002) as well as from a similar, but smaller, reflective high in the accretionary complex known as Southeast Knoll (Figs. F1B, F3B). Because the seafloor at all three sites is well within the GHSZ (Fig. F3A), the presence of methane bubbles beneath and at the seafloor suggests rapid transport of methane to the seafloor from sediments beneath the GHSZ. Because seawater is undersaturated in methane, their persistence in the water column suggests that they are protected by a thin coating of hydrate (Suess et al., 2001; Rehder et al., 2002; Heeschen et al., pers. comm., 2002). Disappearance of the acoustic "bubble" plumes at 450–500 m below the sea surface (near the top of the hydrate stability zone) suggests that the hydrate shell dissociates and that most of the methane in the bubble plumes is dissolved in the ocean rather than reaching the atmosphere. Another objective of Leg 204 is to determine the mechanism whereby free gas migrates through the GHSZ to reach the water column.

### **Biological Communities Associated with Hydrate and Geochemical Implications**

Communities of tube worms, bacterial mats, clams, and other fauna are associated with seafloor hydrates and methane vents on Hydrate Ridge (Fig. F4D) and elsewhere (e.g., Kulm et al., 1986; MacDonald et al., 1989; Suess et al., 1999, 2001; Sassen et al., 2001). Microorganisms are at the base of the food chain in these communities. Recent work suggests complex complementary relationships between sulfate-reducing, methanogenic, and methanotrophic microorganisms in hydrate-bearing sediments (e.g., Parkes et al., 2000; Boetius et al., 2000). These microorganisms must be playing an important role in methane formation and oxidation and are, therefore, a critical component of the hydrate system.

Identification of these organisms and determination of their abundances, spatial variability, and activity rates is just beginning.

Particularly interesting are recently discovered organisms that play a critical role in anaerobic methane oxidation (AMO), which generates isotopically light dissolved inorganic carbon and results in the formation of authigenic carbonates. These carbonates remain in the geologic record as evidence of past fluid flow and hydrate formation and dissociation (e.g., Sample and Kopf, 1995; Bohrmann et al., 1998; Greinert et al., 2001). Very high rates of AMO have been measured in sediment overlying massive gas hydrates on southern Hydrate Ridge (Boetius et al., 2000) and attributed to structured aggregates consisting of a central cluster of methanotropic Archaea coated by sulfate reducing bacteria. That microbes oxidize methane by utilizing sulfate in the absence of oxygen was long suspected by geochemists based on interstitial sulfate and methane gradients (e.g., Claypool, 1974). Borowski et al. (1996) showed that steep sulfate gradients and shallow depths to the sulfate/methane interface (SMI) are a consequence of the increased influence of AMO, and Boetius et al. (2000) were the first to observe the microorganisms that presumably catalyze AMO. These microbial aggregates appear to be abundant in sediments of Hydrate Ridge and mediate AMO when enough sulfate is available.

Analysis of sulfide minerals provides a possible opportunity to reconstruct past biological activity because most of the reduced sulfide produced during microbial sulfate reduction is ultimately sequestered in various iron phases, which usually involve multiple steps terminating in the formation of sedimentary pyrite. The burial of these mineral phases contributes significantly to the oxygen level of the atmosphere, the sulfate concentration in seawater, and the pH of the oceans over geologic timescales (e.g., Garrels and Perry, 1974; Holland, 1978; Boudreau and Canfield, 1993). Anomalous intervals of high greigite content have been reported in intervals from which gas hydrates were recovered or were inferred to exist (Housen and Musgrave, 1996). Based on the rock magnetic properties at Site 889, Housen and Musgrave (1996) inferred the presence of a "fossil gas hydrate zone," which may have extended downward to 295 mbsf during the last glaciation. Data acquired during Leg 204 will be used in several shore-based studies to further understand the relationships between bacterial activity and sulfide mineralogy.

## **HIGH-RESOLUTION 3-D SEISMIC DATA**

Prior to acquisition of a 3-D high-resolution seismic site survey in 2000 (Trehu and Bangs, 2001), the relationship between subsurface reflections and the summit vents was not known because no profiles crossed the summit. The 3-D survey covers a 4 km × 10 km region that includes the southern summit and an adjacent slope basin. Shots from two generator-injector guns fired simultaneously were recorded on the Lamont portable 600-m-long 48-channel towed streamer and on an array of 21 University of Texas Institute for Geophysics four-component ocean-bottom seismometers. The locations of the ship and of the streamer were determined via differential global positioning satellites and four compasses, respectively, and 3-D fold was monitored during the cruise to identify locations where additional data were needed. Excellent data quality was obtained in spite of strong winds and high seas. The data contain frequencies up to ~250 Hz, providing considerable stratigraphic and structural resolution.

Figure F5 shows EW Line 230 from the data volume. The profile is coincident with Line 2 from the 1989 site survey (Fig. F2B). Locations of Sites 1244, 1245, 1246, and 1252 are shown. Features in the data that were particular targets of Leg 204 are labeled. An upper facies of folded and uplifted sediments unconformably overlies a stratigraphic sequence in which layering is less pronounced. This facies, in turn, overlies a low-frequency incoherent zone interpreted to be highly deformed accretionary complex material. The upper two facies were sampled during Leg 204. Figure F6 shows seismic profiles that trend

approximately north-south and illustrate the setting of Sites 1245, 1247, 1248, 1249, and 1250, which form a transect from the flank to the summit.

A strong BSR, which is a negative-polarity reflection generally thought to result from free gas underlying gas hydrate at the base of the GHSZ, is seen everywhere along the profiles of Figures F5 and F6, except for locally near Site 1252. The data also show considerable stratigraphic and structural complexity both above and below the BSR. Certain reflective horizons are anomalously bright, and these amplitude anomalies are consistent for hundreds of meters.

### **Horizon A**

In particular, we point out the event labeled “A” on Figure F5. This reflection has an amplitude that is ~10 times greater than that of adjacent stratigraphic events and 2 times that of the BSR. Horizon A gets shallower and brightens toward the summit, as shown on relative true-amplitude seismic sections in Figure F6. Maps of the two-way traveltime (TWT) to this surface, of the time between this surface and the BSR, and of the amplitude and dominant frequency of the seismic wavelet are also shown in Figure F6. These maps show that the updip change in amplitude follows depth beneath sea level (or hydrostatic pressure) rather than depth beneath the seafloor. Speculations that this horizon is a major path transporting methane-rich fluids to the summit of Hydrate Ridge and that the change in amplitude results from the onset of pressure release degassing of fluids migrating along Horizon A (Trehu et al., 2002) were tested during Leg 204 by drilling at Sites 1245, 1247, 1248, and 1250.

### **Seismic Signature of the Southern Summit**

Figure F7 shows the characteristics of Reflection A and of overlying actively venting features near the southern summit of Hydrate Ridge. Locations of sections are shown on a map of seafloor reflectivity obtained by deep-towed side scan (Johnson and Goldfinger, pers. comm., 2002) to illustrate the relationship between seafloor manifestations of venting and subsurface reflectivity. Chaotic bright reflectivity is observed just beneath the seafloor at the summit (Line 300) (Fig. F7B). This reflectivity pattern is observed only at the summit and is almost exactly coincident with the “tongue” of intermediate strength seafloor reflectivity northeast of the Pinnacle observed in the deep-towed side-scan data. This pattern also underlies the acoustic bubble plume that was observed each time the southern summit was crossed during the seismic data acquisition cruise. We speculated that this pattern indicates the depth extent of surface massive hydrate (Trehu et al., 2002) and tested this speculation by drilling at Site 1249. It appears that Reflection A is a primary source of fluids for the summit vents (the mechanism whereby methane migrates to the seafloor), is not imaged in the seismic data. We speculated that the region between Reflection A and the seafloor is broken by small faults that are not well resolved in the seismic data but that permit methane-rich fluids to rise vertically from Reflection A to the seafloor. This speculation was tested by drilling at Site 1250.

### **Horizons B and B' on the Eastern Flank of Hydrate Ridge**

Complicated reflectivity patterns are also observed east of the southern Hydrate Ridge axis and are associated with an active secondary anticline (Anticline A) (Fig. F5). The “double BSR” originally identified on Line 2 from the 1989 site survey (Fig. F5C) shallows to the south and merges with the BSR along 3-D Line 274. It is continuous with a package of bright regionally extensive reflections that cut across the BSR (Fig. F5). Reflections B and B' are pervasively faulted, with offsets consistent with tensional

cracking in response to uplift and folding. We speculated that Reflection C represents the top of the accretionary complex and that Horizons B and B' might be permeable stratigraphic horizons transporting fluids from the accretionary complex into the GHSZ. The lack of consistent amplitude and polarity changes across the BSR, however, makes this interpretation quite uncertain. During Leg 204, Sites 1244 and 1246 were designed to sample Horizons B and B' above and below the BSR.

### **Slope Basin East Of Hydrate Ridge**

Site 1251 is located in the slope basin east of Hydrate Ridge. The seismic setting of the BSR in this basin is similar to that of the BSR beneath the Blake Ridge. Sediments are accumulating rapidly in this basin, and the BSR is characterized by a change in amplitude of dipping stratigraphic horizons, with large amplitudes indicative of free gas beneath the BSR (Fig. F8). This site was, therefore, chosen for drilling to provide a relative reference site where the processes controlling hydrate formation were hypothesized to be similar to those on the Blake Ridge. A secondary objective was to sample a layer in the center of the basin (labeled DF1 in Fig. F8) that was interpreted to represent a massive debris flow based on the basis of the absence of internal reflectivity. This horizon is one of two such thick events that can be traced through much of the 3-D data set.

Site 1252 was chosen to sample the underlying seismically chaotic sediments where they are uplifted to form Anticline B. Here the sediments appear to be less deformed than beneath the crest of Hydrate Ridge and retain some coherent internal structure. Another objective at Site 1252 was to determine the reason for the absence of a BSR at Site 1252, in contrast to the very strong BSR observed only ~300 m to the east in the core of Anticline B. A third objective was to sample the lower inferred debris flow, which appears to have been blocked by Anticline B. Anticline B must have represented a topographic high when these sediments were deposited.

## **SCIENTIFIC OBJECTIVES**

### **Stratigraphic and Structural Controls on Hydrate Development**

The structural and stratigraphic setting of Hydrate Ridge contrasts with that of the adjacent slope basin to the east. Beneath the slope basin, the seismic indicators of hydrate and free gas are similar to those on the Blake Ridge, with an intermittent BSR and enhancement of stratigraphic reflectivity beneath the BSR (Holbrook et al., 1996). The sedimentation rate in this basin was expected to be very high. During Leg 204, we tested the hypothesis that the distribution, texture, and chemistry of hydrate and related pore fluids beneath Hydrate Ridge differ from those on the slope basin.

### **Formation of Massive Hydrate near the Seafloor**

The presence of massive hydrate near the seafloor is enigmatic, as most models for hydrate formation in a region of diffuse fluid flow predict a decreasing gradient in hydrate concentration above the BSR (e.g., Paull et al., 1994; Rempel and Buffett, 1998; Xu and Ruppel, 1999). Several explanations have been proposed, including formation in the past when the stability boundary was near the seafloor, formation at depth and exposure by erosion (Bohrmann et al., 1998), and transport of methane through the hydrate stability field as free gas isolated from water (Suess et al., 2001). One objective of Leg 204 was to obtain constraints on the rate of hydrate formation, the depth extent of the massive hydrate, and mechanisms for transporting free gas to the seafloor.

## **Methane Sources and Geochemical Effects of Hydrate Formation and Dissociation**

It has been well established that fluids play a major role in many aspects of the geologic evolution of convergent margins. Changes in the chemical and isotopic composition of interstitial fluids with depth have been shown to be powerful tracers of fluid sources and migration patterns. Important objectives of Leg 204 were to document the fluid flow regime and evaluate role of fluid flow on the formation of gas hydrates, specifically as they might provide clues to the source and flux of methane to the GHSZ. Since hydrate formation and destabilization modify the isotopic composition of the pore water, a high-resolution set of pore water samples was collected during Leg 204, with the goal of using the dissolved chloride and the isotopic composition of these waters to constrain models of formation and destabilization of gas hydrates on this margin.

### **Geochemical Impact on the Geological Record**

Changes in the isotopic composition of the dissolved carbonate resulting from oxidation of methane enriched on  $^{12}\text{C}$  are thought to be incorporated into calcareous fossil tests (Wefer et al., 1994; Dickens et al., 1995, 1997; Kennett et al., 1996) and authigenic carbonate phases (e.g., Sample and Kopf, 1995; Bohrmann et al., 1998). An objective of Leg 204 is to determine the isotopic composition of the pore fluids and carbonates associated with gas hydrates to provide the framework needed to unravel the history of gas hydrate formation and destabilization recorded in benthic foraminifer and authigenic carbonate phases elsewhere.

### **Calibration of Geophysical Estimates of Hydrate and Gas Volumes**

Better calibration of regional estimates of gas hydrate and free-gas volumes based on geophysical mapping and modeling techniques is of critical importance toward estimating the global abundance of hydrate and evaluating its role in climate change and potential for economic exploitation. During Leg 204, we drilled through hydrates in a variety of settings with different seismic characteristics, measured in situ physical conditions, and conducted a series of nested seismic experiments to calibrate various techniques for remote sensing of hydrate distribution and concentration.

### **Hydrates and Slope Stability**

The possible relationship between hydrates and slope failure is presently poorly understood. On the one hand, hydrates may stabilize slopes by cementing sediment grains. On the other hand, if hydrates impede fluid flow, they may weaken the underlying sediment by trapping fluids and free gas. Several investigators have noted the possible correlation of hydrates and slope instability (e.g., Booth et al., 1994; Trehu et al., 1995; Paull et al., 1996) and have discussed how such slope instability might release massive amounts of methane into the ocean (Paull et al., 1996; Nisbet and Piper, 1998). One objective of Leg 204 was to determine the mechanical and hydrological properties of hydrate-bearing sediment to better constrain models of slope instability.

### **Biological Communities Associated with Hydrate and Underlying Free-Gas Zones**

Microorganisms play an important role in both methane formation and oxidation and are, therefore, a critical component of the hydrate system. Identification of these organisms and determination of their

abundance, spatial variability, and rates of activities is just beginning. Important questions addressed during Leg 204 included the following:

- What impact do these organisms have on the volume of methane produced and oxidized beneath Hydrate Ridge?
- At what depths are they concentrated?
- What effect do they have on sediment diagenesis and the development of magnetic minerals?
- Does the hydrate-related biosphere differ between Hydrate Ridge and the adjacent slope basin?
- How do microorganisms affect sediment and pore water chemistry and texture, and vice-versa?

## **DRILLING STRATEGY**

To test the hypotheses discussed above, we originally proposed three primary drill sites extending to depths of 400–700 mbsf. Preliminary analysis of the 3-D seismic data confirmed the rationale behind these three sites but led to minor modifications of site locations. It also led to the addition of seven shallow-penetration (<260 mbsf) sites to sample the massive hydrate at the summit and to determine updip changes along subsurface horizons that appeared to be fluid pathways feeding the summit vents. Four of these additional sites were primary sites and three were alternates as described in the Leg 204 Scientific Prospectus; all were approved for drilling by Pollution Prevention and Safety Panel (PPSP). We drilled all sites except for alternate site HR1c, for a total of nine sites. Locations of the sites drilled are overlain on a map showing seafloor bathymetry in Figure F1C.

Leg 204 started with 3 weeks dedicated to LWD. For safety reasons, Site 1244 (proposed Site HR1a) was cored to 350 mbsf depth prior to LWD, allowing for sampling of all seismic facies that were to be drilled. We had approval from the PPSP to proceed with LWD prior to coring at all additional sites, or until the time allocated to LWD was expended, if no safety issues were encountered while drilling at Site 1244. Our objective was to use the LWD data to determine where to use time-consuming special downhole tools prior to coring. The LWD data turned out to be of excellent quality, and this strategy proved to be very useful.

Another novel aspect of this leg was the use of IR thermal imaging to systematically scan each core (at least those from within and near the hydrate stability zone) as soon as it was brought on board. Because hydrate dissociation is a strongly endothermic process, cold spots thus detected permitted us to quickly confirm what portions of the core contained significant amounts of gas hydrate. Experiments were designed to determine whether the original amount of hydrate present could be determined based on the change in temperature with time by calibrating the temperature record obtained by the IR scanner with concentration estimates obtained from closely spaced pore water chloride concentration sampling.

## **OPERATIONAL SUMMARY**

Leg 204 was originally scheduled to begin in San Francisco, California, and end in San Diego, California. As a result of an impending West Coast dock strike, both port calls were ultimately moved to Victoria, British Columbia, Canada. Leg 204 officially began with the first line ashore, Westcan Terminal B at 0655 hr on 7 July 2002.

In many ways, the leg turned out to be extraordinary. Almost all science objectives were successfully achieved during the course of drilling/coring the seven primary sites and two alternate sites. In addition, a

series of holes geared specifically toward the rapid recovery and preservation of hydrate samples was cored at the end of the leg at Site 1249 as part of a hydrate geiatric study funded by the Department of Energy.

Some significant statistics of Leg 204 are listed below, followed by a more descriptive discussion:

Water depths ranged from 788.5 to 1228.0 meters below rig floor.

Eight of nine sites were drilled using LWD technology.

Overall, a total of 45 holes were drilled/cored at nine separate drill sites.

Eleven holes were drilled with a tricone bit for LWD/resistivity-at-the-bit (RAB)-8 or wireline logging.

Thirty-three holes were cored with the advanced piston corer (APC) and/or extended core barrel (XCB) coring systems, and one hole was rotary core barrel (RCB) cored.

A total of 3674.5 m were cored with 3068.3 m (83.5%) recovered.

Of a 57.1-day leg, 50.4 days, or 88.3%, of the time was spent on site operating and 6.7 days in port/transit.

Twenty-nine nautical miles (43.8 hr) were covered during 23 moves between sites, using dynamic positioning.

Seven helicopter and two supply boat rendezvous were conducted, resulting in 42 personnel exchanges.

Visitors included two journalists (Dallas Morning News and American Geophysical Union/Eos), two engineering observers (Department of Energy and Chevron/Texaco), and a two-man German film crew from Context TV.

Whirl-Pak glass microbeads and perflouorocarbon tracers were used on 85 cores that were sampled for microbiology.

Fifty meters of hydrate core was recovered and stored under pressure in a methane environment; 35 m of additional samples was recovered and stored in six liquid nitrogen dewars.

Special tool deployments and successes during the leg included the following:

Thirty of thirty-nine successful runs with PCS;

Sixteen of sixteen successful runs with the Davis-Villinger Temperature-Pressure Probe (DVTPP);

Eight of eight successful runs with the Davis-Villinger Temperature Probe (DVTP);

Sixty-one of sixty-one successful runs with APC temperature tool (APCT);

One hundred and seven of one hundred and ten successful runs with the APC-methane tool (APC-M);

One of two successful deployments of the Fugro-McClelland piezoprobe;

Two of ten cores successfully recovered with pressure using the deployment of the Fugro Pressure Corer (FPC) on hydrates;

Four of eight cores successfully recovered under pressure using the HYACE Rotary Corer (HRC);

Twenty-eight runs with the Lamont-Doherty Earth Observatory (LDEO) Drill String Acceleration (DSA) tool; seventeen were all or partially successful; and

Eight of eight cores successfully recovered using the RAB-8 logging-while-coring (LWC) technology.

Operations on the southern Hydrate Ridge also required coordination with several other oceanographic research vessels. The *Somme*, a German research vessel, operated in the same area, deploying and recovering instrumented seafloor landers. The *Ewing*, from LDEO, worked in conjunction with the *JOIDES Resolution* conducting two-ship seismic operations and independent research, including the setting of ocean-bottom seismometer (OBS) packages on the seafloor. The *Atlantis*, from Woods Hole Oceanographic Institution,



was on site for 4 days of *Alvin* diving at the ridge crest. And finally, the *New Horizon*, a Scripps Institution of Oceanography vessel, was on location briefly doing independent oceanographic research work.

The leg also included a two-ship seismic program conducted in conjunction with the *Ewing* to acquire vertical, constant-offset, and walk-away VSPs. A new Schlumberger tool called the Vertical Seismic Imager (VSI) was used for most of the VSP work, whereas the older Well Seismic Tool (WST) was used for the remaining holes. Deployment of the VSI tool was problematic because of its fragile construction and because the tool is not designed to have the electric line slacked off during the data acquisition period. Nonetheless, the tool worked well enough to achieve most of the seismic objectives.

Eight of the sites were drilled using LWD technology. A developmental LWC system, jointly developed by LDEO, Anadrill, and Texas A&M University (TAMU), was also successfully tested using a RAB-8 LWD tool. This marked the first time that core samples have been recovered simultaneously with LWD data.

Several other specialized tools developed all or in part by TAMU were successfully deployed during the leg. These include the PCS, MT, APCT shoe, DVTP, and DVTPP.

Two other developmental pressure coring systems developed by the European consortium (HYACINTH) were deployed. These tools were designed to allow transfer of a pressurized core sample from the downhole tools autoclave chamber to a pressurized logging chamber. The FPC and HRC were deployed 10 times and 8 times, respectively. Two runs with the FPC and four runs with the HRC successfully recovered core at or near in situ pressure. Functionally, the pressurized core transfer and logging chambers worked well, although some tolerance variations with the FPC made the transferring of the FPC cores more problematic.

Prior to the leg, TAMU worked with Fugro-McClelland on the adaptation of their piezoprobe tool to the ODP/TAMU bottom-hole assembly (BHA). This tool was deployed twice on the first site, with the second attempt fully successful. Data from this electric line-deployed tool will be compared to DVTPP data. The DVTPP tool is deployed in a much faster and simpler fashion by being free-fall deployed and then recovered using the standard ODP coring line.

LDEO deployed its DSA tool to gather downhole data in support of the HYACINTH tool deployments and also as part of an experimental study using the APC as an energy source. The APC impact energy was recorded using OBS stations placed on the seafloor earlier by the *Ewing*. Initial results indicated that this experiment was successful and that useful data were obtained.

The scientific and operational achievements were impressive; however, the leg was extremely demanding because of the confined operating area. All nine drill sites were located within 3.6 nmi of each other. As a result of the close proximity of the sites, all moves between sites were done using the ship's dynamic positioning system. Because of the commonality of the coring BHAs to be used, most of these moves were made with the pipe suspended below the ship. When a BHA change or bit replacement was required, the move was made simultaneously with the pipe trip to and from the surface. With no transit time, other than traveling to and from port and limited pipe trips between sites, the operating time available for drilling and coring was considerable. For the 57.1-day leg, 50.4 days, or 88.3%, of the available time was spent on site. The remaining 6.7 days was spent in port (4.14 days) and under way (2.54 days).

Leg 204 operations were confined to an area located ~50 nmi off the coast of Oregon. The close proximity of land meant that this leg was a candidate for numerous changes of personnel and equipment. An initial supply boat rendezvous was planned to allow removal of specialized and expensive VSP equipment along with an Anadrill VSP engineer. This soon grew to include numerous other personnel changes via helicopter, and another supply boat brought out special pressure vessels, dewars, and liquid nitrogen to support the add-on effort to recover and preserve the additional hydrate samples. Ultimately,

there were a total of nine rendezvous completed with the *JOIDES Resolution*, including seven helicopters and two supply vessels.

Leg 204 officially ended at 0900 hr on 2 September 2002, with the first line ashore Westcan Terminal Pier B in Victoria.

## **SITE SUMMARIES**

In this section, we describe and discuss the primary results at each site. Relationships among sites are also discussed using figures that compare data from several sites. In general, sites fall into two primary groupings. Sites 1245, 1247, 1248, 1249, and 1250 form a north-south transect that documents the evolution of the southern Hydrate Ridge (SHR) gas hydrate system from the flank to the summit and explores the role of Horizon A. Sites 1245, 1246, 1244, 1252, and 1251 form an east-west transect that compares the west and east flanks of SHR to the adjacent slope basin. Lithology at all sites is similar, with abundant turbidites, some debris flows, and several notable ash layers (Fig. F9). These ash layers are responsible for the largest-amplitude seismic reflections and play a major role in focusing fluid flow and hydrate distribution in this system.

### **Site 1244**

Site 1244 (proposed Site HR1a) is located in 890 m of water on the eastern flank of Hydrate Ridge, ~3 km northeast of the southern summit (Fig. F1). The 3-D seismic data available from a Leg 204 site survey show that the BSR is present at a depth of ~125 mbsf at this site (Fig. F5). The temperature and pressure at the seafloor are well within the GHSZ (Fig. F3), indicating that gas hydrates can exist within the entire stratigraphic section above the BSR if hydrate-forming gases are available in concentrations that exceed their in situ solubility. The 3-D seismic data also image a zone of incoherent seismic reflections that forms the core of Hydrate Ridge. At Site 1244, the top of this incoherent zone is located at a depth of ~300 mbsf. This facies has been interpreted to comprise fractured accretionary complex material. Dipping, faulted, and strongly reflective strata interpreted to be an uplifted and deformed slope basin overlie this facies.

The primary drilling objectives at this site were to (1) determine the distribution and concentrations of gas hydrate within the GHSZ; (2) determine the nature of a pair of strong reflections (referred to as B and B') that underlie much of the eastern flank of Hydrate Ridge; (3) determine the composition, structure, and fluid regime within the seismically incoherent unit underlying the stratified sediments; and (4) sample the subsurface biosphere associated with these features.

### **Operations**

Five holes were cored at Site 1244, and an additional hole was drilled (Table T1). Hole 1244A was abandoned when the first core overshot and did not record a mudline. Hole 1244B was abandoned at 53.1 mbsf after six cores were obtained because the BHA had to be brought to the surface to retrieve a downhole instrument (Fugro piezoprobe) that had become unscrewed from the Schlumberger conductor cable. One APCT measurement was taken at 35.1 mbsf in this hole. Hole 1244C, which comprises 39 cores, began at the seafloor and continued to 334 mbsf. Special tools used in Hole 1244C included three APCT (at 63, 82, and 110 mbsf), one DVTP (at 64 mbsf), one DVTPP (at 150 mbsf), and three PCS (at 120, 131, and 142 mbsf) runs. Hole 1244C was abandoned 17 m above the target depth of 350 mbsf, when hole conditions suggested that a change from XCB to RCB coring would be appropriate. Examination of the core and the initial chemical data from this depth suggested that we had reached the deepest target (i.e.,

the accretionary complex). We had, thus, fulfilled the PPSP requirement that we core the primary facies we expected to encounter during LWD prior to proceeding with LWD at all sites. We returned later in the leg to drill Hole 1244D, which was dedicated to wireline and seismic work, to 380 mbsf. This was followed by a Hole 1244E, which was cored to 136 mbsf and extensively sampled for geochemistry, gas hydrates, and microbiology, and Hole 1244F, which was cored to 24 mbsf primarily for high-resolution microbiological sampling.

### **Principal Scientific Results**

On the basis of visual observations, smear slides, and correlation with physical property data (especially magnetic susceptibility [MS]), the sedimentary sequence can be divided into three primary lithostratigraphic units, with three subdivisions in the second unit. Lithostratigraphic Units I (from the seafloor to 69 mbsf) and II (69–245 mbsf) are both characterized by hemipelagic clay interlayered with turbidites, with thicker, coarser turbidites common in lithostratigraphic Unit II. Individual turbidites are characterized by sand and silt layers that fine upward to bioturbated sulfide-rich silty clay and clay. The turbidites are particularly well developed in the interval from 160 to 230 mbsf. A 60-cm-thick layer at 216 mbsf that is especially rich in detrital volcanic ash shards corresponds to a strong regional seismic reflection referred to here as Reflection B' (Fig. F5).

The lithology changes to more indurated and fractured claystone interbedded with glauconite-bearing to glauconite-rich silts and sands below 245 mbsf, lithologies referred to as Unit III. The boundary between lithostratigraphic Units II and III corresponds to the top of the seismically incoherent zone that underlies the slope basins (Fig. F5) and was interpreted to represent highly deformed sediments of the accretionary complex.

Biogenic components vary downcore, with a predominance of siliceous microfossils. Biostratigraphic boundaries based on diatoms correlate fairly well with lithostratigraphic unit boundaries and with seismic stratigraphic boundaries identified in the 3-D seismic data, although there are some inconsistencies among these three data sets when comparisons are made among sites. Sediments immediately above a regional unconformity at ~240 mbsf (approximately the boundary between lithostratigraphic Units II and III) yield diatoms that indicate the age to be younger than 1.6 Ma. Sediment immediately below the unconformity yields nannofossils that indicate the age to be older than 1.7 Ma. This unconformity is also sampled at Site 1251 at 300 mbsf and at Site 1252 at 130 mbsf (Fig. F10). Lithostratigraphic Unit III is older than 1.7 Ma.

Physical property data are generally consistent with the lithostratigraphic, biostratigraphic, and seismic stratigraphic boundaries. The boundary between lithostratigraphic Units I and II is marked by a localized decrease in wet bulk density. As mentioned above, the turbidites of lithostratigraphic Unit II are particularly well developed in the interval from 160 to 230 mbsf. This interval is characterized by high values of whole-core MS. The widest and strongest MS peak, at 168 mbsf, correlates with the seismic reflector known as Horizon B. This horizon is also coincident with an increase in wet bulk density. There is also excellent correlation between moisture and density (MAD) measurements on core samples and measurements of density and porosity obtained via LWD.

One novel aspect of Leg 204 is the regular use of both hand held and track-mounted IR cameras to image all cores. Cores from within the GHSZ were imaged several times by the physical property scientists. The hand held IR camera proved to be very effective for rapid identification of the location of hydrate specimens within the cores (Fig. F12). Gas hydrate samples were recovered as whole rounds in Cores 204-1244C-8H and 10H (samples from 63, 68, and 84 mbsf) and preserved for detailed shore-based studies. A

few pieces were dissociated for chemical analysis (discussed below). In all three cases, the hydrate was present as layers or nodules several millimeters to 1.5 cm thick, aligned at an angle of 45°–60° to the core liner, suggesting formation along steeply dipping fractures.

The track-mounted IR camera imaged the cores systematically, and these records were used to confirm the presence of hydrates spotted by the hand held cameras to develop techniques for detecting more subtle signatures of disseminated hydrate and to track the temporal evolution of the thermal signature of hydrate dissociation. The IR thermal imaging of the cores on the catwalk indicated the presence of numerous nodular and/or disseminated hydrates extending from ~45 mbsf to the BSR at 124 mbsf. The presence of these are shown in Figure F13 as temperature anomalies in which local temperature along the core is 1°–7° ( $\Delta T$  in Fig F13) lower than in the adjacent sediments.

The LWD data obtained at this site are of excellent quality and provide spectacular images of electrical resistivity within the borehole (Fig. F13). High-amplitude variable resistivity from 40 to 130 mbsf (Fig. F11) suggests the presence of hydrate and correlates well with the depth range of the IR temperature anomalies and with geochemical indicators of hydrate presence discussed below. We note that this is the only site at which the LWD data were acquired after coring. At other sites, the pattern of high-amplitude variable resistivity was used as a predictor the presence of hydrate prior to coring. Sinusoidal patterns in the resistivity images of the borehole wall suggest that gas hydrate is concentrated in steeply dipping fractures as well as along bedding planes (Fig. F14). The data also show strong borehole breakouts in Unit III, which are indicative of a northeast-southwest-oriented axis of least compressive stress.

Geochemical analysis of interstitial waters has revealed that depth variations in the concentration of several different chemical species correlate with the hydrate stability zone. The most direct correlation is seen in Cl concentrations. Above the first occurrence of hydrate (from the seafloor to ~45 mbsf), Cl concentration in the pore water is similar to that in seawater (Fig. F14). Between 45 mbsf and the BSR at ~125 mbsf, there are numerous low Cl spikes that likely reflect the freshening effect of dissociated hydrate on the interstitial waters. Correlation of Cl data with the IR camera data indicates that the spatial sampling of Cl anomalies is biased, which smooths estimates of hydrate concentration based on Cl anomalies. Experiments to better quantify this bias were conducted at several other sites. Nevertheless, these data can be used to obtain a rough estimate of hydrate concentration if a “no hydrate” background concentration can be estimated. At Site 1244, Cl concentrations from the BSR to 300 mbsf decrease linearly at a rate of ~0.35 mM/m. This suggests a diffusive gradient between seawater and low Cl fluids in the accretionary complex. The reduced chloride concentration at depth may reflect dehydration of clay minerals deeper in the accretionary complex. Considering uncertainties in the background concentration of Cl, we estimate that 2%–8% of the pore space is occupied by hydrate, with locally higher and lower concentrations. The Cl concentration profile within the deepest incoherent seismic facies is approximately constant, suggesting a zone of fluid advection and mixing consistent with LWD, physical properties, and core observations, all of which suggest a pervasively fractured medium.

The methane/ethane ( $C_1/C_2$ ) ratio also shows a clear correlation with the presence of gas hydrate (Fig. F15). Gases obtained by the headspace technique and by sampling void space in the cores show a steplike decrease in the  $C_1/C_2$  ratio at the BSR. This was observed to a varying degree at all sites and will be discussed further in the site summary for Site 1251. Slightly lower  $C_1/C_2$  ratios are observed in gas obtained by dissociating discrete hydrate samples (Fig. F15), suggesting some fractionation of  $C_2$  into hydrate.

After the first two cores, the cores were pervasively cracked and contained many voids, both of which are indications of degassing during recovery. The PCS offers the only opportunity to measure in situ

methane concentrations directly. At Site 1244, in situ methane concentrations are below the solubility predicted for in situ conditions at depths of 24, 40, 120, and 131 mbsf and are above predicted solubility at 72 and 103 (Fig. F17). These are the first in situ gas concentrations obtained from Hydrate Ridge. They corroborate the relatively low estimates of gas hydrate concentration obtained from the chloride data.

The downhole temperature measurements (including the average of waterline temperatures) were used to define a linear temperature gradient of  $0.0575^{\circ}\text{C}/\text{m}$  (Fig. F18), very similar to the temperature gradient determined at ODP Site 892 during Leg 146 (Shipboard Scientific Party, 1994). This temperature gradient predicts that the BSR should be at a depth of 135 mbsf, based on the pure methane and seawater stability curve and seismic velocities obtained from the 2000 3-D OBS. The apparent ~10-m mismatch between the BSR depth determined from the seismic data and that calculated from the observed temperature gradient is probably within the uncertainty of the data.

Seismic data at this site include high-frequency sonic log data and lower-frequency vertical, offset, and walk-away seismic profiles. Preliminary data from automatic picks of the VSP indicate that the velocities used for initial mapping of the 3-D seismic reflection data from TWT to depth were quite close (Fig. F19). The data also indicate that positive velocity anomalies resulting from hydrate presence above the BSR and low-velocity anomalies resulting from free gas below the BSR are small and local.

The pore pressure dissipation measurement made by the DVTPP follows the expected pattern, but detailed analyses to determine whether in situ pressure departs from hydrostatic pressure awaits postcruise study.

Samples were taken to support a range of shore-based microbiological studies, but there are no results to report at this time. Measurements of sulfate concentration in the interstitial waters, which indicate that the SMI is present at 8 mbsf at this site, were used to guide high-resolution sampling for microbiological studies.

## **Summary**

Site 1244, which is the first site that was logged and cored during Leg 204, provides strong evidence that gas hydrates are common within the hydrate stability zone on the Oregon continental margin and that they are a major factor influencing the biogeochemical evolution of the margin. It is also clear that the integration of geophysical remote sensing data such as 3-D seismic reflection surveying, LWD, and IR thermal scanning provides a reliable road map to guide further sampling and analysis.

## **Site 1245**

Site 1245 (proposed Site HR3a) is located in 870 m of water on the western flank of Hydrate Ridge, ~3 km northwest of the southern summit (Fig. F1). The 3-D seismic data show that the BSR is at a depth of ~134 mbsf at this site. As at all sites drilled during Leg 204, the temperature and pressure at the seafloor at Site 1245 are well within the GHSZ, indicating that gas hydrates can exist within the entire stratigraphic section above the BSR if hydrate-forming gases are available in concentrations that exceed their in situ solubility. A faint reflection that underlies the BSR and is approximately parallel to it has tentatively been interpreted to be a second BSR that may indicate the base of the stability zone of hydrates that include higher-order hydrocarbons. This site also samples Horizon A. Horizon A can be mapped from the northern boundary of the seismic survey (where it clearly follows stratigraphic boundaries) to the summit (where it appears as a “bright spot” beneath the BSR). On its downdip edge, it appears to lap onto the boundary between coherent folded strata and the seismically incoherent facies interpreted to represent highly deformed sediments of the accretionary complex. It has been interpreted to be a “conduit” that

transports fluids from the accretionary complex to the summit. Several unconformities, referred to as Horizons Y and Y', overlie Horizon A and appear to represent discontinuities in sediment accumulation in a slope basin that was formed during growth of an underlying accretionary anticline.

Primary objectives at Site 1245 were to (1) determine the distribution, composition, and concentration of gas hydrate in the sediments on the western flank of Hydrate Ridge and contrast these parameters with those on the eastern flank of the ridge and in the adjacent slope basin where the sub-BSR fluid migration pathways inferred from seismic data are distinctly different; (2) sample sediments and fluids from seismic Horizon A; and (3) sample the sedimentary section of the western flank of Hydrate Ridge below the BSR to provide constraints for interpreting variations in BSR strength across the western flank. Site 1245 is also a reference site for a north-south-trending transect that extends from Site 1245 to the summit and includes Sites 1247, 1248, 1249, and 1250.

## **Operations**

Hole 1245A was drilled to a depth of 380 mbsf (without coring) to obtain the initial LWD data for this site. Hole 1245B was cored to 473.7 mbsf using the APC and XCB. Holes 1245C and 1245D were cored to 201.7 and 24 mbsf, respectively, for extensive high-resolution geochemical and microbiological sampling. Hole 1245E was drilled to 473.7 mbsf and then cored to 540.3 mbsf using the RCB. Coring in Hole 1245E stopped short of the originally planned depth of 700 mbsf because of deteriorating hole conditions. The hole began to collapse, trapping the BHA. Fortunately, it was not necessary to sever the pipe, although preparations were made to do so. The upper 300 mbsf of Hole 1245E was used for wireline logging. Plans for conventional, offset, and walk-away seismic lines were abandoned when the downhole seismometer would not clamp in Hole 1245E and the hole continued to collapse. The APCT was run eight times, the DVTP was run three times, and the PCS was run five times at this site. There were also two runs each of the HYACINTH HRC and FPC devices. Eleven whole-round samples of sediment thought to contain gas hydrate were preserved in liquid nitrogen or in pressure vessels for postcruise studies.

## **Principal Scientific Results**

Biostratigraphic observations from the 540 m of core recovered at Site 1245 indicate that the entire 540-m-thick sequence is younger than 1.65 Ma (Fig. F10). Distinct changes in sedimentation rate occurred at 55 and 150 mbsf. Sediments deeper than 150 mbsf were deposited from 1.0 to 1.65 Ma at a rate of ~62 cm/k.y., whereas the overlying strata were deposited at a slower rate of 10–23 cm/k.y. (Fig. F11). Lithostratigraphic analysis indicates that the dominant lithologies in the upper 0–31 mbsf are clay with carbonate concretions and foraminifer-rich interlayers. From 31.5 to 212.7 mbsf, the sediments are mainly diatom-bearing clay and silty clay with frequent sand-rich turbidites containing a few glass-rich layers. Included within this deeper sequence is seismic Horizon A, characterized by multiple ash-rich sandy layers between 176 and 183 mbsf. Between 212.7 and 419.3 mbsf, nannofossil-rich claystone and silty claystone with glauconite layers and turbidites are present, underlain by claystone containing thick turbidites and heterogeneous mud clasts.

The precruise 3-D seismic reflection site survey (Figs. F5, F6) and the LWD data (Fig. F13) obtained from Hole 1245A provided a roadmap that was used to guide the sampling and analysis strategy at this site. The logging data, which are of excellent quality, show a marked increase in the amplitude and variability of formation resistivity between 48 and 131 mbsf (logging Unit II). As discussed for Site 1244, this resistivity pattern is interpreted to indicate the zone within which gas hydrates are present. High-resistivity layers are both subhorizontal, indicating accumulation of gas hydrate parallel to bedding, and steeply dipping,

indicating that hydrate fills fractures. Archie's Law (Archie, 1942) saturation calculations (Collett and Ladd, 2001) predict a hydrate concentration of ~10%–30% of the pore volume in layers distributed throughout this interval.

The estimated depth distribution of gas hydrate obtained from the LWD data was confirmed by several other chemical and physical proxies. Low chloride concentration anomalies (Fig. F14) were detected in samples of interstitial waters from 55 to 125 mbsf (Fig. F14) and are interpreted to reflect in situ hydrate concentrations that are generally below 3%, with one anomaly suggesting a concentration of 15%. Low-temperature anomalies were observed with the IR cameras between 50 and 129 mbsf (Fig. F13). Preliminary estimates of total in situ methane concentration obtained from a PCS at 57 mbsf indicated a concentration very close to in situ saturation, and a PCS located at 120 mbsf indicated that in situ methane concentration just above the BSR is an order of magnitude greater than saturation at in situ conditions (Fig. F16). Two PCS runs below the BSR yielded concentrations that are apparently slightly lower than saturation. The consistency between these multiple independent estimates of the depth range of the zone where hydrate is present gives us considerable confidence in the validity of these estimates. Models will be investigated postcruise to relate the depth of the first occurrence of hydrate to the depth of the SMI (observed at ~7 mbsf at this site) and to more precisely estimate the in situ methane concentration as a function of depth within the hydrate stability zone.

The IR camera was used to rapidly identify the temperature range and potential location of hydrate samples in cores on the catwalk. In addition, the IR data were used to estimate the distribution and texture of gas hydrate downhole. Approximately 80 IR anomalies were identified and classified (Fig. F13). In Hole 1245B, 75% of the anomalies suggested disseminated hydrate and 25% suggested nodular hydrate; in Hole 1245C, 60% of the anomalies suggested disseminated hydrate and 17% suggested nodular hydrate. The IR data were also used to select a section of core (Section 204-1245C-7H-5) for an experiment to investigate the relationship between IR imaging, chloride concentration anomalies in pore water, and hydrate distribution in the core. When the core liner was split and removed, a 2-cm-thick, steeply dipping layer of hydrate was found. After allowing the hydrate to dissociate for 90 min, closely spaced sediment samples were taken near the hydrate, including one sample from where the hydrate had been. The chloride concentration anomaly is strongly attenuated 5 cm away from the hydrate sample and has disappeared 10 cm from the hydrate. Since normally only two interstitial water samples are taken in each 9.5-m-long core, the chloride concentration measurements are spatially biased. Frequent low-chloride concentration anomalies downcore must indicate extensive distribution of hydrate. Additional comparison and calibration between data sets with different length scales and sensitivity to hydrate concentration should improve our ability to estimate in situ concentrations from such data.

A major objective at Site 1245 was to sample seismic Horizon A. At Site 1245, as well as at the other three sites where Horizon A was crossed during the LWD phase of Leg 204 (Sites 1247, 1248, and 1250), it is characterized by a very distinctive strong double-peaked low-density anomaly that is 3–4 m wide. At Site 1245, the density of Horizon A is  $<1.5 \text{ g/cm}^3$  compared to  $1.85 \text{ g/cm}^3$  in adjacent sediments. Coincidence of this LWD density anomaly with the estimated depth of Horizon A in the seismic data provided confirmation that the velocities used for converting the seismic data to depth were accurate enough to predict the depth of target horizons to within a few meters. This was confirmed by sonic velocity measurements. The direct correlation between the low-density layers and the thick ash layers discussed above was confirmed by bulk density and MS measurements made on the cores.

Another major result of drilling at Site 1245 was the discovery of significant concentrations of higher-order hydrocarbons beneath the BSR. Methane/ethane ( $C_1/C_2$ ) ratios in headspace samples reach values  $<100$  between 130 and 180 mbsf (Fig. F15). When combined with the measured in situ temperature

gradient ( $\sim 0.055^\circ\text{C}/\text{m}$ ) and the observation that the  $C_1/C_2$  anomaly is due entirely to an increase in ethane concentration, the data suggest that thermogenic hydrocarbons are migrating from deeper in the accretionary complex. Dissolved lithium anomalies observed in association with Horizon A support this interpretation. In addition to  $C_2$ , enrichments in  $C_3$  and other higher-order hydrocarbons were also observed. At Site 1245, the minimum in the  $C_1/C_2$  ratio is present at  $\sim 150$  mbsf,  $\sim 30$  m above Horizon A.

## **Summary**

Site 1245 provided confirmation that multiple proxies for in situ hydrate presence (including electrical resistivity measured downhole, core temperatures measured on the catwalk, chloride anomalies measured in interstitial waters, and direct measurements of gas concentration) are generally consistent in predicting the distribution and concentration of gas hydrates in the subsurface. Additional analysis is needed to more precisely understand and calibrate these different proxies. Drilling at this site also demonstrated that seismic Horizon A results from the presence of a pair of low-density ash-bearing sand layers that are likely to be fluid conduits. Shipboard data provide evidence for migration of higher hydrocarbons beneath the GHSZ, although determining details of the role of seismic Horizon A in this migration will only be resolved through integration of data from several sites. Finally, this site provided important lithostratigraphic and biostratigraphic data for reconstructing the geologic history of this hydrate-bearing system, including the rate at which the system formed and lithologic controls on fluid migration and hydrate distribution.

## **Site 1246**

Site 1246 (proposed Site HR1b) is located in 848 m of water near the crest of Hydrate Ridge,  $\sim 3$  km north of the southern summit (Fig. F1). The 3-D seismic data show that the BSR is at a depth of  $\sim 114$  mbsf at this site. This site also samples a pair of bright regional seismic reflectors, referred to as Horizons B and B', at depths of  $\sim 60$  and 100 mbsf, respectively. At this site, the temperature and pressure at the seafloor are well within the GHSZ, indicating that gas hydrates can exist within the entire stratigraphic section above the BSR if hydrate-forming gases are available in concentrations that exceed their in situ solubility.

The primary objective at Site 1246 was to sample Horizons B and B' where they are within the GHSZ. By comparing this site to Site 1244, where Horizons B and B' are below the GHSZ, we hope to constrain lithologic and hydrologic explanations for the strong reflectivity of these seismic horizons, obtain insights into the processes that transport fluids into and through the GHSZ, and develop more effective strategies to predict hydrate presence from seismic and other remote sensing data.

## **Operations**

Hole 1246A was drilled to a depth of 180 mbsf without coring to obtain the initial LWD data for this site. In Hole 1246B, we obtained 16 APC cores, sampling to a depth of 136.7 mbsf with 99% recovery. The APCT was run five times; no other special tools were deployed. These cores were sampled for headspace and void gas analyses, chemical analysis of interstitial water (two per core), basic physical property measurements, biostratigraphic analysis, and lithostratigraphic description.



## **Principal Scientific Results**

The precruise 3-D seismic reflection site survey and the LWD data obtained in Hole 1246A provided a roadmap that was used to guide the sampling and analysis strategy at this site. As mentioned above, the seismic data define the link between Sites 1244 and 1246 and suggest approximate depths to Horizons B and B' and the BSR of ~60, 100, and 114 mbsf, respectively. The LWD data were processed and available for interpretation for 3 weeks prior to coring. These logs provided a first look at the probable distribution of hydrate within the GHSZ. Based on the Archie's Law relationships between electrical resistivity and porosity, LWD data suggest that hydrate should be present intermittently between 53 and 109 mbsf (Fig. F13). The LWD data also indicate that Horizon B is characterized by relatively high density and resistivity, as was found at Site 1244. Unlike Site 1244, no prominent low-density anomaly is found associated with Horizon B' at Site 1246.

Use of the IR camera continued both to rapidly identify gas hydrate through the core liner and to investigate the distribution and texture of hydrate in the cores and visualize the process of dissociation. Temperature anomalies in the IR thermal images suggest the intermittent presence of hydrate from ~15 to 117 mbsf (Fig. F13), a somewhat more extensive depth range than is indicated by other hydrate proxies (see discussion of interstitial waters and LWD). In addition, several of the IR thermal anomalies are correlated with changes in the lithologic and physical properties of the sediments and with anomalies in chemistry of the pore waters. These changes are in turn correlated with seismic Horizon B. Whole rounds of core containing particularly strong IR temperature anomalies, and therefore suspected of containing gas hydrate veins or nodules, were recovered from 66.5, 96.6, and 105.0 mbsf and preserved in liquid nitrogen for detailed shore-based studies. A gas hydrate sample recovered from 109.5 mbsf was divided into two pieces; one piece was allowed to dissociate on board for chemical analysis (discussed below), and the other was preserved.

On the basis of visual sediment descriptions, examination of smear slides, and correlation with physical property data (especially MS), the sedimentary sequence can be divided into two primary lithostratigraphic units (Fig. F10). Lithostratigraphic Unit I (from the seafloor to 21.7 mbsf) is a late Pleistocene–Holocene unit characterized by dark greenish gray diatom and nannofossil-bearing hemipelagic clay. Lithostratigraphic Unit II, which extends to the base of the Hole 1246B, is defined by the onset of graded silt and sand layers, which represents a series of turbidites of varying thicknesses bounded by erosional contacts and separated by periods of bioturbated hemipelagic sedimentation. Layers composed of >50% sand are found at 62, 71, and 136 mbsf, respectively. The sandy layer at 62 mbsf (found in Core 204-1246B-8H) can be correlated with the base of seismic Horizon B. (Note that the thickness and base of this layer are not defined because whole rounds were taken for microbiology and interstitial water analyses prior to core description). The overlying graded sequence is ~2 m thick and gray colored, in sharp contrast to most of the sediment cored during this leg. The gray color results from a high percentage of quartz grains. This zone contains fewer biogenic components than adjacent strata, suggesting rapid deposition. A similar sequence is found at 56 mbsf in Core 204-1246B-7H, although the base of this upper turbidite sequence contains less sand.

Detailed analysis of physical property data reveals that the two turbidite sequences that comprise Horizon B are characterized by high density and high MS anomalies and that each layer is ~2.5 m thick (Fig. F17). Preliminary synthetic seismograms, calculated based on the density log, confirm that the resulting double-peaked density anomaly extending from 54 to 67 mbsf explains the complicated waveform of seismic Horizon B at this site. The relatively high density probably results from the grain size and packing of the sediments. The source of the high MS has not yet been identified. A thin (<50 cm

thick) high-resistivity anomaly also appears near the base of each of these turbidites, suggesting the presence of gas hydrate. Low temperatures measured on the catwalk with the IR camera are additional indirect indicators for the presence of gas hydrate in the lowermost coarse-grained portion of each turbidite sequence. A sample thought to contain hydrate was recovered from the base of the lower turbidite (Sample 204-1246B-8H-4, 25–30 cm) and was preserved in liquid nitrogen for postcruise analysis. Samples of this coarse-grained layer were also taken for interstitial water and microbiology studies.

The correlation between physical properties, lithology, and seismic Horizon B' at Site 1246, where it is present a few meters above the BSR, is not clear. A thin (<1 cm thick) volcanic ash-rich layer is observed at 96 cm depth in Section 204-1246B-11H-4, 96 cm (~95 mbsf). Strong, narrow (<1 m), high-resistivity, and thermal anomalies indicative of the presence of gas hydrate are observed at 96–97 mbsf in the LWD and IR data, respectively. A sample thought to contain hydrate was recovered in Core 204-1246B-11H-5 at this depth. Recovery in Core 204-1246B-11H was 80%, and the primary lithologic source of Horizon B' may not have been recovered. Shore-based studies are planned to determine the age and provenance of this ash and to compare it to the ash recovered from Site 1244. The ash data will complement the biostratigraphic ages, which suggest an age of ~0.3 Ma at Horizon B'. Seismic modeling will also provide constraints on the nature of fluids in this horizon. At Site 1244, where Horizon B' is found at 216 mbsf (well below the GHSZ), it is associated with a 60-cm-thick layer that is rich in detrital shards of volcanic glass and corresponds to a distinctive low-density anomaly in the LWD and shipboard physical property data. We will test the model that Horizon B' contains free gas at Site 1244 and that the disappearance of the density anomaly at Site 1246 results from incorporation of free gas into gas hydrate.

Geochemical analyses of interstitial waters made during Leg 204 revealed variations in the concentration of several different chemical species with depth that correlate with the GHSZ. At Site 1246, the most direct correlation is based on chloride concentrations, which show a pattern similar to those observed at most other sites, with the exception of those at the southern summit of Hydrate Ridge (Fig. F14). From the seafloor to ~40 mbsf, the chloride concentrations is similar to that of seawater, suggesting that no hydrate is present. Between 40 mbsf and the BSR at ~114 mbsf, there are numerous low-chloride spikes that likely reflect the dilution of pore water by water from dissociated hydrate. The lowest chloride value at this site (~430 mM) is from a sample that fortuitously coincided with the coarse-grained basal zone of the Horizon B turbidite discussed above. Assuming that an in situ no hydrate background concentration of chloride (as was estimated for Site 1244), the amplitude of this chloride anomaly suggests that 23% of the pore space in this layer is filled by hydrate. Ba, Li, and Na are depleted in this interval, and Ca, Mg, and Sr are depleted in the overlying sample located ~3 m higher in the section. The correlation of interstitial water chemistry with specific horizons defined by lithologic and physical properties suggests that modeling of these chemical data may provide constraints on the origin, evolution, and flow rate of fluids that transport methane into and through the GHSZ.

Analyses of the organic chemistry of gases at Site 1246 indicate that processes here are similar to those at Site 1244. The ratio of methane to ethane ( $C_1/C_2$ ) shows a steplike decrease at the BSR, which reflects an increase in  $C_2$  beneath the BSR rather than a change in methane concentration. The presence of propane ( $C_3$ ) below the BSR suggests the upward migration of higher hydrocarbons from below, and the absence of  $C_3$  within the GHSZ (with one exception at ~22 mbsf) indicates that gas above solubility in this zone should be in the form of Structure I rather than Structure II hydrate. The apparent fractionation of  $C_2$  into gas hydrate, which was reported at Site 1244, is not apparent here. However, this may be an artifact of sampling because only one hydrate sample was available for gas analysis at Site 1246. Because no PCS runs were made at this site, no in situ gas concentration estimates are possible.

The methane/sulfate boundary at Site 1246 falls between 4 and 7 mbsf but is poorly defined as a result of sparse sampling; it is slightly shallower than at Site 1244, where it is identified at 9 mbsf (Fig. F18). Variations in the depth of the methane/sulfate boundary among Leg 204 sites will be compared to variations in depth to the first occurrence of hydrate as part of a postcruise study.

Five downhole temperature measurements were made at Site 1246 (Fig. F18). The apparent temperature at the seafloor appeared to change abruptly by  $-2^{\circ}\text{C}$  between the first and second runs, suggesting a problem with the instrument. This was confirmed when the probe indicated a temperature of  $-2.53^{\circ}\text{C}$  after being placed in an ice-water bath. The APCT tool that was used showed a short offset of  $-2^{\circ}\text{C}$  between the first and second runs. Correcting for this offset, the data suggest a temperature gradient of  $0.049^{\circ}\text{C}/\text{m}$ , which is lower than the gradient of  $0.057^{\circ}\text{C}/\text{m}$  measured at Sites 1244 and 1251. This temperature gradient predicts that the BSR should be present at 150 mbsf, considerably deeper than the observed depth of  $\sim 114$  mbsf. This observation is consistent with results from other sites near the crest of Hydrate Ridge, whereas sites located away from the crest show much less difference between measured and predicted temperatures at the BSR.

## **Summary**

There are multiple correlations between geological and geophysical parameters and the presence of gas hydrate at Site 1246. The primary preliminary result is that seismic Horizon B is caused by a pair of high-MS, high-density, and low-porosity layers  $\sim 2.5$  m thick and spaced 10 m apart. Sedimentological analysis indicates that each layer is formed by a turbidite sequence with a complicated internal structure indicating deposition, erosion, and redeposition. Electrical resistivity, IR temperature, and geochemical anomalies are associated with the basal coarser-grained layers of each of the two turbidites that constitute Horizon B, indicating that hydrates preferentially form here. Indirect and direct indicators of hydrate were also found associated with Horizon B'. Postcruise work is planned to determine the source of the MS anomaly and to correlate lithologic and physical properties of these horizons between Site 1244 and Site 1246. Additional efforts will be focused on modeling the seismic response of this horizon as it changes from a fluid-rich layer beneath the BSR to a hydrate-bearing layer above it and to constrain the source and evolution of the fluids using the geochemical data.

## **Site 1247**

Site 1247 (proposed Site HR4c) is located in  $\sim 845$  m of water on the western flank of Hydrate Ridge,  $\sim 800$  m northwest of the southern summit and approximately halfway between Site 1245 and the summit (Fig. F1). The 3-D seismic data indicate that the seismic stratigraphic setting is similar to that of Site 1245 (Fig. F5). The BSR is at a depth of  $\sim 121$ – $124$  mbsf at this site. Horizon A is brighter and shallower ( $\sim 160$  mbsf) at Site 1247 than at Site 1245; Horizon Y is also shallower ( $\sim 60$  mbsf) at this site.

A faint negative-polarity reflection  $\sim 40$  m below the BSR is observed in this region. The possibility that this event is a source artifact has not been definitively ruled out. However, the abrupt decrease in the amplitude of Horizon A as it crosses this reflection and approaches the BSR from below suggests that it might be a "second BSR" resulting from the presence of more stable hydrate structures that contain higher-order hydrocarbons, as has been suggested for similar features observed elsewhere.

The primary objective at Site 1247 was to sample sediments and fluids from Horizon A, approximately halfway between Site 1245 and the summit (Site 1249), in order to determine updip variations in the physical and chemical characteristics of this horizon and, thus, understand the role it plays in fluid migration and formation of hydrate on the seafloor at the summit. A second related objective was to

investigate the origin of the second BSR. Although they are only 75 m apart, the two holes drilled at this site sample parts of Horizon A with distinctly different seismic characteristics.

## **Operations**

Hole 1247A was drilled without coring to a depth of 270 mbsf to obtain LWD data for this site. We returned to core Hole 1247B, which was offset from Hole 1247A ~75 m to the east. Hole 1245B was cored to 220 mbsf using the APC and XCB. The APCT was run six times (including a mudline run to obtain seafloor temperature), the DVTP was run twice, and the PCS was run three times in this hole. The HYACINTH, HRC, and FPC devices were not run at this site. Hole 1247B was then logged using the triple combination (triple combo) and Formation MicroScanner (FMS)-sonic tools. After wireline logging, a vertical and an offset VSP covering the interval of 104–214 mbsf was acquired by alternately shooting from the *JOIDES Resolution* and the *Ewing*, which held station ~700 m away. Plans to conduct walk-away VSPs were abandoned when the Schlumberger VSI tool would no longer clamp in the hole.

Samples suspected of containing hydrate based on IR temperature anomalies were recovered from 93 and 113 mbsf and were stored temporarily in liquid nitrogen. However, on later inspection, it was discovered that although the samples showed textures indicative of hydrate dissociation, no hydrate was actually preserved.

## **Principal Scientific Results**

Biostratigraphic observations from the 220 m of core recovered in Hole 1247B indicate that the entire sequence is younger than 1.65 Ma (Fig. F11). Sediments deeper than ~165 mbsf were deposited at a rapid but poorly constrained rate. These strata can be correlated with strata yielding a linear sedimentation rate of 62 cm/k.y. at Site 1245. The interval from ~150 to 165 mbsf, which contains Horizon A, yields a relatively slow sedimentation rate of 4 cm/k.y. based on nannofossils. The overlying sediments were deposited at a rate of 9–22 cm/k.y., similar to what was observed at Site 1245.

Lithostratigraphic analysis indicates that the dominant lithologies are clay with authigenic carbonates and foraminifer-rich interlayers in the upper 0–27 mbsf (lithostratigraphic Unit I). This unit is underlain by diatom-bearing clay and silty clay with frequent sand-rich turbidites containing a few glass-rich layers from 27 to 212.7 mbsf (Unit II). Lithostratigraphic Unit III (60–220 mbsf) is distinguished from Unit II by an increase in turbidites and biogenic components. Included in lithostratigraphic Unit II is seismic Horizon A. Unlike at the other sites where Horizon A was sampled and found to correspond with volcanic ash layers, at Site 1247B a soft-sediment debris flow bounded by turbidites was found. Because the signature of Horizon A in the LWD data from Hole 1247A (located only 75 m from Hole 1247B) is very similar to that observed at Sites 1245, 1248, and 1250, we conclude that the change in amplitude of Horizon A between the two holes at Site 1247 results from a dramatic local change in lithology rather than from processes related to gas hydrates.

As at other sites, the apparent top of the zone where hydrate is present, as indicated by a variety of different proxies, is generally consistent. The onset of high and variable electrical resistivity and of thermal anomalies observed with the IR camera on the catwalk are both at ~45 mbsf (Fig. F13). High-resistivity layers are subhorizontal, indicating accumulation of gas hydrate parallel to bedding, and steeply dipping, indicating that hydrate fills fractures. The onset of low chloride concentration anomalies is at ~55 mbsf (Fig. F14). The onset of in situ methane oversaturation as projected from headspace and PCS measurements is at ~38 mbsf (Fig. F16).

The above proxies are also consistent with similar depths for the base of the GHSZ. The deepest IR thermal anomaly is at 118 mbsf (Fig. F13). The deepest chloride concentration anomaly is at 114 mbsf (Fig. F14). A PCS core, indicating a volume of methane greater than in situ concentration, was taken at 123 mbsf. Seismic velocities from the sonic log and the VSP complement these interpretations by clearly resolving a velocity decrease indicative of the presence of free gas beneath 129–134 mbsf.

The significant concentrations of higher-order hydrocarbons found beneath the BSR at Site 1245 were also observed at Site 1247 (Fig. F15). Here, low values of the methane/ethane ratio ( $C_1/C_2 < 100$ ) persist to a slightly deeper depth than at Site 1245 (~220 mbsf compared with ~180 mbsf at Site 1245). Hole 1247B did not extend deep enough to resolve whether the  $C_1/C_2$  ratio returns to normal at greater depth, as it did at Site 1245.

One of the notable results from this site was identification of a new hydrate proxy that has the potential to provide valuable constraints on the dynamics of hydrate formation. It was found that many samples collected from the depth range in which other proxies indicate the presence of hydrate showed ethane enrichment and propane depletion. This was attributed to fractionation of ethane and exclusion of propane ( $C_3$ ) during the formation of Structure I hydrate. The observed pattern of anomalies, relative to baseline  $C_1/C_2$  and  $C_1/C_3$  concentrations defined by the majority of samples, can be explained by invoking the presence of gas hydrates within those samples that dissociated on recovery.

Another interesting result was that Horizon A shows a low-amplitude chloride concentration low and methane high. Given the expectation that Horizon A should be more permeable where it is characterized by coarse-grained ash-rich layers than where it consists of a clay-rich debris flow, these observations are surprising and have not yet been explained. At this horizon, there is also Li enrichment similar in magnitude to that observed at other sites, supporting the interpretation of a stratigraphic horizon that transports fluids from greater depth.

The depth of the SMI at this site is well constrained by high-resolution samples and is determined to be at 11 mbsf. Assuming that this depth is entirely controlled by AMO, a methane flux of  $2.5 \times 10^{-3}$  mM/cm<sup>2</sup>/yr is inferred, which is ~1.4 times greater than at the Blake Ridge and ~30% less than at Site 1251. However, the assumptions on which this estimate is based may not be valid for the entire interval above the SMI, leading to considerable uncertainty in this estimate.

The in situ temperature measurements in Hole 1247B yielded a very precisely defined slope of 0.0524°C/m (correlation coefficient = 0.999) and did not reveal any sign of a positive temperature anomaly at Horizon A. This observation will be used to place an upper bound on the rate of fluid transport from depth along this horizon that can be compared to rates obtained from the chemical anomalies.

## **Summary**

Site 1245 provided further confirmation that multiple proxies for the presence of in situ hydrate are consistent with direct measurements of gas concentration in predicting the distribution and concentration of gas hydrates in the subsurface. These include electrical resistivity and porosity measured downhole via LWD, core temperatures measured on the catwalk, and chloride anomalies measured in interstitial waters extracted from sediment samples. A new proxy, ethane enrichment and propane depletion, was discovered and holds promise for constraining hydrate dynamics. Results from this site also indicate that lateral changes in the amplitude of Horizon A in the interval between the BSR and a faint second BSR probably result from lithologic changes rather than from the presence of more stable hydrates of higher-order hydrocarbons, as had been speculated, which leaves open the question of the

origin of this second BSR. Finally, the small chloride concentration depletion and methane enhancement associated with Horizon A, which is not observed at Sites 1245, 1248, and 1250, leads to the apparently contradictory conclusion that Horizon A is a more active conduit for deeper fluids where it is composed of a clay-rich debris flow than where it is composed of coarse-grained ash-rich sandy silt.

### **Site 1248**

Site 1248 (proposed Site HR6) was drilled in a 832 depth of water, ~300 m northwest of the southern Hydrate Ridge summit (Fig. F1). This site is located in the middle of a small (~150 m diameter) high-reflectivity spot on the seafloor imaged by a deep-towed side-scan sonar survey (Fig. F7). The small spot is located 300 m north of a larger circular high-reflectivity patch around the Pinnacle, a well-known active carbonate chemoherm. These are the only two locations on southern Hydrate Ridge where high backscatter reflectivity is observed and is interpreted as seafloor manifestations of fluid venting. Television-sled surveys revealed some evidence for the presence of scattered authigenic carbonate fragments within the small high-reflectivity patch, which might be responsible for the higher backscatter signal observed in the side-scan sonar data. The 3-D seismic data show attenuation of the underlying stratigraphic reflectivity, similar to what is observed beneath the Pinnacle (Fig. F7). Both areas of high backscatter overlie the intersection of seismic Horizon A and the BSR.

The principal objectives at Site 1248 were to (1) investigate whether the sediments below the high-reflectivity seafloor spot contain evidence of active fluid advection and (2) if these fluids are supplied by Horizon A.

### **Operations**

Three holes were drilled at Site 1248. LWD measurements were made in Hole 1248A down to 194 mbsf. Hole 1248B was abandoned at 17 mbsf after three cores. Coring disturbance because of massive near-seafloor gas hydrate presence and a shattered liner during retrieval of Core 204-1248B-3H resulted in poor core recovery (44%). Of the 17 cores from Hole 1248C, 5 XCB cores were drilled to 48 mbsf, followed by 11 APC cores and 1 XCB core to 149 mbsf. After poor core recovery (23%) in Cores 204-128C-1X through 5X, recovery increased to 90%. Temperature measurements were made using one DVTP (at 19 mbsf), three APCT (at 26, 86, and 105 mbsf), and two DVTPP (at 105 mbsf and at the bottom of the hole at 149 mbsf) runs.

### **Principal Scientific Results**

Three lithostratigraphic units were recognized at Site 1248. The uppermost sediments that comprise Units I and II (Holocene–late Pleistocene age) are characterized by dark greenish gray diatom-bearing clay and silty clay and extend from the seafloor to 39 mbsf. These fine-grained lithologies are commonly structureless except for sulfide mottles. Lithostratigraphic Unit III (39–149 mbsf), of middle–early Pleistocene age, is dominated by homogenous silty clays with varying amounts of biogenic components. Sand- and silt-sized turbidites are intercalated as minor lithologies throughout this unit.

High concentrations of beige to white volcanic glass shards were observed in the tail of a few turbidites near 130 mbsf in Core 204-1248C-14H (Fig. F9). These glass-rich layers are the lithologic signature of seismic Horizon A, which appears in the LWD data as a 2-m-thick interval characterized by high resistivity and low density values within the depth interval from 126 to 128 mbsf. Physical property measurements on discrete samples of the cores from Site 1248 confirm the low-density character of Horizon A sediments,

which is interpreted to be a result of the reduced grain density of the ash. The presence of volcanic ash in Horizon A reduces the grain density because amorphous silica particles in the ash have distinctly lower grain densities than other sedimentary components like quartz, feldspar, and clay minerals. Sediments from the interval of Horizon A do not show higher porosity values than the surrounding sediments. The distinctly larger grain size of the ash-rich sediments, however, implies a different packing structure and possibly higher permeability in these intervals, supporting the idea that Horizon A is a potential fluid migration conduit.

Organic geochemistry measurements on gases from Site 1248 reveal high methane contents throughout. In addition to the high methane levels, there is a surprising variation in ethane content with depth.  $C_1/C_2$  is  $< 1,000$  near the seafloor, increasing to 10,000 near the base of the GHSZ, then decreasing sharply below the BSR. In addition to ethane, propane ( $C_3$ ) is present in relatively high concentrations in the upper 120 mbsf and is even more abundant in headspace gas below that depth. The gas analyses at Site 1248 reflect the complex mixing of gases from two hydrocarbon sources (Fig. F15). Mixed microbial and thermogenic gases are present in the uppermost 40 mbsf followed downhole by an intermediate interval (40–100 mbsf) dominated by microbial gas. Mixed microbial and thermogenic gas is also present in the deepest sediments at Site 1248 (below 100 mbsf), with thermogenic gas possibly being injected at Horizon A at ~130 mbsf. The data, thus, suggest rapid advection of deeper gas to the seafloor, bypassing the lower part of the GHSZ.

Analyses of gases from dissociated hydrate samples collected from the shallow zone above 40 mbsf showed that, even though methane occupies most of the water cages of the hydrate structure, higher-order hydrocarbons are also present. Gas hydrates at Site 1248 are probably primarily Structure I hydrate that incorporates ethane molecules within their cage structure. However, in Sample 204-1248C-2H-2, 0–10 cm (7.37 mbsf), a higher concentration of propane than ethane suggests that Structure II hydrate is present. Although thermogenic Structure II gas hydrates are common in petroleum provinces such as the Gulf of Mexico and the Caspian Sea (Sassen et al., 2001; Ginsburg and Soloviev, 1998), this hydrate type was not known to be at Hydrate Ridge prior to Leg 204.

Interstitial water geochemistry results clearly show the influence of gas hydrate formation at Site 1248 (Fig. F14). Based on the chloride distribution in the pore water, the presence of hydrate is suggested from the seafloor to the BSR at 115 mbsf. The data indicate 25% gas hydrate content in the pore space of the uppermost 20 mbsf, whereas LDW resistivity data indicate up to 50% occupancy by gas hydrates. Below 20 mbsf, gas hydrate content calculated from chloride anomalies ranges from 2% to 5% pore volume saturation. This pattern of chloride distribution is well documented by direct gas hydrate sampling and by the hydrate-related fabrics observed at this site by the sedimentologists. Soupy and mousselike textures are predominantly present in silty clay and diatom-bearing silty clay after dissociation of hydrates. These were particularly common in the uppermost 20 mbsf. At these depths, more massive gas hydrate samples were recovered; in contrast, farther downcore, small nuggets and thin veins of hydrate were sampled. The samples were identified by thermal IR data imaging of cores on the catwalk using a hand held IR camera. Postacquisition processing of the IR data shows a good correlation with the pore volume saturation derived by LDW resistivity logs, the chloride pore water data, and the sedimentological observations of the presence of dissociated hydrate layers.

High advective flow rates in the uppermost 20 mbsf of the sediments drilled at Site 1248 are indicated by several findings. Sulfate concentrations were near zero even in the shallowest pore water sample, implying a high methane flux from below that feeds microbial AMO. By consuming the near-seafloor sulfate, a consortium of bacteria and Archaea is responsible for AMO close to the seafloor, during which millimolar quantities of dissolved sulfide are created. High sulfide concentrations were found within the

the uppermost core. In addition, authigenic carbonates that were described in the cores are probably caused by higher dissolved carbon dioxide production, as evidenced in high alkalinity values.

Temperature measurements from downhole tools (three APCT, one DVTP, and two DVTPP runs) were used to calculate a temperature gradient of 0.038°C/m, considerably lower than expected. However, if two outlier measurements are excluded, the gradient is 0.055°C/m, identical to the gradient determined from nine measurements at Site 1245. This temperature gradient predicts the base of the GHSZ at 130 mbsf, assuming methane and standard mean seawater for the calculation. This is 15 m deeper than that indicated by the seismic and LWD data and is consistent with a general pattern of greater mismatch between measured in situ temperature and BSR depth near the summit of Hydrate Ridge, the cause of which has not yet been determined.

### **Summary**

Gas hydrate is present throughout the sediment column from the seafloor to the BSR at Site 1248, as documented by IR imaging, LWD data, chloride anomalies in the pore water, analyses of sedimentary fabric, and direct sampling of gas hydrates in a couple of intervals. The Holocene–Pleistocene sediments drilled here indicate strong advective fluid flow near the summit of southern Hydrate Ridge. There is abundant hydrate in near-surface sediments and no sulfate in the shallowest interstitial water samples collected at Site 1248, clearly indicating active flow of methane-bearing fluids. Authigenic carbonate formation is present close to the seafloor, probably induced by AMO. The presence of authigenic carbonate as well as gas hydrate probably causes the high reflectivity that was mapped during the deep-towed side-scan sonar survey of the seafloor. Advective flow is also indicated by the shallow presence of thermogenic hydrocarbons mixed with microbial gases. Gases obtained from dissociation of a shallow gas hydrate sample revealed a higher concentration of propane than ethane ( $C_3 > C_2$ ) in addition to methane. Such a gas composition should form Structure II hydrate, although we were not able to confirm this on board. Structure II gas hydrate is well known from petroleum basins like the Gulf of Mexico (Sassen et al., 2001), although this is the first indication of Structure II hydrate along an accretionary margin.

### **Site 1249**

Site 1249 (proposed Site HR4b) was drilled in 778 m of water on the summit of southern Hydrate Ridge (Fig. F1). This area is characterized by massive gas hydrate deposits at the seafloor (Suess et al., 2002). Vigorous streams of bubbles are known to emanate from the seafloor, as documented by submersible observations and high-frequency echo-sounding surveys, which have repeatedly imaged bubble plumes in the water column (Trehu and Bangs, 2000; Heeschen et al., pers. comm., 2002). These observations are interpreted to indicate that some of the methane rising through the sediment column is trapped as hydrate near the seafloor and that some escapes into the water column (Suess et al., 2001).

The seafloor in this area is anomalously reflective (Johnson and Goldfinger, pers. comm., 2002), and the seafloor reflectivity is spatially correlated with subsurface seismic reflectivity that extends to ~30 mbsf (Fig. F7). These geophysical observations have been interpreted to indicate the spatial extent of lenses of massive hydrate intercalated with sediment (Trehu et al., 2002). Seismic data also indicate that the BSR at this site is at ~115 mbsf. However, coring was only permitted to 90 mbsf because of the possibility of trapped gas beneath the BSR at this structural high.

The objectives at Site 1249 were to (1) determine the distribution and concentration of gas hydrate with depth at the southern summit of Hydrate Ridge and to investigate processes that allow methane gas



bubbles to coexist with gas hydrate and pore water within the hydrate stability field and (2) test whether the pattern of chaotic reflectivity accurately predicts the spatial extent of massive hydrate lenses.

## **Operations**

Twelve holes were drilled at Site 1249 (Table T1). LWD measurements were made during drilling in Hole 1249A. Hole 1249B was drilled using the new RAB-8 LWD and coring system, which permits simultaneous acquisition of core and logging data. For this test, we washed down to 30 mbsf before beginning RAB coring operations; eight cores (4.5 m long) were taken with liners followed by 9-m-long cores without liners until we reached the permitted penetration depth of 90 mbsf. Following this test, the 90-m sediment sequence was APC sampled in Holes 1249C through 1249F, with core recoveries of <30% in the uppermost 20 mbsf and increased core recovery (up to 70%) deeper in the holes. Six holes (Holes 1249G–1249L) were APC/XCB cored for a special shore-based “geriatrics” study, in which several means of preserving gas hydrates for future study will be compared. During this effort, 244 m of gas hydrate-bearing sediments were cored with 35% core recovery. The samples were either stored in liquid nitrogen or steel pressure vessels, which were repressurized using methane gas and water.

All pressure coring systems available (PCS, HRC, and FPC) were used at Site 1249 (Tables T2, T3). The ODP PCS was deployed seven times in Hole 1249C (33.5, 63.5, and 88.5 mbsf), in Hole 1249E (9.08 mbsf), and in Hole 1249F (13.5, 58.9, and 71.4 mbsf). The FPC was used in Hole 1249D (8 mbsf), in Hole 1249H (70.4 mbsf), and in Hole 1249G (13.5 mbsf). The HRC was deployed in Holes 1249F and 1249G (8 and 13.5 mbsf, respectively). Temperature measurements were made using the DVTP (30.4 and 90 mbsf) and the APCT (16.5, 24.0, 32.5, 37.5, 39.9, 58.9, 70.4, and 90.0 mbsf).

## **Principal Scientific Results**

Based on visual observations, smear slide analyses, physical property measurements, seismic stratigraphy, and logging data, the sediments at Site 1249 were divided into three lithostratigraphic units. Each of the three units correlates well with lithostratigraphy of other sites on the western flank of Hydrate Ridge (Fig. F10). Because of poor core recovery resulting at least, in part, from the presence of massive hydrate, lithostratigraphic Units I and II at Site 1249 were combined into a single unit referred to as Unit I-II. This unit, of Holocene–early Pleistocene age, is composed of clay and silty clay; the biogenic component changes from nannofossil bearing to diatom bearing and diatom rich. Lithostratigraphic Unit III, of early Pleistocene age, has similar lithologies to Unit I-II. The boundary between Unit III and Unit I-II is defined by the presence of visible turbidites in the cores, an increase in grain size, a slight increase in calcareous components, and a slight decrease in biogenic opal. This boundary varies in depth among the holes (from 51 to 59 mbsf) and is coincident with seismic Horizon Y (Figs. F5, F7), which is interpreted to be a regional angular unconformity.

During Leg 204, the highest concentration of gas hydrates was encountered at Site 1249, leading to considerable whole-round sampling. Massive gas hydrate pieces were recovered in the uppermost two cores. Layers of apparently pure gas hydrate up to several centimeters thick were interbedded with soft sediment. Temperature anomaly profiles from the catwalk-track IR camera support this generalized model for gas hydrate distribution. Downhole gas hydrate presence can also be inferred from LWD resistivity data, and the Archie’s Law relationship between resistivity and porosity implies gas hydrate saturations in the pore space at Site 1249 that range from 10% to 92% of the pore space.

As a result of dissociation of gas hydrate during core recovery, cores were highly disturbed and most of the original gas hydrate fabric was probably not preserved. Soupy and mouselike textures, probably

related to gas hydrate presence, were commonly observed. Soupy textures are thought to result from the dissociation of massive gas hydrate, a process that releases a considerable amount of water. Mousseliike textures result from the dissociation of disseminated gas hydrates in fine-grained sediments.

Pore fluids recovered from the upper 20 mbsf show pronounced enrichment in dissolved chloride concentration. The highest chloride concentration measured is 1368 mM in a sample collected from the working half of the core. This sample was selected because it showed a dry-looking coherent fabric and is, therefore, thought to represent the in situ pore fluid with minimal overprint from addition of water from hydrate dissociation during recovery. The observed enrichment in dissolved chloride is only possible in a system in which the rate of gas hydrate formation exceeds the rate at which excess salts can be removed by diffusion and/or advection. The presence of brines in the upper 20 mbsf is also reflected by the concentration of other dissolved species such as  $\text{Na}^+$ ,  $\text{K}^+$ ,  $\text{Ba}^{2+}$ ,  $\text{Sr}^{2+}$ , and  $\text{Mg}^{2+}$  because these ions are excluded from the hydrate structure and enriched in the residual pore water. Superimposed on the dissolved ion enrichment resulting from brine formation, the interstitial chemistry water also reflects the effect of rapid advection of deeply sourced fluids and diagenetic processes occurring in near-surface sediments. Below 20 mbsf, small negative chloride anomalies have been attributed to hydrate dissociation during core recovery.

In comparison to other sites, headspace samples at Site 1249 showed extremely high methane contents consistent with the presence of gas hydrate in the headspace samples. Ethane and propane are also present in high concentrations, indicating migration of thermogenic hydrocarbons. Gases from decomposed hydrate samples show that some of the gas hydrates contain propane and butane, suggesting the presence of Structure II hydrate.

In order to determine in situ methane concentrations, PCS cores were successfully obtained at 14, 34, and 72 mbsf (Fig. F16). The degassing experiments document methane concentrations that range from 200 to 6000 mM, methane concentrations above saturation at in situ temperature and pressure conditions.

One of the highlights of Site 1249 was the successful recovery of gas hydrate at in situ pressure using the new HYACINTH pressure sampling tools. HRC and FPC cores from 14 mbsf both contained high concentrations of gas hydrate. Gamma density logs show a spectacular interlayering of sediments, with some layers having density slightly lower than  $1 \text{ g/cm}^3$ . Since pure methane hydrate has a density of  $\sim 0.92 \text{ g/cm}^3$ , we interpret these low-density layers to be relatively pure hydrate layers. In addition, a low-density spike ( $0.75 \text{ g/cm}^3$ ) in a 8-cm-thick gas hydrate layer reveals the presence of free gas within a massive gas hydrate layer. A second indicator of free gas came from the HRC core. A small explosion pushed gas hydrate and sediment interlayers out of the liner from two intervals while the core was being transferred from the pressure vessel to liquid nitrogen. This sudden gas release can only be explained by the expansion of small volumes of free gas that existed in situ within the gas hydrate layer.

Downhole temperatures derived from the APCT define a temperature gradient of  $0.047^\circ\text{--}0.051^\circ\text{C/m}$  and predict a depth to the base of the GHSZ that is 20 m deeper than the BSR. The data at this site show more scatter than is observed at other sites, where a comparable number of measurements were made. Some possible explanations for this scatter are that thermal conductivities measured on core samples are not representative of in situ thermal conductivity when large concentrations of hydrate are present or that dissociation of hydrate resulting from frictional heating when the temperature probe is inserted affects the measurements. This will be investigated further as part of shore-based recalibration and reanalysis of the downhole temperature data.

## **Summary**

Holocene–early Pleistocene sediments of lithostratigraphic Units I-II and II at Site 1249 are well correlated with other sites along the western flank of southern Hydrate Ridge. Site 1249 was cored to a depth of 90 mbsf; thus, this entire sequence lies within the GHSZ, and large quantities of gas hydrates were sampled. Core recovery at this site was limited because of the presence of massive gas hydrate close to the seafloor. Rapid formation of massive hydrates in the uppermost 20 mbsf at this site induces a brine formation, with chloride values in the interstitial water of up to 1368 mM. This is the greatest chloride enrichment as a result of gas hydrate reported to date. Degassing of the PCS from Core 204-1249F-4P revealed 95 L of gas, which is the largest volume of gas ever measured with the PCS. At this site, we obtained the first density measurements from gas hydrates under in situ conditions using the HYACINTH pressure coring and laboratory transfer systems. One HYACINTH core showed direct evidence for free gas within gas hydrate layers at 13 mbsf.

## **Site 1250**

Site 1250 (proposed Site HR4a) was drilled in 792 m of water, ~100 m west of the southern summit of Hydrate Ridge and ~100 m east of the Pinnacle (Fig. F1). On southern Hydrate Ridge, the Pinnacle is the only carbonate mound, whereas at northern Hydrate Ridge several major chemoherm are known. The Pinnacle has near-vertical flanks rising ~40 m above the seafloor and a diameter of ~150 m. The carbon source for formation of the Pinnacle is known to be biogenic methane from the very low  $\delta^{13}\text{C}$  values (Teichert et al., in press).  $^{230}\text{Th}/^{234}\text{U}$  data indicate that the Pinnacle formed during the last 12 k.y. (Teichert et al., in press). It is located in the middle of a high-reflectivity patch (mapped by a deep-towed side-scan sonar survey) (Johnson and Goldfinger, pers. comm., 2002), which might be created by scattered carbonates close to the seafloor and/or the presence of shallow gas hydrates. Site 1250 lies close to the eastern rim of the high-reflectivity patch (Fig. F7). The precruise 3-D seismic reflection survey data show that seismic Horizon A (~150 mbsf at Site 1250) meets the BSR (~114 mbsf at Site 1250) just below the Pinnacle (Fig. F7).

The primary objective at Site 1250 was to sample the sediments, fluids, gases, and gas hydrates under the high backscatter seafloor flanking the Pinnacle. The sediments at Site 1250 were expected to be strongly affected by the upward fluid migration that has resulted in the formation of the Pinnacle chemoherm. In this context, understanding the role of Horizon A as a conduit for fluid flow and its interaction with the BSR was of special interest.

## **Operations**

Five holes were drilled at Site 1250. Recording of the LWD RAB tool failed during the first run in Hole 1250A because of depleted batteries; therefore, the LDW operation was repeated in Hole 1250B, which was drilled to 180 mbsf. Holes 1250C and 1250D were APC/XCB cored down to 145 mbsf. At Holes 1250C and 1250D 19 cores were recovered, with average recovery of 82% of the total penetration (Table T1). Two cores were recovered at Hole 1250E, which was dedicated to biogeochemical sampling, with 92% core recovery. Because of relatively high levels of higher-order hydrocarbons encountered near Horizon A at Site 1248, we decided not to penetrate Horizon A until a better understanding of possible hazards associated with this horizon had been obtained from drilling through it further downdip. After coring through Horizon A at Sites 1245 and 1247, we returned to Site 1250 to APC/XCB core Hole 1250F from 100 to 180 mbsf.

The PCS was deployed two times in Hole 1250C (71 and 130 mbsf), three times in Hole 1250D (35, 103, and 135 mbsf), and three times in Hole 1250F (119, 130, and 132 mbsf). HYACINTH autoclave pressure coring tools were deployed in Hole 1250C (FPC; 137.5 mbsf) and Hole 1250D (HRC; 134.2 mbsf). Special tools were used for temperature measurements in Hole 1250C, including five APCT runs at 33, 52, 71, 82.5, and 92 mbsf and two DVTP runs. Temperature measurements in Hole 1250D included four APCT runs at 35, 46.5, 65.5, and 103.5 mbsf and two DVTP runs. Wireline logging was performed in Hole 1250F using separate runs of the triple combo tool (Temperature/Acceleration/Pressure [TAP] tool/Dual Induction Tool [DIT]/Hostile Environment Litho-Density Tool [HLDT]/Accelerator Porosity Sonde [APS]/Hostile Environment Gamma Ray Sonde [HNGS]/QSST) and the FMS-sonic tool string (FMS/Dipole Sonic Imager [DSI]/Scintillation Gamma Ray Tool [SGT]) down to 180 mbsf. Vertical and offset VSPs were acquired with the *JOIDES Resolution* and the *Ewing* (located at an offset of ~700 m) alternating shots. This was followed by walk-away VSPs shot by the *Ewing* to downhole seismometers clamped at 91, 138, and 172 mbsf.

### **Principal Scientific Results**

On the basis of visual sediment descriptions, physical property measurements, LWD data, and seismic correlation, the sedimentary sequence at Site 1250 was divided into three lithostratigraphic units. Lithostratigraphic Unit I, Holocene–late Pleistocene in age, extends from the seafloor to 9.5 mbsf and is mainly composed of dark greenish gray clay or silty clay, which is generally diatom bearing or diatom rich. Lithostratigraphic Unit II (9.5–14 mbsf), of late Pleistocene age, is principally composed of lithologies similar to those in Unit I but intercalated with thin silt and fine sand layers not found in Unit I. Based on their appearance, these multiple layers of coarser grain size are clearly single events that were deposited rapidly from turbidity currents. Lithostratigraphic Unit III (14–181 mbsf) consists of silty clay that is nannofossil rich or diatom rich, with an age range of late–early Pleistocene.

The boundary between lithostratigraphic Units II and III is correlated with Horizon Y, a seismic reflector that corresponds to a regional stratigraphic unconformity. This boundary is well defined by a 6-m-thick sequence of coarse-grained high-frequency thin turbidite layers, which includes individual sand layers up to 20 cm thick. LWD recorded a high-density peak around seismic Horizon Y, which was confirmed by shipboard physical property measurements of core samples. In addition, shipboard multisensor track (MST) data reveal a large positive excursion of MS caused by a higher content of magnetic minerals within the sand layers at the boundary between lithostratigraphic Units II and III.

Lithostratigraphic Unit III at Site 1250 is divided in two subunits. Subunit IIIA includes several mass-wasting deposits, of which a debris-flow layer between 86.5 and 100 mbsf is the most pronounced example. This deposit is characterized by the presence of mud clasts up to 5 cm in diameter, similar to those observed at other sites (Fig. F9) and several soft sediment deformation features. Subunit IIIB has a distinctly higher abundance of calcareous nannofossils and foraminifers than Subunit IIIA. The boundary between the stratigraphic Subunits IIIA and IIIB is marked by several light-colored ash-rich layers that are composed of volcanic glass–rich silt to silty volcanic ash, typically a few centimeters thick. This ash-rich interval is well defined in the LWD data by a low-density anomaly and corresponds to the regional seismic reflector known as Horizon A. Physical property measurements on discrete samples at Site 1250 revealed low grain densities in this depth interval, which are partly explained by the low grain density of the amorphous silicate components of the ash. Free gas in this interval probably also contributes to the low densities and high resistivities recorded in the LDW data and to the low seismic velocities recorded by the sonic logs and VSPs.

IR imaging of the cores on the catwalk using a hand held camera enabled us to identify 20 whole-round samples likely to contain gas hydrates. The hydrate samples show a wide range of morphologies, ranging from massive to nodular, and are often embedded in soupy sediments, which are interpreted to result from decomposition of disseminated hydrate and fluidization of the sediment by hydrate water.

In addition, IR imaging with the track-mounted camera revealed 40 temperature anomalies between 14 and 109 mbsf in Hole 1250C and 57 anomalies between 6 and 113 mbsf in Hole 1250D. The depth range of the cold-temperature anomalies correlates well with the depth distribution of moussey and soupy textures observed by the sedimentologists during core description. The lowermost gas hydrate piece was sampled in Hole 1250F at 100.23 mbsf, which is slightly above the base of the GHSZ at 114 mbsf as defined in the *P*-wave sonic log.

Chloride concentrations in the pore water at Site 1250 document the different geochemical processes linked to the presence of gas hydrates. As observed at Site 1249, an enrichment in dissolved chloride in the upper 20–30 mbsf at Site 1250 shows the effect of rapid and recent gas hydrate formation. Below 20–30 mbsf, the chloride shows a gently sloping baseline toward fresher chloride values. Using this baseline curve, the negative chloride anomalies were used to calculate the amount of gas hydrate responsible for the dilution of each sample. The peak amounts are up to 15% gas hydrate filling of the available pore space with average values ranging from 0% to 6%.

Interstitial water chemistry documents upward fluid advection and near-surface diagenetic processes. Sulfate is depleted even in the shallowest sample because of the upward methane flux and methane oxidation. Alkalinity is anomalously high in the upper tens of meters, reflecting fluid advection. Authigenic carbonate formation is documented by very low Ca concentration in the pore fluids and discrete carbonate samples close to the seafloor. Interstitial water chemistry also documents migration of fluids from a deep source. A downhole linear increase in lithium concentration with depth is believed to reflect the diagenetic remobilization of lithium at depth in the accretionary wedge where the temperature exceeds 80° C. Superimposed on this downhole lithium increase there is a peak in the pore fluid concentration around seismic reflector Horizon A, indicating focused fluid transport along this high-permeability pathway.

Gas samples from Site 1250 show high methane content throughout the sediment sequence, and there is no decrease in the in the shallow samples. This is in agreement with the lack of sulfate in the pore water and the inferred high advection rates. Void gas samples show that the ethane content is relatively high. The observed enrichment of higher hydrocarbons (C<sub>3</sub>–C<sub>5</sub>) close to the seafloor indicates lateral migration of wet gas hydrocarbons that must have originally been derived from a deep source. A distinct increase in ethane observed near the BSR could be a result of release of ethane from decomposed gas hydrate. An increase in propane and *n*-butane probably reflects migration of hydrocarbons from deeper depths.

In order to obtain in situ gas concentrations, the PCS was deployed successfully five times. Three PCS deployments above the BSR show concentrations clearly above methane saturation, which predicts gas hydrate concentrations of 0.6%–2.2% within the pore volume of the cores. A second sample, from Core 204-1250D-18P, collected ~24 m below the BSR, indicates a gas concentration below saturation at in situ conditions.

Nine APC temperature measurements were made at this site, and they yielded a temperature gradient of 0.049°C/m, which is lower than expected and predicts the base of the GHSZ at 138 mbsf, assuming methane and standard mean seawater for the calculation. This is 26 m deeper than the level of the GHSZ indicated by the seismic and LWD data and is consistent with a general pattern of greater mismatch between measured in situ temperature and BSR depth near the summit of Hydrate Ridge. The cause of this discrepancy is yet not known.

## **Summary**

At Site 1250, hemipelagic fine-grained sediments interbedded with turbidites are Quaternary in age (younger than 1.6 Ma) and contain gas hydrates in varying amounts. Positive chloride anomalies in the pore water in the upper 20–30 mbsf reveal rapid and active formation of gas hydrates during recent times, consistent with LWD resistivity data and direct sampling. High methane concentration, no sulfate, high alkalinity, and carbonate diagenesis in the uppermost sediments document high advection rates of fluid migration, similar to what was observed at the other seep-related sites (Sites 1248 and 1249). Below 30 mbsf, chloride anomalies in interstitial water samples and direct measurement of in situ gas concentrations using the PCS indicates that gas hydrates occupy <1% to a few percent of the pore space. The presence of free gas just below the BSR is documented by the concentrations of methane well above in situ solubility found in a PCS core from below the BSR and from *P*-wave data obtained by sonic logs and VSPs.

## **Site 1251**

Site 1251 (proposed Site HR2alt) was drilled in a water depth of 1216 m, ~5.5 km east of the southern summit of Hydrate Ridge (Fig. F1). The site is located in a slope basin where well-stratified sediments were apparently deposited at a rapid rate. Seismic data record a history of deposition, tilting, folding, and depositional hiatuses in the basin that is probably related to the evolution of Hydrate Ridge. A strong BSR suggests that the base of the GHSZ is at ~196 mbsf at this site.

The principal objectives at Site 1251 were to (1) determine the source of water and gases forming gas hydrates in a setting that is characterized by rapid deposition of hemipelagic sediments and mass-wasting deposits, in contrast to the uplifted sediments of the accretionary complex; (2) determine the distribution of gas hydrates in relation to the typical lithologic parameters for the basin; (3) test general models for hydrate formation in regions of rapid sediment accumulation that were developed in the Blake Ridge area from results of ODP Leg 164; and (4) provide age constraints on the geological history recorded by seismic stratigraphy.

## **Operations**

Six holes were drilled at Site 1251. In Hole 1251A, LWD measurements were made using a variable, but generally low, rate of penetration (ROP) in the upper 30 mbsf followed by an increased ROP of ~50 m/hr from 30 mbsf to the bottom of the hole (at 380 mbsf). The LWD string included the RAB tool, measurement-while-drilling [MWD], NRT (natural magnetic resonance [NMR]-LWD), and Vision Neutron Density (VDN) tools. Hole 1251B was APC cored (Cores 204-1251B-1H through 24H, including PCS deployments at 105 and 154 mbsf and an FPC deployment at 172 mbsf) with an average core recovery of 80.6% down to 194.6 mbsf, where more lithified sediments significantly reduced the penetration of the bit. Coring continued using the XCB down to 445.1 mbsf (Cores 204-1251B-25X through 53X) with an average recovery of 85.5%. In addition to the XCB coring, the three pressure coring tools (PCS, FPC, and HRC) were used at 291, 330, and 397 mbsf, respectively. Special tools in Hole 1251B included four APCT (37.6, 66.1, 94.6, and 125.1 mbsf) and two DVTTP (156.6 and 293.6 mbsf) runs. Hole 1251C was terminated after two cores. In Hole 1251D, which comprises 30 cores, 3 XCB cores were drilled to 26.9 mbsf followed by 15 APC cores to 173.4 mbsf and 6 XCB cores to 226.5 mbsf. Furthermore, a series of special tools were deployed in Hole 1251D: one APCT (173.4 mbsf), two DVTTP (175.4, and 198.2 mbsf), four PCS (46, 77, 173, and 228 mbsf), one FPC (227 mbsf), and one HRC (230 mbsf). Holes 1251E and

1251F were each cored by APC to 9.5 mbsf for high-density sampling. Hole 1251G was washed to 2.5 mbsf before one APC core was taken for special sampling of turbidite layers. The hole was then washed down to 20 mbsf before an additional PCS (at 21 mbsf) was deployed.

### **Principal Scientific Results**

Based on the major and minor lithologies and additional criteria like sediment fabric, physical properties, microscopic, chemical, and XRD analysis, the hemipelagic strata and turbidite sequences recovered at Site 1251 were divided in three lithostratigraphic units. Lithostratigraphic Unit I, subdivided into three subunits, extends from the seafloor to 130 mbsf and is characterized dominantly by dark greenish gray clay to silty clay ranging from Holocene to Pleistocene age (0--0.3 Ma). The sediments of Subunit IA (0--23 mbsf) are characterized by clay and silty clay, some of which is diatom bearing, interlayered with several coarse-grained turbidites. Subunit IB (23--34 mbsf) is characterized by unsorted pebble-sized mudclasts in a clay matrix and a series of soft-sediment deformation fabrics representing a debris flow unit. This unit can be traced regionally based on its chaotic character in seismic reflection records (Fig. F8) and reaches a maximum thickness of ~70 m in the center of the slope basin. Stratified diatom-bearing silty clays comprise Subunit IC (34--130 mbsf), which shows clear seismic stratification. The base of Subunit IC is defined to correspond to a prominent angular unconformity imaged in the seismic data, although there is no apparent lithologic discontinuity at that boundary.

Hemipelagic clays of middle Pleistocene age, partly enriched in siliceous and calcareous biogenic components, form lithostratigraphic Unit II (130--300 mbsf). Unit III (300--443 mbsf) consists of partly lithified clays that show a downcore transition to claystones. A distinct enrichment of green glauconite grains in a 120-cm-thick interval on top of lithostratigraphic Unit III is probably associated with a major unconformity or period of very low sedimentation rate that lasted from 1.6 to 1.0 Ma, as defined by biostratigraphic data (Fig. F11). Between 320 and 370 mbsf, the sediments contain a higher amount of biogenic opal, which is well documented by smear slide estimates and XRD analyses. Authigenic carbonates of various morphologies and mineralogical compositions as well as glauconite grains are scattered throughout this unit. Biostratigraphic investigations using diatoms and calcareous nannofossils assign these sediments to an early Pleistocene and late Pliocene age. The Pleistocene/Pliocene boundary is present at ~375 mbsf.

Major downcore changes in physical property data are generally in agreement with seismic stratigraphy and lithostratigraphic boundaries. The uppermost sediments of lithostratigraphic Units I and II are characterized by increasing bulk density values that follow a standard compaction curve. A generally increasing trend in bulk densities measured with the MST and in density measurements on discrete samples (MAD) is interrupted by a 50-m-thick sediment sequence between 320 and 370 mbsf, in which the bulk densities drop significantly and porosity values increase. This change in physical properties is caused by higher amounts of biogenic opal-A, an amorphous silica phase having low grain density and high skeleton porosity. MS values at Site 1251 are characterized by generally uniformly low values. Various high-amplitude MS peaks are correlated with either turbidites, enrichments of magnetic minerals resulting from low sedimentation rates, or diagenetic iron sulfide minerals.

Thermal imaging of cores using the IR cameras was used to detect intervals of disseminated gas hydrate between 40 and 200 mbsf. Discrete samples of hydrate were not seen in Hole 1251B, although several cold anomalies were observed. As a result of low recovery of this interval, the BSR was not sampled in Hole 1251B. The IR temperature anomalies observed in Hole 1251B were relatively small ( $\Delta T = \sim 1^{\circ}\text{--}1.5^{\circ}\text{C}$ )

compared to an IR temperature anomaly ( $\Delta T = \sim 6^\circ\text{C}$ ) encountered in Hole 1251D between 190 and 197 mbsf, which corresponds to the interval just above the BSR.

Interstitial water geochemistry at Site 1251 focused on hydrate-related changes in chloride concentration pattern, changes in fluid composition in relation to dewatering of the sediments, and biogeochemical processes within the sediments. As observed at Sites 1244 and 1252 as well as in other accretionary wedges, the profile of dissolved chloride at Site 1251 decreases downcore from present seawater values close to the seafloor. At Site 1251, the chloride decrease in the interstitial water corresponds to an increase in dissolved lithium, revealing a fluid source from deeper sediments of the accretionary complex. The dissolved chloride distribution at Site 1251 shows only one distinct negative anomaly, seen in several samples taken just above the BSR from  $\sim 190$  to 200 mbsf. This is consistent with the IR temperature and visual observations, indicating the presence of disseminated hydrate just above the BSR. Based on the lowest chloride value measured relative to an estimated background concentration, gas hydrate occupies up to 20% of the pore space in this zone. This finding is in contrast to other sites drilled during the leg, where repeated excursions to low chloride concentration values record the presence of gas hydrate over much larger depth intervals above the BSR (Fig. F21). We note that this low chloride anomaly was missed completely in Hole 1215B because of poor recovery of this interval. Special care was taken to sample this interval in Hole 1251C.

As at other sites on Hydrate Ridge, a number of different processes control whether methane reaches levels above saturation within the GHSZ. An important process controlling the methane distribution in the sediments at Site 1251 is methane consumption by AMO using sulfate as an oxidant. Methane flux at the SMI can be estimated from the sulfate and methane concentration gradients. At Site 1251, over half the sulfate being reduced is a result of AMO. Sulfate depletion at the SMI at 4.5 mbsf also leads to high dissolved barium concentrations below the SMI.

Methane concentrations obtained from headspace analyses increased rapidly below the level of sulfate depletion. Nine PCS deployments revealed methane concentrations from 46.4 to 158.4 mM at depths ranging from 20 to 290 mbsf. The methane concentration at 20 mbsf is compatible with the shallower headspace methane estimates and provides the gradient from which the methane flux is calculated. Based on measured methane concentrations slightly above solubility, two PCS deployments within the GHSZ (at 45 and 104 mbsf) show methane concentrations with values above saturation, implying the presence of methane hydrate. Observations below the BSR are ambiguous. A PCS sample from 32 m below the BSR did not show methane concentration above solubility, whereas one from 100 m below the BSR did.

In addition to methane ( $C_1$ ), higher molecular weight hydrocarbons such as ethane ( $C_2$ ), ethylene ( $C_2^=$ ), and propane ( $C_3$ ) traces were also detected throughout the sequence cored at Site 1251. As at Sites 1244 and 1246, the composition of gas samples recovered from both expansion voids in the core liner and headspace measurements show a systematic in decrease in  $C_1/C_2$  ratios below the BSR (Fig. F15). This order of magnitude decrease in the  $C_1/C_2$  ratio is caused by an abrupt increase of ethane rather than by a change in methane concentration. Two possible mechanisms have been considered to explain this observation. In the first mechanism, ethane preferentially stored in hydrates and then released when the ethane-enriched gas hydrates at the base of the GHSZ dissociate in response to subsidence of the slope basin and the resulting upward migration of the GHSZ through the sediment column. In the second mechanism, the GHSZ is a barrier to  $C_2$  migration. Additional analysis of the gas composition in hydrate samples from Leg 204 should permit us to distinguish between these two mechanisms.

Temperature measurements obtained with five APCT and three DVTTPP deployments were used to calculate a linear temperature gradient of  $0.0575^\circ\text{C}/\text{m}$  at Site 1251, which is very similar to temperature



profiles from other sites on Hydrate Ridge. Extrapolating laboratory measurements of gas hydrate stability for pure methane in water of 3.5% salinity, this temperature gradient predicts the base of the GHSZ to be at ~196 mbsf, which is in excellent agreement with the calculated BSR depth of ~196 mbsf determined from 3-D seismic reflection and OBS-derived seismic velocity data.

The recorded LWD data in the basin sediments in Hole 1251A are of high quality even though data were collected at a faster penetration rate than at other sites. There is minimal loss of vertical resolution. Resistivity and density log variations indicate thin-bedded changes in lithologies throughout the hole below 130 mbsf, which most likely reflect the downhole presence of interbedded turbidites that were observed during core description. There is a little direct evidence for the presence of gas hydrate in the LWD data, except for the depth interval from 90 to 110 mbsf and again immediately above the BSR. The Archie's Law relation for estimating gas hydrate saturation from the resistivity log data implies gas hydrate saturation up to 18% in the sediments just above the BSR, in excellent agreement with the estimate based on the maximum chloride anomaly. The resistivity data also indicate the presence of free gas extending for ~100 m below the BSR. Borehole breakouts are well developed below 300 mbsf and indicate an east-west axis of compressive stress.

## **Summary**

Drilling at Site 1251 recovered a sequence of well-stratified hemipelagic sediments of the slope basin adjacent to Hydrate Ridge. Major lithostratigraphic units were characterized and are, in most cases, separated by clearly defined unconformities in the seismic record. Thermal, sedimentological, geophysical, and geochemical proxies for the presence of hydrate, as well as direct sampling, were used to document the presence of gas hydrates in host sediments younger than 500,000 yr old. At this site, significant hydrate accumulations seem to be limited to two intervals, 90–110 mbsf and just above the BSR at 190–200 mbsf. This contrasts with the hydrate distribution at the other sites cored during Leg 204, where hydrate is found throughout most of the hydrate stability zone.

## **Site 1252**

Site 1252 (proposed Site HR5a) was drilled in 1039 m of water, ~4.5 km east of the southern summit of Hydrate Ridge. The site is located on the western flank of a secondary anticline that is located east of the crest of Hydrate Ridge. The sediments in the core of the anticline appear to be continuous with the accretionary complex sediments sampled near the base of Site 1244 (~1.5 km to the west). Although there is an anomalously bright BSR at a depth of ~170 mbsf within the core of the anticline, the BSR disappears abruptly at an apparent stratigraphic boundary within the accretionary complex sequence and does not extend beneath Site 1252. Sediments onlapping the anticline from the west can be correlated with sediments sampled at Site 1251.

The principal objectives at Site 1252 were to (1) sample the sediments in the core of the anticline to determine whether they are compositionally and biostratigraphically similar to those at the base of Site 1244; (2) determine the structure of these sediments in order to constrain the mode of growth of the anticline/diapir; (3) determine whether hydrates are present at a site near a very strong BSR but where no BSR is present; and (4) provide age constraints on the geological history recorded by seismic stratigraphy.

## **Operations**

One hole was drilled at Site 1252, comprising 28 cores (14 APC and 14 XCB) and sampling sediments to a depth of 260 mbsf. The APCT tool, which was deployed six times to measure in situ temperature, was the only special downhole tool used at this site (Tables T2, T3). This is also the only site where we did not acquire LWD. Wireline logging data were acquired, including one run with the triple combo tool string and one run with the FMS-sonic tool string. This was an alternate site and was the last site drilled during Leg 204.

## **Principal Scientific Results**

Drilling at Site 1252 showed evidence for only very limited presence of gas hydrate. Nonetheless, it is a very interesting site in that it showed very clear correlations between lithostratigraphic observations, physical property measurements, and wireline logging results throughout the entire cored sequence. It is the only site to show significant postdepositional carbonate formation beneath the upper tens of meters.

Based on the major and minor lithologies and additional criteria like fabric, physical properties, and microscopic analysis, the sediments recovered at Site 1252 were divided in three lithostratigraphic units. Lithostratigraphic Unit I, subdivided into four subunits, extends from the seafloor to 96.5 mbsf and is dominated by dark greenish gray clay to silty clay ranging in age from 0 to ~0.3 Ma. Subunit IA is characterized by a strong negative density gradient in the MST data, which probably results from the onset of gas exsolution at ~7 mbsf. The lower boundary of Unit I is defined by the same unconformity that was sampled at a depth of 130 mbsf at Site 1251. At both sites, this unconformity is clearly seen in seismic data and is compatible with biostratigraphic data but does not have a striking lithologic signature. At Site 1252, the unconformity is overlain by an apparent debris flow called Subunit ID, the top of which corresponds to a strong anomaly in MS. Subunit ID pinches out just west of Site 1251 and was not sampled there. In contrast, the debris flow that comprises Subunit IB at Site 1251 is not present at Site 1252 (Fig. F8). Subunit IC at both sites is strikingly similar in its lithologic description and its seismic reflection character.

Unit II at Site 1252 is a dark green foraminifer-rich silty clay that is intercalated with lighter-colored fine sand and coarse silt turbidite layers. These thin turbidites result in a nearly continuous zone of high MS. In contrast to Site 1251, where Unit II is ~180 m thick, Unit II at Site 1252 is only ~20 m thick. This is primarily due to the location of this site, where Unit II laps onto the west flank of uplifted accretionary complex sediments. Subunits IB and IC through Unit II are characterized by a normal increase in density and decrease in porosity with depth that is probably caused by sediment compaction.

The boundary between Unit II and Unit III is marked by a 5-m-thick series of glauconite-rich sands, including a 2-cm-thick layer of almost pure glauconite. This is underlain by a layer of authigenic carbonate that required a transition from APC to XCB coring at 125 mbsf. Wireline density, resistivity, and chemical (uranium and potassium) logs all show very high values in a 6-m-thick interval at this depth, consistent with extensive carbonate precipitation forming concretions and cement. The top of Unit III corresponds closely with the top of the uplifted accretionary complex sediments in the core of the anticline/diapir and is referred to as Subunit IIIA (1310–210 mbsf). It is underlain by Subunit IIIB (210–260 mbsf), which is distinguished from Subunit IIIA by an increase in biogenic opal and a decrease in silt. The biostratigraphic age of Unit III is 1.6–>2 Ma.

The density profile of Unit III is unusual. Physical property measurements (MST GRA logs and MAD bulk density) indicate that the density decreases by 0.2 g/cm<sup>3</sup> (from 1.8 to 1.6 g/cm<sup>3</sup>) over a distance of ~25 m below the carbonate-rich zone and is then variable but with an average value of ~1.7 g/cm<sup>3</sup>. No

systematic increase in density is observed until the base of the hole at 260 mbsf. The wireline density logs show similar behavior, with a local increase to nearly 2.0 g/cm<sup>3</sup> in the carbonate layers underlain by a nearly constant density of 1.7 g/cm<sup>3</sup> with occasional thin (~2 m thick) low-density (~1.5 g/cm<sup>3</sup>) excursions. This anomalous density profile, similar to but better defined than what was observed in lower part of the section at Sites 1244 and 1251, suggests that density-driven diapirism may be a mechanism contributing to the tectonic evolution of the accretionary prism.

Thermal imaging of cores using the IR cameras indicated only very limited hydrate presence at Site 1252. Two possible hydrate samples were preserved from depths of 83 mbsf (in Subunit ID) and 99 mbsf (in Unit II). The chloride concentration in the pore water and the C<sub>1</sub>/C<sub>2</sub> ratios in void-space gas samples did not show anomalies indicative of dissociated hydrate, unlike what was observed at other sites (see, for example, discussion of Site 1247). In contrast, Subunit IIIA showed several examples of classic moussey and soupy texture in cores recovered from above the base of the GHSZ. A sample of the soupy sediment was taken for postcruise chloride analysis.

The chloride profile shows a general decrease with depth similar to those observed at Sites 1244 and 1251. This decrease has been attributed to diffusion or slow advection of low chloride concentration pore waters generated by dewatering of aluminosilicates deeper in the accretionary complex. A closer look at the chloride profile suggests segments of different slope that can be roughly correlated with lithologic boundaries, suggesting lithologic control on permeability.

The thermal gradient of 0.059°C/m measured at Site 1252 is similar to the gradients of 0.057° and 0.058°C/m measured at Sites 1251 and 1244, respectively, and predicts the base of gas hydrate stability at 170 mbsf, which is consistent with the estimate of 170 mbsf obtained by lateral projection of the BSR observed in the core of the anticline.

## **Summary**

Site 1252 provided the best sampling of the older (>1.65 Ma) sediments that comprise the uppermost part of the seismically incoherent facies referred to as the accretionary complex. This zone is characterized by a density inversion relative to the base of the overlying slope basins and an anomalous density vs. depth profile. This observation suggests that gravitational instability should be considered as a possible driving force contributing to the evolution of forearc structure here. The data from this site also reinforce previous observations that the accretionary complex is characterized by low chloride concentration interstitial waters and is relatively permeable. Although this site yielded little direct evidence of gas hydrate, sediment textures and limited IR thermal anomalies indicate that some hydrate was present even though no BSR is observed at this site.

## **CONCLUSIONS**

In this section, we summarize some of the general conclusions that emerge from the above discussions of preliminary results at each site. We also point out additional questions that are the focus of ongoing postcruise data integration and modeling efforts.

***Multiple proxies for hydrate presence and concentration are consistent and complementary. They indicate that gas hydrate is present, concentrated in relatively coarse-grained layers, over a broad depth range between the seafloor and the BSR.*** One of the main conclusions to emerge from the shipboard analysis of the data collected during Leg 204 is that gas hydrates are distributed through a broad depth range within the GHSZ. Electrical resistivity anomalies measured downhole with LWD and wireline logging, low-

temperature anomalies measured with IR camera scans immediately after cores came on deck, low chloride concentration measured in interstitial waters, anomalously low  $C_1/C_2$  ratios measured in vacutainer samples, and gas volumes measured from pressure core samples are all proxies for the presence of gas hydrate in the subsurface. All are consistently observed to start at a similar depth at a given site (~30–50 mbsf at sites away from the summit and at the seafloor near the summit). With the exception of local gas concentrations measured in PCS samples that are greater than the predicted solubility, none of these proxies extend below the BSR, which is the seismically predicted base of the gas hydrate stability field. The different proxies thus lead to consistent conclusions about the distribution and concentration of gas hydrate beneath Hydrate Ridge.

The various proxies for the presence of gas hydrate measure different length scales and have different sensitivity to hydrate concentration. Electrical resistivity, seismic velocity and attenuation, and temperature anomalies in recovered cores can be continuously measured on scales of centimeters and indicate that hydrate concentration probably varies considerably on scales of tens of centimeters. These data provide continuous profiles of relative hydrate concentration and indicate that hydrate is distributed over a broad depth range, with concentration controlled primarily by lithology. Exceptions are Site 1251 in the eastern slope basin, where hydrate is concentrated in a 10-m-thick zone just above the BSR, and sites near the summit, where it is concentrated near the seafloor. These geophysical parameters, however, do not give a direct measurement of concentration, although concentration can be estimated through physical models (e.g., through Archie's Law relation in the case of resistivity) (see Collett and Ladd, 2001).

The PCS data give a direct measurement of gas concentration in situ. The concentration of gas hydrate or free gas may be estimated by comparing the in situ gas concentration to the predicted in situ solubility. These measurements, however, are restricted to only a handful at each site because of logistical constraints. The ODP PCS provides measurements of concentration averaged >1 m, whereas the newer HYACE tools demonstrated the potential to provide additional information about the scale length of hydrate distribution and the presence of free gas within the GHSZ.

Chloride concentration measurements provide robust estimates of hydrate concentration if the background chloride concentration profile can be constrained. However, they are still spatially aliased because it is not practical to routinely obtain measurements less than several meters apart. Leg 204 has demonstrated that, except for near the summit where the background chloride concentration cannot be determined because of very rapid hydrate formation (see discussion of Site 1249), background chloride concentration can be well defined. Maximum concentrations are ~20% of pore space. It also demonstrates that it is essential to extend measurements well below the base of the GHSZ because there is a clear freshening of the interstitial waters as a result of diffusion of a low chloride concentration source at depth (probably water derived from dehydration of subducted minerals). Estimates that do not take this into account will overestimate the in situ hydrate concentration.

$C_1/C_2$  ratios have the potential to become a new proxy for hydrate concentration. Leg 204 data suggest preferential incorporation of ethane in the hydrate, which results in a signal that can be detected in routine headspace and vacutainer measurements. Additional analysis of the data from Leg 204 is underway to better calibrate quasicontinuous geophysical data using robust geochemical estimates of in situ hydrate concentration. This will result in greatly improved estimates of the total amount of methane and other hydrocarbon gases sequestered in the gas hydrate system on the Oregon continental margin. The calibrated downhole geophysical results will then be used to calibrate surface and seafloor seismic reflection and refraction data, which will provide tools to more robustly estimate hydrate distribution and concentration elsewhere.

*Horizon A is an ash-rich layer that serves as a fluid pathway transporting methane and other hydrocarbons from the accretionary complex to the summit of Hydrate Ridge.* Determining the origin and significance of a strong seismic reflection (Horizon A), which underlies the BSR and shallows toward the southern summit of Hydrate Ridge, was an important objective of Leg 204. This reflection was crossed at Sites 1245, 1247, 1248, and 1250. In the LWD data, it is characterized by a strong 2- to 4-m-wide double-peaked low-density and low-resistivity anomaly.

Cores at Sites 1245, 1248, and 1250 reveal several coarse-grained layers at this depth. Microscopic analysis of these sediments reveals that the sediment is composed primarily of relatively fresh glass shards indicating volcanic ash. The number and thickness of the ash layers could not be determined precisely because of generally poor recovery of this interval, probably because of high fluid content and possible overpressure. Grain density is low, probably because of vesicles within the glass shards. The age and provenance of the ash will be determined postcruise.

Although the physical properties of Horizon A are remarkably similar from site to site, hydraulic properties determined from chemical analysis of gases and interstitial waters are more complicated. Positive lithium anomalies are clearly associated with this horizon, supporting the interpretation that it is a conduit for fluids coming from greater depth. However, no thermal anomaly is detected, placing an upper limit on flow rate. Relatively high levels of higher hydrocarbons are observed in a 30- to 50-m-thick zone below the BSR at all sites, but the maximum level of higher hydrocarbons does not generally coincide with Horizon A (Fig. F15). A qualitative explanation for these observations is that diffusion away from Horizon A is superimposed on accumulation of hydrocarbons beneath the BSR. Postcruise modeling is needed to quantitatively test this hypothesis.

*Massive hydrate lenses extend to a depth of ~30 mbsf near the summit of South Hydrate Ridge, and hydrate formation here is very rapid.* Prior to Leg 204, it was known that methane bubbles were venting from the southern summit of Hydrate Ridge and that massive hydrate was present at the seafloor; however, the rate of hydrate formation and the depth to which massive hydrate is present were unknown. Seismic reflection data suggested that this zone extends to ~30 mbsf (Trehu et al., 2002) (Fig. F7). Electrical resistivity anomalies recorded in LWD data, however, indicate extremely high resistivities (approximately two orders of magnitude greater than observed at other sites) from 0 to 40 mbsf. The resistivity is higher than at other sites logged during Leg 204 to a depth of ~70 mbsf.

In the upper 10–20 mbsf near the summit at Sites 1249 and 1250, interstitial fluids are high chlorite brines, cores contain pervasive gas hydrate veins and nodules, and pressure core samples indicate the presence of massive hydrate. Moreover, core recovery from this interval was poor, probably because of massive hydrate presence. Below 15–30 mbsf, high-chloride brines give way to the low-chloride anomalies characteristic of dissociation of hydrate relative to background interstitial waters that do not retain the signature of hydrate-driven brine, presumably because of much slower rates of hydrate formation. At these depths, core recovery improved significantly. Both of these observations indicate a change from a shallow zone in which methane is provided through vigorous advection and hydrate forms rapidly to a zone in which methane flux is slower and hydrate formation is slower, perhaps because of limited availability of water. Below ~20–30 mbsf, lenses of massive hydrate containing significant pockets of free gas are not likely, although both hydrate and free gas in disseminated form may be present in relatively large concentration. The cause of the very high resistivity from 30 to 70 mbsf remains poorly understood and is a focus of postcruise research as is estimation of hydrate formation rate from the positive chloride concentration measurements.

*Free gas is trapped in gas hydrates tens of meters beneath the seafloor at the southern summit of Hydrate Ridge.* Gamma density logging of a HYACE RPC core from 14 mbsf at Site 1249 indicated the presence of

several layers of massive hydrate, one of which contained material with very low density indicating the presence of free gas. This is the first direct evidence for free gas in the GHSZ, although the presence of free gas had previously been hypothesized based on observations of gas bubbles emanating from the seafloor (Suess et al., 2001; Torres et al., 2002). The new data provide strong support for the hypothesis that hydrate formation locally uses up all available water, isolating pockets of free gas. Modeling of elastic wave velocities and attenuation should further constrain the presence and distribution of free gas. The presence of free gas shallows within the stability zone has important implications for seafloor stability.

***Lithology is a major factor influencing hydrate concentration.*** Integrated analysis of Horizon B provides an excellent example of the impact of lithology on hydrate distribution (see discussion of Sites 1244 and 1246). Detailed analysis of physical properties and IR thermal anomalies combined with lithologic description demonstrates that gas hydrates are concentrated in the coarse-grained layers in this ash-rich turbidite section.

***Ethane is enriched beneath the BSR.*** All sites show an abrupt decrease in  $C_1/C_2$  at the BSR except for Site 1252 (where there is no BSR). This effect is most evident at Sites 1244 and 1251, where this signal is not obscured by additional effects of Horizon A and results from an increase in  $C_2$  rather than a decrease in  $C_1$ . There are at least two possible mechanisms to explain this observation. In one model, the BSR serves as a barrier to upward flow of ethane. In the other model, ethane is preferentially incorporated into hydrate; dissociation of the hydrate at a later time in response to tectonic uplift recycles ethane into the free-gas zone beneath the hydrate. Relative enrichment of ethane observed in gases from several dissociated hydrate samples support the second mechanism. Discontinuities at the BSR in several other chemical species support the first mechanism. It is possible that both mechanisms operate simultaneously.

***There is less free gas beneath the BSR here than beneath north Hydrate Ridge or the Blake Plateau.*** One of the more surprising results of Leg 146 on north Hydrate Ridge and Leg 164 on the Blake Ridge was the depth to which free gas is present beneath the BSR. Seismic experiments at both of these sites indicated that free gas is present in the sediments for several hundred meters below the BSR (MacKay et al., 1994; Holbrook et al., 1996; Trehu and Flueh, 2001). In contrast, PCS measurements of gas concentration and seismic measurements during Leg 204 indicate that free gas is present beneath the BSR but only in thin layers.

***The accretionary complex is permeable and is a source of fresh water, which must be accounted for when estimating hydrate concentration from chloride concentration anomalies.*** Data acquired during Leg 204 confirm the interpretation that the boundary in the 3-D seismic reflection data between stratified sediments and seismically incoherent material represents an unconformity between slope basin material and older indurated and fractured sediments. In addition, interstitial waters from sites on the eastern flank of Hydrate Ridge (Sites 1244, 1251, and 1252) show a decrease in chloride concentration and an increase in lithium with depth, which indicates that fresh water migrates from deeper in the accretionary complex where it probably originates from dehydration of subducted oceanic crust and sediment. The slope of the mixing curve between seawater and water from this deep source changes at the top of the accretionary complex, implying that the accretionary complex is more permeable than the overlying deformed slope basin and that diffuse vertical migration of fluids through this material is significant. Although this freshening effect has been documented previously from Cascadia (Kastner et al., 1995), implications for estimation of hydrate concentration from salinity has not been fully appreciated. Leg 204 provides a systematic transect across the margin that can be integrated with structural information to constrain depth and volume of dewatering and the mechanism of fluid expulsion.

## REFERENCES

- Arsenault, M.A., Trehu, A.M., Bangs, N., and Nakamura, Y., 2001. P-wave tomography of Hydrate Ridge, Oregon continental margin. *Eos, Trans.*, 82:604. (Abstract).
- Boetius, A., Ravensschlag, K., Schubert, C.J., Rickert, D., Widdel, F., Gieseke, A., Amann, R., Jorgensen, B.B., Witte, U., and Pfannkuche, O., 2000. Microscopic identification of a microbial consortium apparently mediating anaerobic methane oxidation above marine gas hydrate. *Nature*, 407:623–626.
- Bohrmann, G., Greinert, J., Suess, E., and Torres, M., 1998. Authigenic carbonates from the Cascadia Subduction Zone and their relation to gas hydrate stability. *Geology*, 26:647–650.
- Bohrmann, G., Linke, P., Suess, E., Pfannkuche, O., and Scientific Party, 2000. R/V SONNE cruise report, SO143 TECFLUX-I-1999. *GEOMAR Rpt.*, 93.
- Bohrmann, G., Suess, E., Greinert, J., Teichert, B., and Naehr, T., 2002. Gas hydrate carbonates from Hydrate Ridge, Cascadia Convergent Margin: indicators of near-seafloor clathrate deposits. *Fourth Int. Conf. Gas Hydrates*, Yokohama, Japan. 102 – 107.
- Booth, J.S., Winters, W.J., and Dillon, W.P., 1994. Circumstantial evidence of gas hydrate and slope failure associations on the United States Atlantic continental margin. In Sloan, E.D., Happel, J., and Hantow, M.A. (Eds.), *Int. Conf. Nat. Gas Hydrates*, 7:487–489.
- Borowski, W.S., Paull, C.K., and Ussler, W., III, 1996. Marine pore-water sulfate profiles indicate in situ methane flux from underlying gas hydrate. *Geology*, 24:655–658.
- Boudreau, B.P., and Canfield, D.E., 1993. A comparison of closed and open system models for porewater and calcite saturation state. *Geochim. Cosmochim. Acta*, 57:317–334.
- Carson, B., Seke, E., Paskevich, V., and Holmes, M.L., 1994. Fluid expulsion sites on the Cascadia accretionary prism: mapping diagenetic deposits with processed GLORIA imagery. *J. Geophys. Res.*, 99:11959–11969.
- Clague, D., Maher, N., and Paull, C.K., 2001. High-resolution multibeam survey of Hydrate Ridge, offshore Oregon. In Paull, C.K., and Dillon, W.P. (Eds.), *Natural Gas Hydrates: Occurrence, Distribution, and Detection*. Am. Geophys. Union, Geophys. Monogr. Ser., 124:297–306.
- Claypool, G.E., and Kaplan, I.R., 1974. The origin and distribution of methane in marine sediments. In Kaplan, I.R. (Ed.), *Natural Gases in Marine Sediments*: New York (Plenum), 99–139.
- Collett, T.S., and Ladd, J., 2000. Detection of gas hydrate with downhole logs and assessment of gas hydrate concentrations (saturations) and gas volumes on the Blake Ridge with electrical resistivity log data. In Paull, C.K., Matsumoto, R., Wallace, P.J., and Dillon, W.P. (Eds.), *Proc. ODP, Sci. Results*, 164: College Station, TX (Ocean Drilling Program), 179–191.
- Dickens, G.R., Castillo, M.M., and Walker, J.G.C., 1997. A blast of gas in the latest Paleocene: simulating first-order effects of massive dissociation of oceanic methane hydrate. *Geology*, 25:259–262.

- Dickens, G.R., O'Neil, J.R., Rea, D.K., and Owen, R.M., 1995. Dissociation of oceanic methane hydrate as a cause of the carbon isotope excursion at the end of the Paleocene. *Paleoceanography*, 10:965–971.
- Dickens, G.R., 2001. Modeling the global carbon cycle with a gas hydrate capacitor: significance for the latest Paleocene thermal maximum. In Paull, C.K., and Dillon, W.P. (Eds.), *Natural Gas Hydrates: Occurrence, Distribution, and Detection*. Am. Geophys. Union, Geophys. Monogr. Ser., 124:19–40.
- Garrels, R.M., and Perry, E.A., 1974. Cycling of carbon, sulfur, and oxygen through geologic time. In Goldberg, E.D. (Ed.), *The Sea* (Vol. 5): *Marine Chemistry: The Sedimentary Cycle*. New York (Wiley), 569–655.
- Ginsburg, G.D., and Soloviev, V.A., 1998. Submarine gas hydrates. *VNIIOkeangeologia*, St. Petersburg, 216.
- Greinert, J., Bohrmann, G., and Suess, E., 2001. Gas hydrate-associated carbonates and methane-venting at Hydrate Ridge: classification, distribution and origin of authigenic lithologies. In Paull, C.K., and Dillon, W.P. (Eds.), *Natural Gas Hydrates: Occurrence, Distribution, and Detection*. Am. Geophys. Union, Geophys. Monogr. Ser., 124:99–114.
- Holbrook, W.S., Hoskins, H., Wood, W.T., Stephen, R.A., Lizzarralde, D., and the Leg 164 Science Party, 1996. Methane gas-hydrate and free gas on the Blake Ridge from vertical seismic profiling. *Science*, 273:1840–1843.
- Holland, H.D., 1978. *The Chemistry of the Atmosphere and Oceans*. New York (Wiley).
- Housen, B.A., and Musgrave, R.J., 1996. Rock-magnetic signature of gas hydrates in accretionary prism sediments. *Earth Planet. Sci. Lett.*, 139:509–519.
- Hovland, M., Lysne, D. and Whiticar, M., 1995. Gas hydrate and sediment gas composition, Hole 892A. In Carson, B., Westbrook, G.K., Musgrave, R.J., and Suess, E. (Eds.), *Proc. ODP, Sci. Results*, 146 (Pt 1): College Station, TX (Ocean Drilling Program), 151–161.
- Kastner, M., Sample, J.C., Whiticar, M.J., Hovland, M., Cragg, B.A., and Parkes, J.R., 1995. Geochemical evidence for fluid flow and diagenesis at the Cascadia convergent margin. In Carson, B., Westbrook, G.K., Musgrave, R.J., and Suess, E. (Eds.), *Proc. ODP, Sci. Results*, 146 (Pt 1): College Station, TX (Ocean Drilling Program), 375–384.
- Katz, M.E., Pak, D.K., Dickens, G.R., and Miller, K.G., 1999. The source and fate of massive carbon input during the latest Paleocene thermal maximum. *Science*, 286:1531–1533.
- Kennett, J., Hندی, I.L., Behl, 1996. First MASTER Workshop on Gas Hydrates, Ghent, Belgium.
- Kulm, L.D., Suess, E., Moore, J.C., Carson, B., Lewis, B.T., Ritger, S.D., Kadko, D.C., Thornburg, T.M., Embley, R.W., Rugh, W.D., Massoth, G.J., Langseth, M.G., Cochrane, G.R., and Scamman, R.L., 1986. Oregon subduction zone: venting, fauna, and carbonates. *Science*, 231:561–566.
- Kvenvolden, K.A., 1995. A review of the geochemistry of methane in natural gas hydrate. *Org. Geochem.*, 23:997–1008.



- Kvenvolden, K.A., and Lorenson, T.D., 2001. The global occurrence of natural gas hydrate. In Paull, C.K., and Dillon, W.P. (Eds.), *Natural Gas Hydrates: Occurrence, Distribution, and Detection*. Am. Geophys. Union, Geophys. Monogr. Ser., 124:3–18.
- Linke, P., Suess, E., and Scientific Party, 2001. R/V SONNE cruise report, SO148 TECFLUX-II-2000. *GEOMAR Rpt.*, 98.
- MacDonald, I.R., Boland, G.S., Baker, J.S., Brooks, J.M., Kennicutt, M.C., II, and Bidigare, R.R., 1989. Gulf of Mexico hydrocarbon seep communities II. Spatial distribution of seep organisms and hydrocarbons at Bush Hill. *Mar. Biol.*, 101:235–247.
- MacKay, M.E., 1995. Structural variation and landward vergence at the toe of the Oregon accretionary prism. *Tectonics*, 14:1309–1320.
- MacKay, M.E., Moore, G.F., Cochran, G.R., Moore, J.C., and Kulm, L.D., 1992. Landward vergence and oblique structural trends in the Oregon margin accretionary prism: implications and effect on fluid flow. *Earth Planet. Sci. Lett.*, 109:477–491.
- MacKay, M.E., Jarrad, R.D., Westbrook, G.K., Hyndman, R.D., and Shipboard Scientific Party, 1994. ODP Leg 146, Origin of BSRs: geophysical evidence from the Cascadia accretionary prism. *Geology*, 22:459–462.
- Milkov, A.V., and Sassen, R., 2002. Economic geology of offshore gas hydrate accumulations and provinces. *Mar. Petr. Geol.*, 19:1–11.
- Nisbet, E.G., 1990. The end of the ice age. *Can. J. Earth Sci.*, 27:148–157.
- Nisbet, E.G., and Piper, D.J., 1998. Giant submarine landslides. *Nature*, 392:329–330.
- ODP Leg 146 Scientific Party, 1993. ODP Leg 146 examines fluid flow in Cascadia margin. *Eos*, 74:345–347.
- Parkes, R.J., Cragg, B.A., and Wellsbury, P., 2000. Recent studies on bacterial populations and processes in marine sediments: a review. *Hydrogeol. Rev.*, 8:11–28.
- Paull, C.K., Matsumoto, R., Wallace, P.J., et al., 1996. *Proc. ODP, Init. Repts.*, 164: College Station, TX (Ocean Drilling Program).
- Paull, C.K., and Ussler W., III, 2001. History and significance of gas sampling during the DSDP and ODP. In Paull, C.K., and Dillon, W.P. (Eds.), *Natural Gas Hydrates: Occurrence, Distribution, and Detection*. Am. Geophys. Union, Geophys. Monogr. Ser., 124:53–66.
- Paull, C.K., Ussler, W., III, and Borowski, W.A., 1994. Sources of biogenic methane to form marine gas-hydrates: in situ production or upward migration? *Ann. N.Y. Acad. Sci.*, 715:392–409.
- Paull, C.K., Ussler, W., III, and Dillon, W.P., 1991. Is the extent of glaciation limited by marine gas-hydrates? *Geophys. Res. Lett.*, 18:432–434.
- Rempel, A.W., and Buffett, B.A., 1998. Mathematical models of gas hydrate accumulation. In Henriot, J.P., and Mienert, J. (Eds.), *Gas Hydrates; Relevance to World Margin Stability and Climate Change*, Spec. Publ.—Geol. Soc. London, 137:63–74.
- Revelle, R., 1983. Methane hydrates in continental slope sediments and increasing atmospheric carbon dioxide. In *Changing Climate: Washington* (National Academy Press), 252–261.

- Ruppel, C., 1997. Anomalously cold temperatures observed at the base of the gas hydrate stability zone on the U.S. Atlantic passive margin. *Geology*, 25:699–702.
- Sample, J.C., and Kopf, A., 1995. Isotope geochemistry of syntectonic carbonate cements and veins from the Oregon Margin: implications for the hydrogeologic evolution of the accretionary wedge. In Carson, B., Westbrook, G.K., Musgrave, R.J., and Suess, E. (Eds.), *Proc. ODP, Sci. Results*, 146 (Pt 1): College Station, TX (Ocean Drilling Program), 137–148.
- Sassen, R., Sweet, S.T., Milkov, A.V., Defreitas, D.A., and Kennicutt, M.C., 2001. Thermogenic vent gas and gas hydrate in the Gulf of Mexico slope: is gas hydrate decomposition significant? *Geology*, 29:107–110.
- Sassen, R., Sweet, S.T., Milkov, A.V., Defreitas, D.A., Kennicutt, M.C., and Roberts, H.H., 2001. Stability of thermogenic gas hydrate in the Gulf of Mexico: constraints on models of climate change. In Paull, C.K., and Dillon, W.P. (Eds.), *Natural Gas Hydrates: Occurrence, Distribution, and Detection*. Am. Geophys. Union, Geophys. Monogr. Ser., 124:131–144.
- Schlüter, M., Linke, P., and Suess, E., 1998. Geochemistry of a sealed deep-sea borehole on the Cascadia margin. *Mar. Geol.*, 148:9–20.
- Suess, E., and Bohrmann, G., 1997. FS SONNE cruise report, SO110:SO-RO (SONNE-ROPOS), Victoria-Kodiak-Victoria, July 9-Aug. 19, 1996. *GEOMAR Rpt.*, 59:181.
- Suess, E., Torres, M.E., Bohrmann, G., Collier, R.W., Rickert, D., Goldfinger, C., Linke, P., Heuser, A., Sahling, H., Heeschen, K., Jung, C., Nakamura, K., Greinert, J., Pfannkuche, O., Trehu, A., Klinkhammer, G., Whiticar, M.J., Eisenhauer, A., Teichert, B., and Elvert, M., 2001. Sea floor methane hydrates at Hydrate Ridge, Cascadia margin. In Paull, C.K., and Dillon, W.P. (Eds.), *Natural Gas Hydrates: Occurrence, Distribution, and Detection*. Am. Geophysical Union, Geophys. Monogr. Ser., 124:87–98.
- Suess, E.M., Torres, M.E., Bohrmann, G., Collier, R.W., Greinter, J., Linke, P., Rehter, G., Trehu, A.M., Wallmann, K., Winckler, G., and Zulegger, E., 1999. Gas hydrate destabilization: enhanced dewatering, benthic material turnover, and large methane plumes at the Cascadia convergent margin. *Earth Planet. Sci. Lett.*, 170:1–15.
- Teichert, B.M.A., Eisenhauer, A., and Bohrmann, G., 2001. Chemoherm buildups at the Cascadia Margin (Hydrate Ridge)—evidence for long-term fluid flow. *2001 MARGINS Meet.*, Kiel, 208.
- Teichert, B.M.A., Eisenhauer, A., Bohrmann, G., Haase-Schramm, A., Bock, B., and Linke, P., in press. U/Th systematics and ages of authigenic carbonates from Hydrate Ridge, Cascadia margin: recorders of fluid flow variations. *Geochm. Cosmochem. Acta*.
- Torres, M.E., Bohrmann, G., Brown, K., deAngelis, M., Hammond, D., Klinkhammer, G., McManus, J., Suess, E., and Trehu, A.M., 1999. Geochemical observations on Hydrate Ridge, Cascadia margin, July, 1999. *Oregon State Univ. Data Rpt.* 174, ref. 99-3.
- Torres, M.E., Colbert, S., Collier, R.W., deAngelis, M., Hammond, D., Heeschen, K., Hubbard, D., McManus, J., Moyer, C., Rehder, G., Trehu, A.M., Tyron, M., and

- Whaling, P., 1998. Active gas discharge resulting from decomposition of gas hydrates on Hydrate Ridge, Cascadia margin. *Eos, Trans.*, 79:461.
- Trehu, A.M., and Bangs, N., 2001. 3-D seismic imaging of an active margin hydrate system, Oregon continental margin, report of cruise TTN112. *Oregon State Univ. Data Rpt.*, 182.
- Trehu, A.M., Bangs, N.L., Arsenault, M.A., Bohrmann, G., Goldfinger, C., Johnson, J.E., Nakamura, Y., and Torres, M.E., 2002. Complex subsurface plumbing beneath southern Hydrate Ridge, Oregon continental margin, from high-resolution 3-D seismic reflection and OBS Data. *Fourth Int. Conf. Gas Hydrates*, Yokohama, Japan, 19023:90–96.
- Trehu, A.M., and Flueh, E., 2001. Estimating the thickness of the free gas zone beneath Hydrate Ridge, Oregon continental margin, from seismic velocities and attenuation. *J. Geophys. Res.*, 106:2035–2045.
- Trehu, A.M., Lin, G., Maxwell, E., and Goldfinger, C., 1995. A seismic reflection profile across the Cascadia subduction zone offshore central Oregon: new constraints on methane distribution and crustal structure. *J. Geophys. Res.*, 100:15101–15116.
- Trehu, A.M., Torres, M.E., Moore, G.F., Suess, E., and Bohrmann, G., 1999. Temporal and spatial evolution of a gas-hydrate-bearing accretionary ridge on the Oregon continental margin. *Geology*, 27:939–942.
- Wefer, G.P., Heinze, M., and Berger, W.H., 1994. Clues to ancient methane release. *Nature*, 369:282.
- Xu, W., and Ruppel, C., 1999. Predicting the occurrence, distribution, and evolution of methane gas hydrate in porous marine sediments. *J. Geophys. Res.*, 104:5081–5096.
- Zwart, G., Moore, J.C., and Cochrane, G.R., 1996. Variations in temperature gradients identify active faults in the Oregon accretionary prism. *Earth Planet. Sci. Lett.*, 139:485–495.

## TABLE AND FIGURE CAPTIONS

**Table T1.** Leg 204 site summary.

**Table T2.** Leg 204 core summary.

**Table T3.** Leg 204 operations summary.

**Figure F1.** A. Tectonic setting of Leg 204 in the accretionary complex of the Cascadia subduction zone. The box shows region of Figure F1B. B. Bathymetric map in the region of Hydrate Ridge. The box shows location of Figure F1C. Locations of ODP Site 892, seismic Line L2-89 (shown in Fig. F2), north Hydrate Ridge (NHR), south Hydrate Ridge (SHR), and Southeast Knoll (SEK) are also shown. C. Detailed bathymetric map of the region of Leg 204. Leg 204 sites are shown along with their site numbers (e.g., Site 1244) and precruise designation (e.g., HR1a). Bathymetry from Clague et al. (2001).

**Figure F2.** A. Schematic line drawing of the crustal structure across Hydrate Ridge based on depth-converted migrated seismic reflection data (from Westbrook et al., 1994). Interpretation is based on Line 9 from the 1989 ODP site survey (MacKay et al., 1992), along which ODP Site 892 was located. On the scale shown here, primary structural features are the same as those along Line 2, which is shown in B. B. Line 2 from the 1989 ODP site survey showing primary structural features of the deformation front and the location of data shown in Figure F5.

**Figure F3.** A. Temperature profiles from conductivity/temperature/depth recorder over southern Hydrate Ridge. The stability boundaries for (A) pure methane hydrate and (B) a mixture of 97.5% methane and 2.5% hydrogen sulfide are shown as are the water depths of Leg 204 sites. B. Echo sounder records (12 kHz) from the region of Hydrate Ridge showing bubbles in the water column.

**Figure F4.** A. A carbonate sample from the top of the Pinnacle showing the porous nature of carbonates from this environment. B. A sample of sediment from near the seafloor at southern Hydrate Ridge showing hydrate lenses parallel to bedding connected to hydrate veins perpendicular to bedding. C. Landscape at southern Hydrate Ridge showing mounds covered by bacterial mats. A clam colony is seen in the right edge of the picture taken during an *Alvin* dive. D. Illustration of the complex biogeochemical relationships expected near the southern summit of Hydrate Ridge.

**Figure F5.** East-west vertical slice through the 3-D seismic data showing the stratigraphic and structural setting of Sites 1244, 1245, 1246, and 1252. Seismic reflections A, B, B', Y, and Y' are anomalously bright stratigraphic events and are discussed further in the text. Seismic reflection AC is the top of the seismically incoherent core of Hydrate Ridge, interpreted to represent older highly deformed rocks of the accretionary complex. The depth scale in meters is shown on the left, assuming a velocity of 1550 m/s above 150 mbsf and 1650 m/s below 150 mbsf. The length of the lines representing sites indicates maximum depth of penetration at that site, and horizontal ticks are located 75 m apart.

**Figure F6.** Panels above, left show north-south–trending vertical slices from the 3-D seismic data volume that extend from the western flank to the summit (see map above, right). Sites drilled during Leg 204 are shown. From left, lower panels are maps of the depth of Horizon A beneath the BSR and the seafloor and of the amplitude of Horizon A. These maps show that changes in the amplitude of Horizon A are correlated with the depth of Horizon A beneath the sea surface (pressure) rather than depth beneath the seafloor (primarily temperature), suggesting that the onset of very strong reflectivity may indicate the onset of gas exsolution within Horizon A. Other labels as in Figure F5. The length of the lines representing sites indicates maximum depth of penetration at that site, and horizontal ticks are located 75 m apart.

**Figure F7.** Seismic details near the summit of southern Hydrate Ridge in the vicinity of Sites 1248, 1249, and 1250. Seafloor reflectivity is also shown (from Johnson and Goldfinger, pers. comm., 2002).

**Figure F8.** East-west–trending vertical slices through the seismic data around Sites 1251 and 1252. The slice for Site 1252 overlaps and extends through the slice shown in Figure F5. The slice for Site 1251 is offset to the south. Sites 1251 and 1252 are on the east and west flanks of anticline B, respectively. This anticline appears to have been active throughout the depositional history of the slope basin on the east flank of Hydrate Ridge, which included an unconformity (U) and two apparent massive debris flows (DF1 and DF2), which can be traced throughout the slope basin. Reflectionary accretionary complex is an unconformity that marks the top of older (>1.6 Ma) indurated and fractured sediments of the accretionary complex.

**Figure F9.** Examples of some of the characteristic lithologic features observed in cores from Leg 204. **A.** Turbidites. **B.** Debris flows. **C.** Volcanic ash and glass horizons.

**Figure F10.** Summary of biostratigraphic and lithologic observations. Seismic correlation of Horizons A, B, B', and Y and of unconformities (U) and the accretionary complex are also shown (see Figs. F5, F6, F8). See text for more detailed descriptions of the characteristics of each lithologic unit. Note that Unit III along the north-south transect is not correlative with Unit III on the east-west transect. Correlation between these two transects is tentative. A comparison between the age constraints shown here and the geometric relationships shown in Figure F5 suggests that Unit III at Site 1245 was deposited very rapidly at the base of the continental slope (i.e., in the trench) and, thus, represents a recent addition to the accretionary complex. Unit II was deposited in a very active tectonic environment on the lower slope and varies laterally in both thickness and lithology. Thorough integration of the seismic, biostratigraphic, and lithologic data is an ongoing postcruise project.

**Figure F11.** Correlation between 3-D seismic data, density, and resistivity measured downhole by LWD (gamma density and magnetic susceptibility measured by MST on cores) and lithology at Sites 1244 and 1246. Seismic data were converted to depth assuming a velocity of 1550 m/s above the BSR and 1700 m/s below the BSR, as suggested by 3-D velocity tomography (Arsenault et al., 2001). VSPs confirmed that the velocities from the tomography study are quite close to in situ velocities (Fig. F19). Seismic Horizon B corresponds to a double-peaked, high-density, high-magnetic susceptibility zone. Lithologic observations indicate that these anomalies result from ash-rich layers that contain a relatively high concentration of gas hydrate.

**Figure F12.** Comparison of IR images and hydrate samples extracted from the core liner. Outer core liner diameter in the IR images is 71.5 mm. Inner core diameter in the photographs is 66 mm.

**Figure F13.** Relative borehole resistivity as imaged by LWD (golden/brown columns) compared to the presence of low temperature anomalies in recovered cores as imaged by IR camera scans (blue spikes). The resistivity data show a clockwise scan from north of the borehole wall. Light shades represent higher resistivity. Horizontal bands are parallel to strata, whereas S-shaped bands represent steeply dipping structures. IR anomalies represent the difference between local and background temperature. Background temperature was determined by eye and can be due to many factors, including air temperature on the catwalk and coring method. The base of the GHSZ (BGHSZ) is defined by the BSR, Horizon A, and the top of accretionary complex as defined by increased fracturing and variable density in the LWD data are also shown.

**Figure F14.** Comparison of the resistivity structure between Sites 1244 and 1248, showing the difference between a site where hydrate fill is primarily along steeply dipping fractures and a site where hydrate fill is primarily along bedding planes.

**Figure F15.** Chloride concentration values measured at all sites. In most cases, samples are spaced at ~5-m intervals (two per core). **A.** Sites on the western flank of Hydrate Ridge. **B.** Sites on the eastern flank of Hydrate Ridge. **C.** Sites near the summit of Hydrate Ridge. BSR depth at each site is shown as a color-coded dashed line.

**Figure F16.**  $C_1/C_2$  values measured at all sites from vacutainer samples. The same patterns are shown in headspace samples, although absolute values of  $C_1/C_2$  are somewhat smaller. Samples are spaced at ~5-m intervals (two per core). **A.** Sites on the western flank of Hydrate Ridge. **B.** Sites on the eastern flank of Hydrate Ridge. **C.** Sites near the summit of Hydrate Ridge. BSR and Horizon A depth at each site is shown as a color-coded dashed line.

**Figure F17.** Methane concentrations determined from PCS measurements. Approximate phase boundaries are shown between fields where dissolved gas, gas hydrates, and free gas are predicted to be present in the subsurface. Uncertainties (~30%) in the position of these boundaries are a result of a number of factors, including variations in subsurface temperature gradient, gas composition, and pore fluid salinity. Although these boundaries give a first order view of where gas hydrate should be present, data points that fall near boundaries should be interpreted with caution. More detailed analysis of the predicted stability fields for conditions measured during Leg 204 is the subject of postcruise research. Near the summit, all PCS measurements from within the GHSZ indicate the presence of gas hydrate, with the highest concentration near the seafloor. On the flanks and in the basin, hydrate presence within the stability zone is intermittent and the highest concentration is just above the BSR (no PCS measurements are available from the thin hydrate-bearing layer just above the BSR at Site 1251) (see Figs. F14, F18).

**Figure F18.** Downhole temperature measurements at all sites. Although temperature gradients are probably known to be better than 0.005°C/m, postcruise calibration of downhole temperature tools is needed to determine absolute temperature. Scatter in the data is greater at sites near the summit, perhaps because of the effect of gas hydrate on in situ thermal conductivity and/or to dissociation of gas hydrate as a result of insertion of the probe.

**Figure F19.** Traveltime picks from vertical seismic profiles. The shallowest point in all profiles is the calculated traveltime to the seafloor. These data confirm the generally very low velocities throughout the GHSZ. Small deflections of the curves that imply a decrease in velocity coincide with the BSR and Horizon A.

**Figure F20.** A. Sulfate and methane concentration at Site 1245 showing the sulfate-methane interface (SMI). B. Summary of sulfate measurements showing the SMI at all sites, except for Sites 1248, 1249, and 1250 where no sulfate was detected in the uppermost sample.

**Figure F21.** Density and RAB recorded through seismic Horizon A at Sites 1245 and 1247. These examples show the remarkable consistency in the signature of this horizon over distances of several kilometers. RAB images are static normalized.

**Figure F22.** A. IR thermal anomalies measured in two different holes at Site 1251. Note that a major thermal anomaly in the 10 m above the BSR observed in Hole 1251D was not observed in Hole 1251B because that interval was not recovered from Hole 1251B (perhaps because of high hydrate concentration in situ). At this site, IR thermal anomalies are generally small and rare compared at most other sites drilled during Leg 204. B. Comparison between chloride anomalies measured from whole rounds and thermal anomalies in Hole 1251D. The IR data suggest two layers of high hydrate concentration immediately above the BSR but do not provide a good constraint on the concentration of hydrate within these layers. Chloride anomalies suggest a hydrate concentration of ~20% of pore space but do not provide a good constraint on the thickness of hydrate-bearing layers because of the small number of samples. Moreover, at this site probable thin hydrate-bearing layers (based on IR and resistivity anomalies) were missed completely geochemical sampling. By calibrating the densely spaced geophysical data using the sparser geochemical data, improved estimates of hydrate distribution and concentration will be obtained.

**Table T1. Leg 204 site summary.**

Drilling order	Site	Hole	Latitude	Longitude	Seafloor (mbrf)	Number	Cored (m)	Recovered (m)	Recovery (%)	Drilled (m)	Penetration (m)	Time on hole		
												(hr)	(days)	
1	HR-1a	1244A	44°35.1701'N	125°7.1906'W	Missed	1	9.5	9.99	105.2	0.0	9.5	10.75	0.45	
2		1244B	44°35.1702'N	125°7.1917'W	906.9	6	54.1	56.85	105.1	0.0	54.1	11.75	0.49	
3		1244C	44°35.1784'N	125°7.1902'W	906.0	39	332.0	315.87	95.1	1.5	333.5	64.75	2.70	
4		1244D	44°35.1865'N	125°7.1900'W	906.0	0	0.0	0.00	NA	380.0	380.0	37.50	1.56	
35		1244E	44°35.1709'N	125°7.1719'W	904.8	19	135.8	137.73	101.4	114.2	250.0	74.75	3.11	
36		1244F	44°35.1691'N	125°7.1705'W	907.4	4	24.1	24.90	103.3	0.0	0.0	5.00	0.21	
Site 1244 totals:						69	555.5	545.34	98.2	495.7	1027.1	204.50	8.52	
5	HR-3a	1245A	44°35.1697'N	125°8.9462'W	886.5	0	0.0	0.00	NA	380.0	380.0	28.75	1.20	
29		1245B	44°35.1587'N	125°8.9455'W	881.0	53	471.7	418.27	88.7	2.0	473.7	80.50	3.35	
30		1245C	44°35.1702'N	125°8.9316'W	880.0	29	198.7	185.31	93.3	3.0	201.7	32.75	1.36	
31		1245D	44°35.1690'N	125°8.9312'W	881.5	3	24.0	24.82	103.4	0.0	24.0	3.50	0.15	
33		1245E	44°35.1702'N	125°8.9605'W	881.0	8	66.6	18.5	27.7	473.7	540.3	104.50	4.35	
Site 1245 totals:						93	761.0	646.88	85.0	858.7	1619.7	250.00	10.42	
6	HR-1b	1246A	44°35.1642'N	125°8.1400'W	861.5	0	0.0	0.00	NA	180.0	180.0	18.25	0.76	
32		1246B	44°35.1644'N	125°8.1235'W	860.8	16	136.7	135.34	99.0	0.0	136.7	18.75	0.78	
Site 1246 totals:						16	136.7	135.34	99.0	180.0	316.7	37.00	1.54	
7	HR-4c	1247A	44°34.6591'N	125°9.0096'W	845.0	0	0.0	0.00	NA	270.0	270.0	21.25	0.89	
37		1247B	44°34.6589'N	125°9.0766'W	845.9	27.0	217.0	212.0	97.7	3.0	220.0	60.5	2.52	
Site 1247 totals:						27	217.0	212.00	NA	273.0	490.0	81.75	3.41	
8	HR-6	1248A	44°34.4515'N	125°9.1548'W	843.0	0	0.0	0.00	NA	194.0	194.0	15.50	0.65	
21		1248B	44°34.4568'N	125°9.1482'W	841.0	3	17.0	7.45	43.8	0.0	17.0	10.75	0.45	
22		1248C	44°34.45'N	125°9.1499'W	841.0	17	149.0	101.56	68.2	0.0	149.0	22.75	0.95	
Site 1248 totals:						20	166.0	109.01	65.7	194.0	360.0	49.00	2.04	
9	HR-4b	1249A	44°34.2246'N	125°8.8423'W	788.5	0	0.0	0.00	NA	90.0	90.0	9.75	0.41	
13		1249B	44°34.2106'N	125°8.8412'W	788.5	8	45.0	14.01	31.1	29.9	74.9	28.00	1.17	
14		1249C	44°34.2368'N	125°8.8410'W	788.5	14	88.5	58.84	66.5	1.5	90.0	22.25	0.93	
26		1249D	44°34.2222'N	125°8.8366'W	788.5	3	16.5	4.78	29.0	2.0	18.5	5.25	0.22	
27		1249E	44°34.2270'N	125°8.3690'W	788.5	3	9.0	4.38	48.7	2.0	11.0	4.75	0.20	
28		1249F	44°34.2317'N	125°8.8377'W	788.5	16	82.5	57.37	69.5	7.5	90.0	22.75	0.95	
39		1249G	44°34.2073'N	125°8.8416'W	788.5	5	43.0	11.24	26.1	0.0	43.0	9.00	0.38	
40		1249H	44°34.2108'N	125°8.8365'W	788.5	6	52.5	27.52	52.4	0.0	52.5	8.50	0.35	
41		1249I	44°34.2111'N	125°8.8437'W	788.5	4	33.6	8.69	25.9	0.0	33.6	6.00	0.25	
42		1249J	44°34.2114'N	125°8.8422'W	788.5	3	32.5	7.69	23.7	0.0	32.5	5.50	0.23	
43		1249K	44°34.2137'N	125°8.8392'W	788.5	5	43.2	16.87	39.1	1.0	44.2	8.25	0.34	
44		1249L	44°34.2119'N	125°8.8439'W	788.5	5	38.5	14.15	36.8	0.0	38.5	10.25	0.43	
Site 1249 totals:						72	484.8	225.54	46.5	133.9	618.7	140.25	5.84	
10		HR-4a	1250A	44°34.1176'N	125°9.0179'W	807.0	0	0.0	0.00	NA	210.0	210.0	20.25	0.84
12			1250B	44°34.1174'N	125°8.9921'W	807.0	0	0.0	0.00	NA	180.0	180.0	19.50	0.81
23	1250C		44°34.1273'N	125°9.0178'W	807.0	19	143.0	117.29	82.0	2.0	145.0	28.50	1.19	
24	1250D		44°34.1063'N	125°9.0182'W	807.0	19	142.0	133.56	94.1	3.0	145.0	26.00	1.08	
25	1250E		44°34.1124'N	125°9.0171'W	807.0	2	16.0	11.93	74.6	0.0	16.0	3.50	0.15	
35	1250F		44°34.1166'N	125°9.0025'W	807.0	13	77.0	70.10	91.0	103.0	180.0	74.25	3.09	
Site 1250 totals:						53	378.0	332.88	88.1	498.0	876.0	172.00	7.17	
11	HR-2alt	1251A	44°34.2197'N	125°4.4521'W	1228.0	0	0.0	0.00	NA	380.0	380.0	25.25	1.05	
15		1251B	44°34.2191'N	125°4.4375'W	1224.4	53	442.1	368.56	83.4	3.0	445.1	86.25	3.59	
16		1251C	44°34.2058'N	125°4.4366'W	1221.4	2	17.6	13.63	77.4	0.0	17.6	4.50	0.19	
17		1251D	44°34.2060'N	125°4.4365'W	1221.4	30	226.5	194.40	85.8	4.0	230.5	38.25	1.59	
18		1251E	44°34.2126'N	125°4.4358'W	1220.0	1	9.5	9.89	104.1	0.0	9.5	1.75	0.07	
19		1251F	44°34.2159'N	125°4.4369'W	1220.0	1	9.5	9.92	104.4	0.0	9.5	0.25	0.01	
20		1251G	44°34.2145'N	125°4.4364'W	1220.0	2	10.5	11.11	105.8	10.5	21.0	4.25	0.18	
34		1251H	44°34.2089'N	125°4.4514'W	1220.0	0	0.0	0.00	NA	445.0	445.0	63.8	2.66	
Site 1251 totals:						89	715.7	607.51	84.9	842.5	1558.2	224.25	9.34	
45		HR-5	1252A	44°35.1671'N	125°5.5691'W	1051.0	28	259.8	253.79	97.7	0.0	259.8	51.00	2.13
Site 1252 totals:						28	259.8	253.79	97.7	0.0	259.8	51.00	2.13	
Totals:						467	3674.5	3068.29	83.5	3475.8	7126.2	1209.75	50.41	



Table T2. Leg 204 coring summary. (Continued on next page.)

Drilling order	Hole	Advanced Piston Corer			Extended Core Barrel			Pressure Core Sampler			Rotary Core Barrel		
		Number	Cored (m)	Recovered (m)	Number	Cored (m)	Recovered (m)	Number	Cored (m)	Recovered (m)	Number	Cored (m)	Recovered (m)
1	1244A	1	9.5	9.99	0	0.0	0.00	0	0.0	0.00	0	0.0	0.00
2	1244B	6	54.1	56.85	0	0.0	0.00	0	0.0	0.00	0	0.0	0.00
3	1244C	15	138.5	138.76	21	190.5	173.85	3	3.0	3.26	0	0.0	0.00
4	1244D	0	0.0	0.00	0	0.0	0.00	0	0.0	0.00	0	0.0	0.00
35	1244E	14	130.8	133.81	0	0.0	0.00	4	4.0	3.00	0	0.0	0.00
36	1244F	3	23.1	23.90	0	0.0	0.00	1	1.0	1.00	0	0.0	0.00
1244 totals:		39	356.0	363.31	21	190.5	173.85	8	8.0	7.26	0	0.0	0.00
5	1245A	0	0.0	0.00	0	0.0	0.00	0	0.0	0.00	0	0.0	0.00
29	1245B	14	127.8	122.14	36	340.9	293.75	2	2.0	2.00	0	0.0	0.00
30	1245C	16	134.6	127.54	7	58.1	53.52	3	3.0	3.00	0	0.0	0.00
31	1245D	3	24.0	24.82	0	0.0	0.00	0	0.0	0.00	0	0.0	0.00
33	1245E	0	0.0	0.00	0	0.0	0.00	0	0.0	0.00	8	66.6	18.48
1245 totals:		33	286.4	274.50	43	399.0	347.27	5	5.0	5.00	8	66.6	18.48
6	1246A	0	0.0	0.00	0	0.0	0.00	0	0.0	0.00	0	0.0	0.00
32	1246B	16	136.7	135.34	0	0.0	0.00	0	0.0	0.00	0	0.0	0.00
1246 totals:		16	136.7	135.34	0	0.0	0.00	0	0.0	0.00	0	0.0	0.00
7	1247A	0	0.0	0.00	0	0.0	0.00	0	0.0	0.00	0	0.0	0.00
37	1247B	13	111.6	114.99	11	102.4	94.01	3	3.0	3.00	0	0.0	0.00
1246 totals:		13	111.6	114.99	11	102.4	94.01	3	3.0	3.00	0	0.0	0.00
8	1248A	0	0.0	0.00	0	0.0	0.00	0	0.0	0.00	0	0.0	0.00
21	1248B	3	17.0	7.45	0	0.0	0.00	0	0.0	0.00	0	0.0	0.00
22	1248C	11	94.0	84.00	6	55.0	17.56	0	0.0	0.00	0	0.0	0.00
1248 totals:		14	111.0	91.45	6	55.0	17.56	0	0.0	0.00	0	0.0	0.00
9	1249A	0	0.0	0.00	0	0.0	0.00	0	0.0	0.00	0	0.0	0.00
13	1249B	0	0.0	0.00	0	0.0	0.00	0	0.0	0.00	0	0.0	0.00
14	1249C	11	85.5	55.84	0	0.0	0.00	3	3.0	3.00	0	0.0	0.00
26	1249D	2	15.5	3.98	0	0.0	0.00	0	0.0	0.00	0	0.0	0.00
27	1249E	2	8.0	3.38	0	0.0	0.00	1	1.0	1.00	0	0.0	0.00
28	1249F	10	73.1	51.38	1	4.4	1.28	3	3.0	3.00	0	0.0	0.00
39	1249G	3	28.5	7.13	1	13.5	3.36	0	0.0	0.00	0	0.0	0.00
40	1249H	4	38.0	25.07	1	13.5	1.70	0	0.0	0.00	0	0.0	0.00
41	1249I	3	20.1	8.29	1	13.5	0.40	0	0.0	0.00	0	0.0	0.00
42	1249J	2	19.0	7.69	1	13.5	0.00	0	0.0	0.00	0	0.0	0.00
43	1249K	4	29.7	16.05	1	13.5	0.82	0	0.0	0.00	0	0.0	0.00
44	1249L	2	19.0	7.15	2	18.5	6.65	0	0.0	0.00	0	0.0	0.00
1249 totals:		43	336.4	185.96	8	90.4	14.21	7	7	7	0	0	0
10	1250A	0	0.0	0.00	0	0.0	0.00	0	0.0	0.00	0	0.0	0.00
12	1250B	0	0.0	0.00	0	0.0	0.00	0	0.0	0.00	0	0.0	0.00
23	1250C	15	133.5	104.80	1	6.5	9.60	2	2.0	2.00	0	0.0	0.00
24	1250D	12	111.0	103.95	3	27.0	26.33	3	3.0	3.00	0	0.0	0.00
25	1250E	2	16.0	11.93	0	0.0	0.00	0	0.0	0.00	0	0.0	0.00
38	1250F	3	19.8	17.47	7	54.2	49.63	3	3.0	3.00	0	0.0	0.00
1250 totals:		32	280.3	238.15	11	87.7	85.56	8	8.0	8.00	0	0.0	0.00
11	1251A	0	0.0	0.00	0	0.0	0.00	0	0.0	0.00	0	0.0	0.00
15	1251B	21	189.6	152.86	26	246.5	210.90	3	3.0	3.00	0	0.0	0.00
16	1251C	1	8.1	8.18	1	9.5	5.45	0	0.0	0.00	0	0.0	0.00
17	1251D	15	142.5	132.49	9	78.0	56.82	4	4.0	4.00	0	0.0	0.00
18	1251E	1	9.5	9.89	0	0.0	0.00	0	0.0	0.00	0	0.0	0.00
19	1251F	1	9.5	9.92	0	0.0	0.00	0	0.0	0.00	0	0.0	0.00
20	1251G	1	9.5	10.11	0	0.0	0.00	1	1.0	1.00	0	0.0	0.00
34	1251H	0	0.0	0.00	0	0.0	0.00	0	0.0	0.00	0	0.0	0.00
1251 totals:		40	368.7	323.45	36	334	273.17	8	8	8	0	0	0
45	1252A	14	125.0	134.10	14	134.8	119.69	0	0.0	0.00	0	0.0	0.00
1252 totals:		14	125.0	134.10	14	134.8	119.69	0	0.0	0.00	0	0.0	0.00
Totals:		244	2112.1	1861.25	150	1393.8	1125.32	39	39.0	38.26	8	66.6	18.48

**Table T2 (continued).**

Drilling order	Hole	Fugro Pressure Corer			Hyacinth Rotary Corer			Logging While Coring			Leg 204 Coring Statistics			
		Number	Cored (m)	Recovered (m)	Number	Cored (m)	Recovered (m)	Number	Cored (m)	Recovered (m)	Number	Cored (m)	Recovered (m)	Recovered (%)
1	1244A	0	0.0	0.00	0	0.0	0.00	0	0.0	0.00	1	9.5	9.99	105.2
2	1244B	0	0.0	0.00	0	0.0	0.00	0	0.0	0.00	6	54.1	56.85	105.1
3	1244C	0	0.0	0.00	0	0.0	0.00	0	0.0	0.00	39	332.0	315.87	95.1
4	1244D	0	0.0	0.00	0	0.0	0.00	0	0.0	0.00	0	0.0	0.00	NA
35	1244E	1	1.0	0.92	0	0.0	0.00	0	0.0	0.00	19	135.8	137.73	101.4
36	1244F	0	0.0	0.00	0	0.0	0.00	0	0.0	0.00	4	24.1	24.90	103.3
1244 totals:		1	1.0	0.92	0	0.0	0.00	0	0.0	0.00	69	555.5	545.34	98.2
5	1245A	0	0.0	0.00	0	0.0	0.00	0	0.0	0.00	0	0.0	0.00	NA
29	1245B	0	0.0	0.00	1	1.0	0.38	0	0.0	0.00	53	471.7	418.27	88.7
30	1245C	2	2.0	1.05	1	1.0	0.20	0	0.0	0.00	29	198.7	185.31	93.3
31	1245D	0	0.0	0.00	0	0.0	0.00	0	0.0	0.00	3	24.0	24.82	103.4
33	1245E	0	0.0	0.00	0	0.0	0.00	0	0.0	0.00	8	66.6	18.48	27.7
1245 totals:		2	2.0	1.05	2	2.0	0.58	0	0.0	0.00	93	761.0	646.88	85.0
6	1246A	0	0.0	0.00	0	0.0	0.00	0	0.0	0.00	0	0.0	0.00	NA
32	1246B	0	0.0	0.00	0	0.0	0.00	0	0.0	0.00	16	136.7	135.34	99.0
1246 totals:		0	0.0	0.00	0	0.0	0.00	0	0.0	0.00	16	136.7	135.34	99.0
7	1247A	0	0.0	0.00	0	0.0	0.00	0	0.0	0.00	0	0.0	0.00	NA
37	1247B	0	0.0	0.00	0	0.0	0.00	0	0.0	0.00	27	217.0	212.00	97.7
1247 totals:		0	0.0	0.00	0	0.0	0.00	0	0.0	0.00	27	217.0	212.00	97.7
8	1248A	0	0.0	0.00	0	0.0	0.00	0	0.0	0.00	0	0.0	0.00	NA
21	1248B	0	0.0	0.00	0	0.0	0.00	0	0.0	0.00	3	17.0	7.45	43.8
22	1248C	0	0.0	0.00	0	0.0	0.00	0	0.0	0.00	17	149.0	101.56	68.2
1248 totals:		0	0.0	0.00	0	0.0	0.00	0	0.0	0.00	20	166.0	109.01	65.7
9	1249A	0	0.0	0.00	0	0.0	0.00	0	0.0	0.00	0	0.0	0.00	NA
13	1249B	0	0.0	0.00	0	0.0	0.00	8	45.0	14.01	8	45.0	14.01	31.1
14	1249C	0	0.0	0.00	0	0.0	0.00	0	0.0	0.00	14	88.5	58.84	66.5
26	1249D	1	1.0	0.80	0	0.0	0.00	0	0.0	0.00	3	16.5	4.78	29.0
27	1249E	0	0.0	0.00	0	0.0	0.00	0	0.0	0.00	3	9.0	4.38	48.7
28	1249F	1	1.0	0.91	1	1.0	0.80	0	0.0	0.00	16	82.5	57.37	69.5
39	1249G	0	0.0	0.00	1	1.0	0.75	0	0.0	0.00	5	43	11.24	26.1
40	1249H	1	1.0	0.75	0	0.0	0.00	0	0.0	0.00	6	52.5	27.52	52.4
41	1249I	0	0.0	0.00	0	0.0	0.00	0	0.0	0.00	4	33.6	8.69	25.9
42	1249J	0	0.0	0.00	0	0.0	0.00	0	0.0	0.00	3	32.5	7.69	23.7
43	1249K	0	0.0	0.00	0	0.0	0.00	0	0.0	0.00	5	43.2	16.87	39.1
44	1249L	0	0.0	0.00	1	1.0	0.35	0	0.0	0.00	5	38.5	14.15	36.8
1249 totals:		3	3	2.46	3	3	1.9	8	45	14.01	72	484.8	225.54	46.5
10	1250A	0	0.0	0.00	0	0.0	0.00	0	0.0	0.00	0	0.0	0.00	NA
12	1250B	0	0.0	0.00	0	0.0	0.00	0	0.0	0.00	0	0.0	0.00	NA
23	1250C	1	1.0	0.89	0	0.0	0.00	0	0.0	0.00	19	143	117.29	82.0
24	1250D	0	0.0	0.00	1	1.0	0.28	0	0.0	0.00	19	142.0	133.56	94.1
25	1250E	0	0.0	0.00	0	0.0	0.00	0	0.0	0.00	2	16.0	11.93	74.6
38	1250F	0	0.0	0.00	0	0.0	0.00	0	0.0	0.00	13	77.0	70.10	91.0
1250 totals:		1	1.0	0.89	1	1.0	0.28	0	0.0	0.00	53	378.0	332.88	88.1
11	1251A	0	0.0	0.00	0	0.0	0.00	0	0.0	0.00	0	0.0	0.00	NA
15	1251B	2	2.0	1.80	1	1.0	0.00	0	0.0	0.00	53	442.1	368.56	83.4
16	1251C	0	0.0	0.00	0	0.0	0.00	0	0.0	0.00	2	17.6	13.63	77.4
17	1251D	1	1.0	0.87	1	1.0	0.22	0	0.0	0.00	30	226.5	194.4	85.8
18	1251E	0	0.0	0.00	0	0.0	0.00	0	0.0	0.00	1	9.5	9.89	104.1
19	1251F	0	0.0	0.00	0	0.0	0.00	0	0.0	0.00	1	9.5	9.92	104.4
20	1251G	0	0.0	0.00	0	0.0	0.00	0	0.0	0.00	2	10.5	11.11	105.8
34	1251H	0	0.0	0.00	0	0.0	0.00	0	0.0	0.00	0	0.0	0.00	NA
1251 totals:		3	3	2.67	2	2	0.22	0	0	0	89	715.7	607.51	84.9
45	1252A	0	0.0	0.00	0	0.0	0.00	0	0.0	0.00	28	259.8	253.79	97.7
1252 totals:		0	0.0	0.00	0	0.0	0.00	0	0.0	0.00	28	259.8	253.79	97.7
Totals:		10	10.0	7.99	8	8.0	2.98	8	45.0	14.01	467	3674.5	3068.29	83.5

**Table T3. Leg 204 operations summary.**

Site	Hole	Drill order	Cored or LWD	Depth		PFT's Wpaks F/MBIO	Number of times deployed					APC-M/PCS	Hyacinth tools	
				Seafloor (mbrf)	Hole (mbsf)		DSA	TAMU PCS	DVTPT	DVTPP	APCT		Number of FPC	Number. of HRC
HR-1a	1244A	1	APC	none	10.0	0	0	0	0	0	0	0	0	0
HR-1a	1244B	2	APC	906.9	54.1	0	1	0	0	0	1	0	0	0
HR-1a	1244C	3	APC/XCB	906.0	333.5	3	3	3	0	2	3	0	0	0
HR-1a	1244D	4	LWD	906.0	380.0	0	0	0	0	0	0	0	0	0
HR-3a	1245A	5	LWD	886.5	380.0	0	0	0	0	0	0	0	0	0
HR-1b	1246A	6	LWD	861.5	180.0	0	0	0	0	0	0	0	0	0
HR-4c	1247A	7	LWD	845.0	270.0	0	0	0	0	0	0	0	0	0
HR6	1248A	8	LWD	843.0	194.0	0	0	0	0	0	0	0	0	0
HR4b	1249A	9	LWD	788.5	90.0	0	0	0	0	0	0	0	0	0
HR-4a	1250A	10	LWD-1	807.0	210.0	0	0	0	0	0	0	0	0	0
HR2alt	1251A	11	LWD	1228.0	380.0	0	0	0	0	0	0	0	0	0
HR-4a	1250B	12	LWD-2	807.0	180.0	0	0	0	0	0	0	0	0	0
HR-4b	1249B	13	RAB-8	788.5	74.9	0	0	0	0	0	0	0	0	0
HR-4b	1249C	14	APC	788.5	90.0	0	0	3	0	1	0	4	0	0
HR-2alt	1251B	15	APC/XCB	1224.4	445.1	6	3	3	0	2	4	3	2	1
HR-2alt	1251C	16	APC/XCB	1221.4	17.6	0	0	0	0	0	0	0	0	0
HR-2alt	1251D	17	APC/XCB	1221.4	230.5	13	2	4	0	2	1	14	1	1
HR-2alt	1251E	18	APC only	1220.0	8.1	1	0	0	0	0	0	0	0	0
HR-2alt	1251F	19	APC only	1220.0	8.1	0	0	0	0	0	0	0	0	0
HR-2alt	1251G	20	APC	1220.0	21.0	0	0	1	0	0	0	1	0	0
HR-6	1248B	21	APC/XCB	841.0	16.0	0	0	0	0	0	1	0	0	0
HR-7	1248C	22	APC/XCB	841.0	149.0	0	0	0	1	2	2	0	0	0
HR-4a	1250C	23	APC/XCB	807.0	145.0	0	1	2	0	2	5	2	1	0
HR-4a	1250D	24	APC/XCB	807.0	145.0	10	1	3	0	2	4	15	0	1
HR-4a	1250E	25	APC	807.0	16.0	2	0	0	0	0	0	0	0	0
HR-4b	1249D	26	APC	788.5	18.5	1	1	0	0	0	0	0	1	0
HR-4b	1249E	27	APC	0.0	18.5	1	0	1	0	0	0	1	0	0
HR-4b	1249F	28	APC	788.5	90.0	11	2	2	0	1	5	3	1	1
HR-3a	1245B	29	APC/XCB	881.0	473.6	7	1	3	3	0	5	2	0	1
HR-3a	1245C	30	APC/XCB	880.0	201.7	12	3	3	0	0	5	15	2	1
HR-3a	1245D	31	APC	881.5	24.0	3	0	0	0	0	0	0	0	0
HR-1b	1246B	32	APC	860.8	136.7	0	0	0	0	0	5	0	0	0
HR-3a	1245E	33	RCB	881.0	540.3	0	0	0	0	0	0	0	0	0
HR-2alt	1251H	34	tricone	1220.0	445.0	0	0	0	0	0	0	0	0	0
HR-1a	1244E	35	APC/XCB	904.8	250.0	12	1	4	0	2	6	16	1	0
HR-1a	1244F	36	APC/PCS	907.4	24.1	3	0	1	0	0	0	1	0	0
HR-4c	1247B	37	APC/XCB	845.9	220.0	0	0	3	2	0	6	16	0	0
HR-4a	1250F	38	XCB ctr bit	807.0	180.0	0	0	3	2	0	0	3	0	0
HR-4b	1249G	39	APC/XCB	788.5	43.0	0	1	0	0	0	1	0	0	1
HR-4b	1249H	40	APC/XCB	788.5	52.5	0	3	0	0	0	0	0	1	0
HR-4b	1249I	41	APC/XCB	788.5	33.6	0	0	0	0	0	0	0	0	0
HR-4b	1249J	42	APC/XCB	788.5	32.5	0	0	0	0	0	0	0	0	0
HR-4b	1249K	43	APC/XCB	788.5	44.2	0	3	0	0	0	0	0	0	0
HR-4b	1249L	44	APC/XCB	788.5	38.5	0	2	0	0	0	1	0	0	1
HR-5a	1252A	45	APC/XCB	1051.0	259.8	0	0	0	0	0	6	14	0	0
Total number of special tool deployments:						85	28	39	8	16	61	110	10	8
Total number of "successful" deployments:						85	17?	30	8	16	61	107	2	4

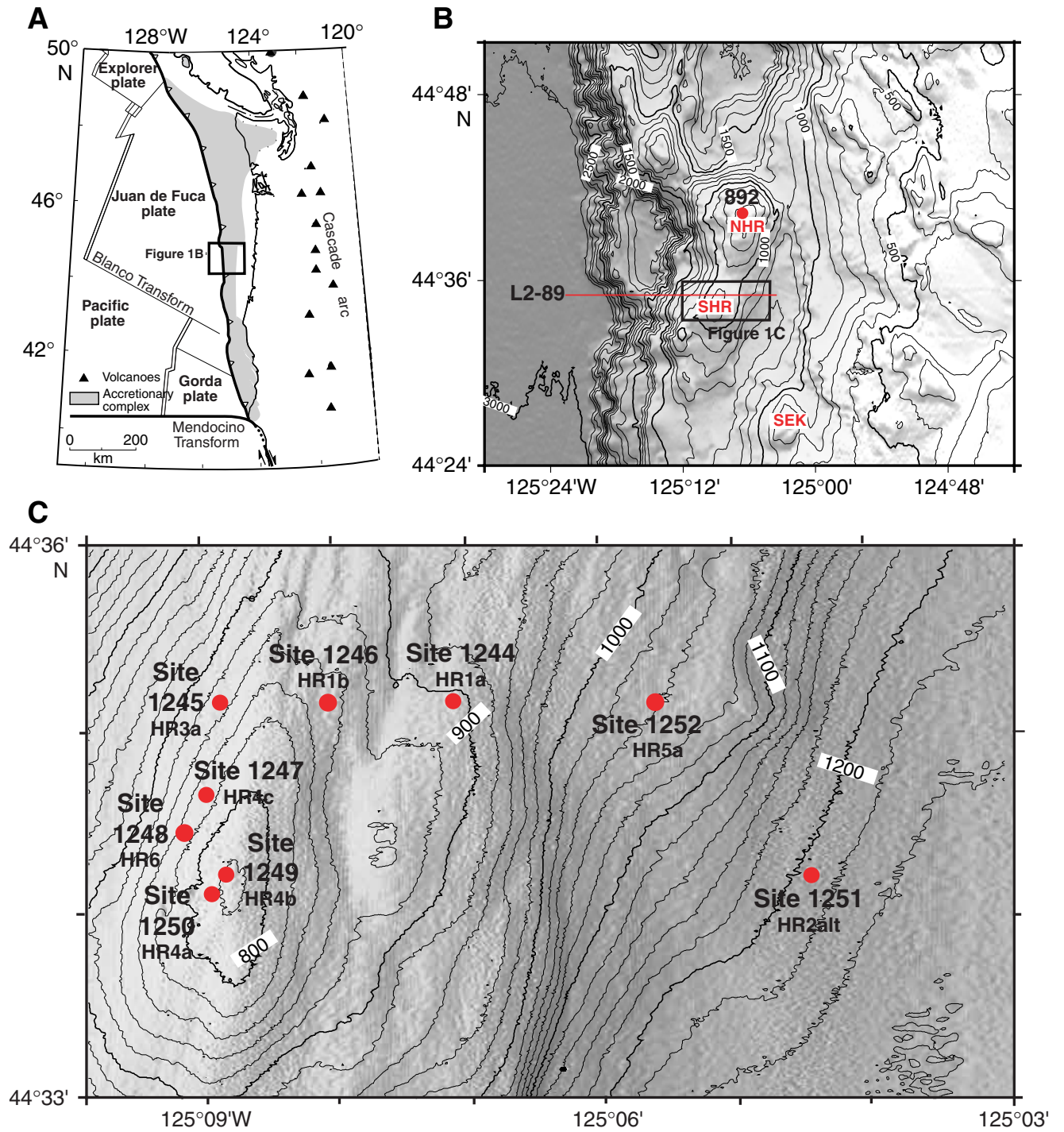


Figure F1

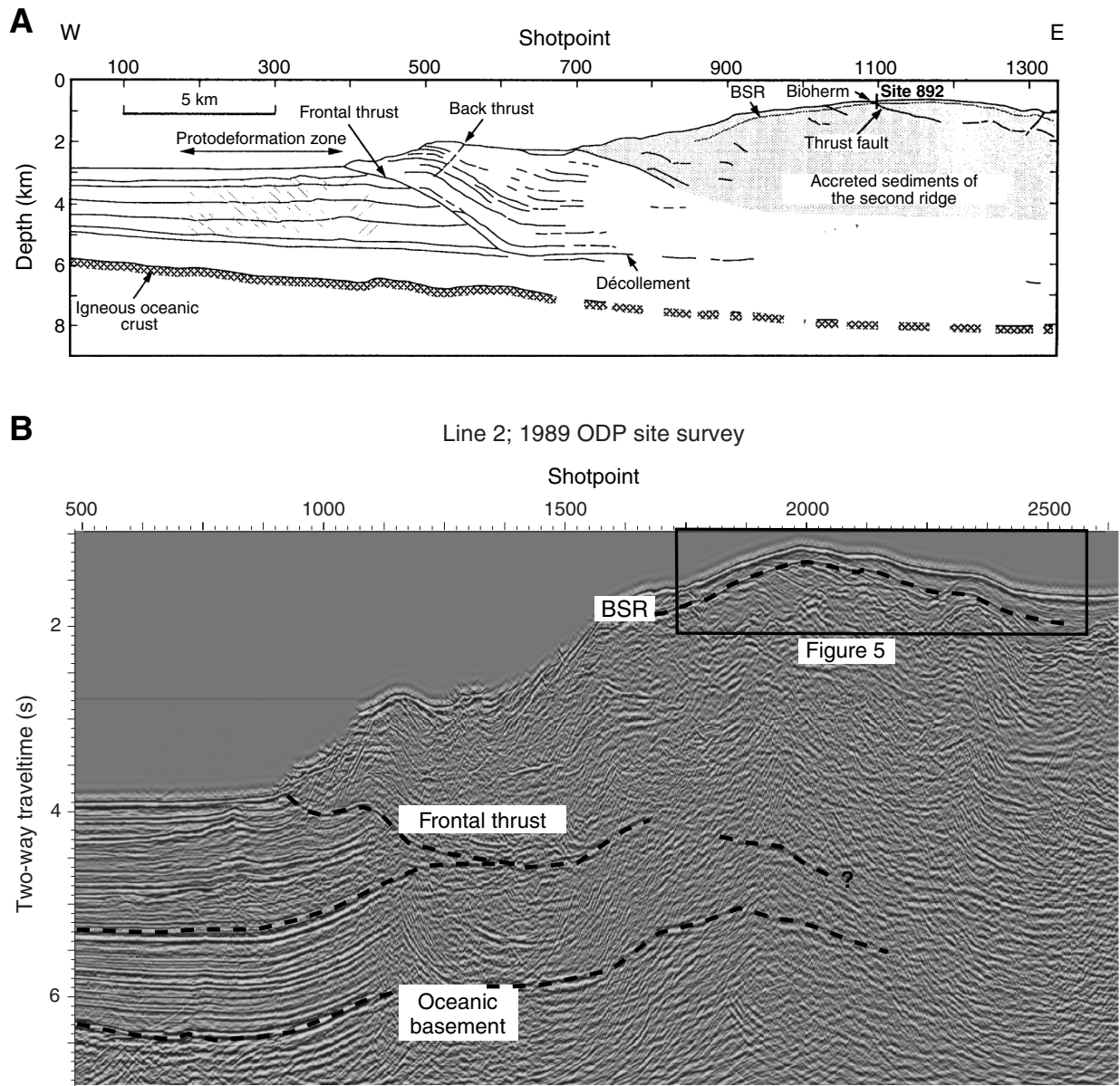


Figure F2

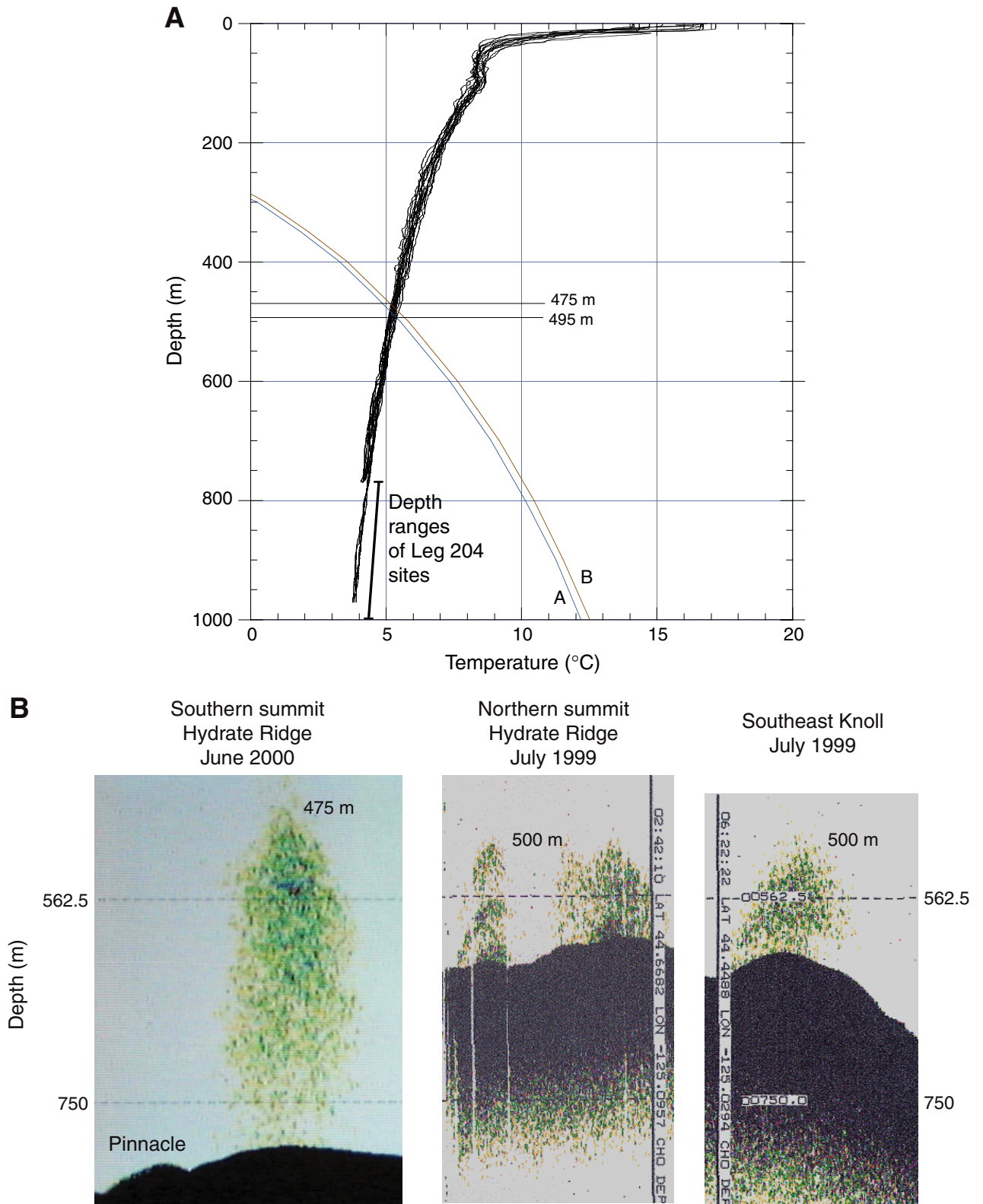


Figure F3

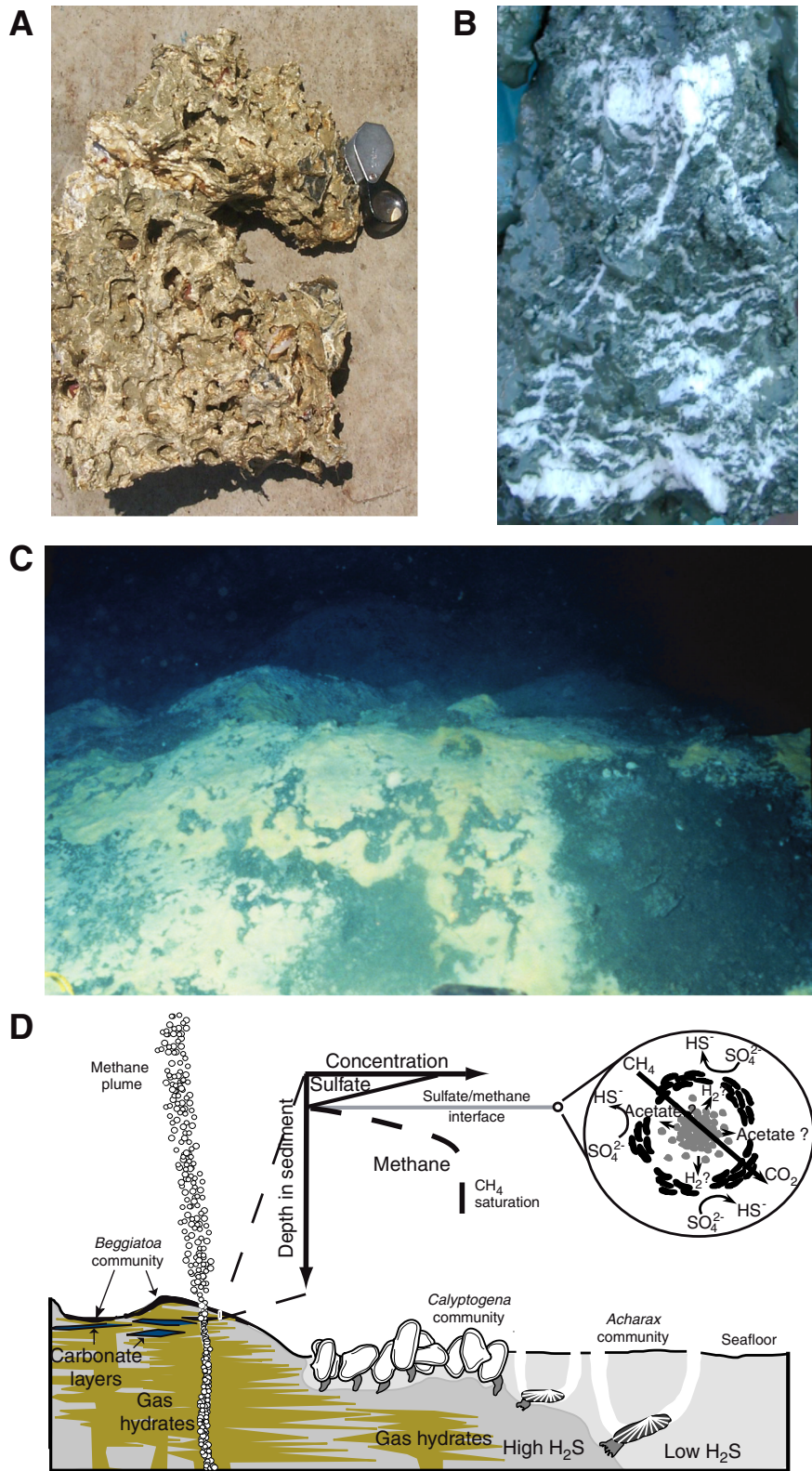


Figure F4

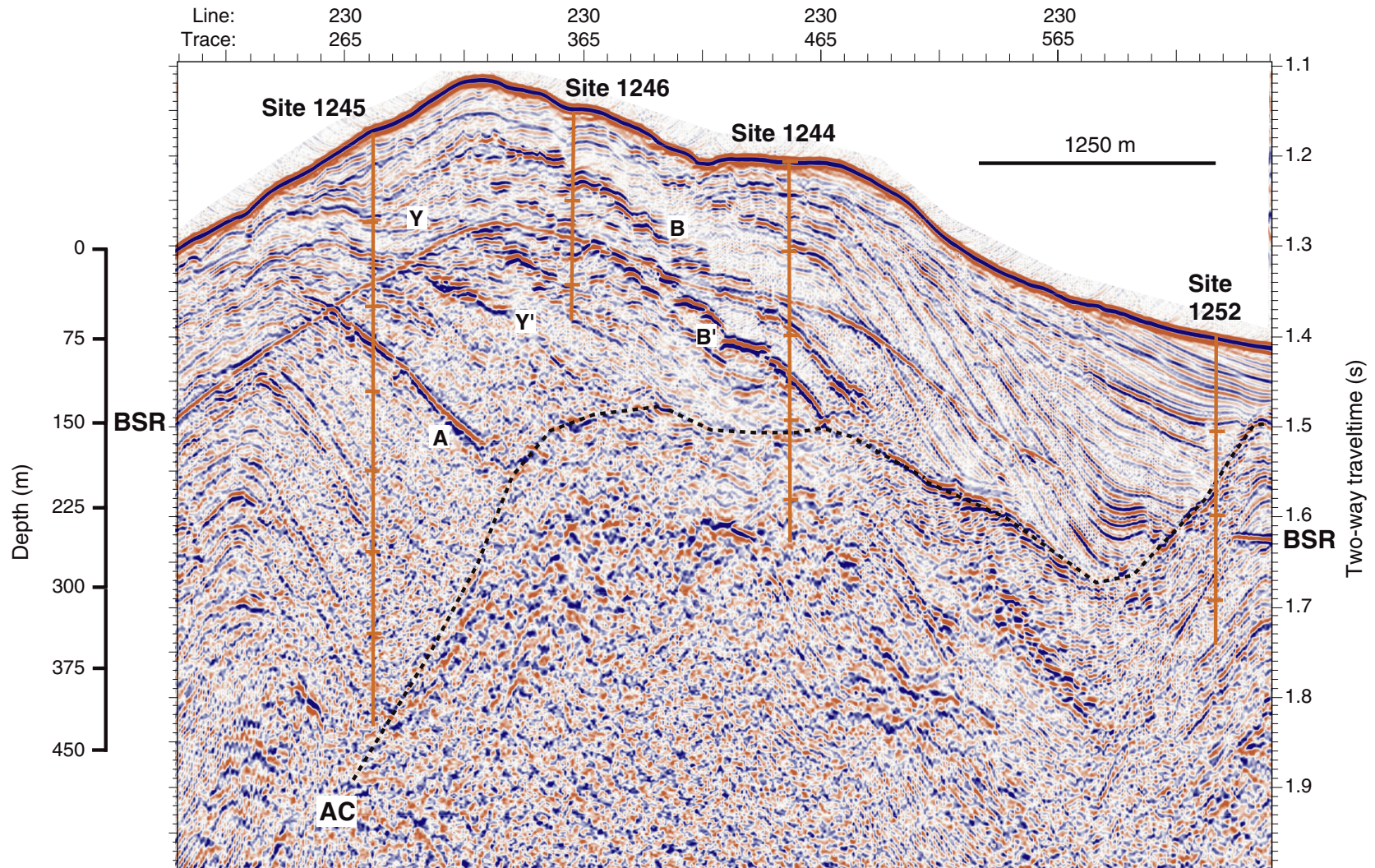


Figure F5



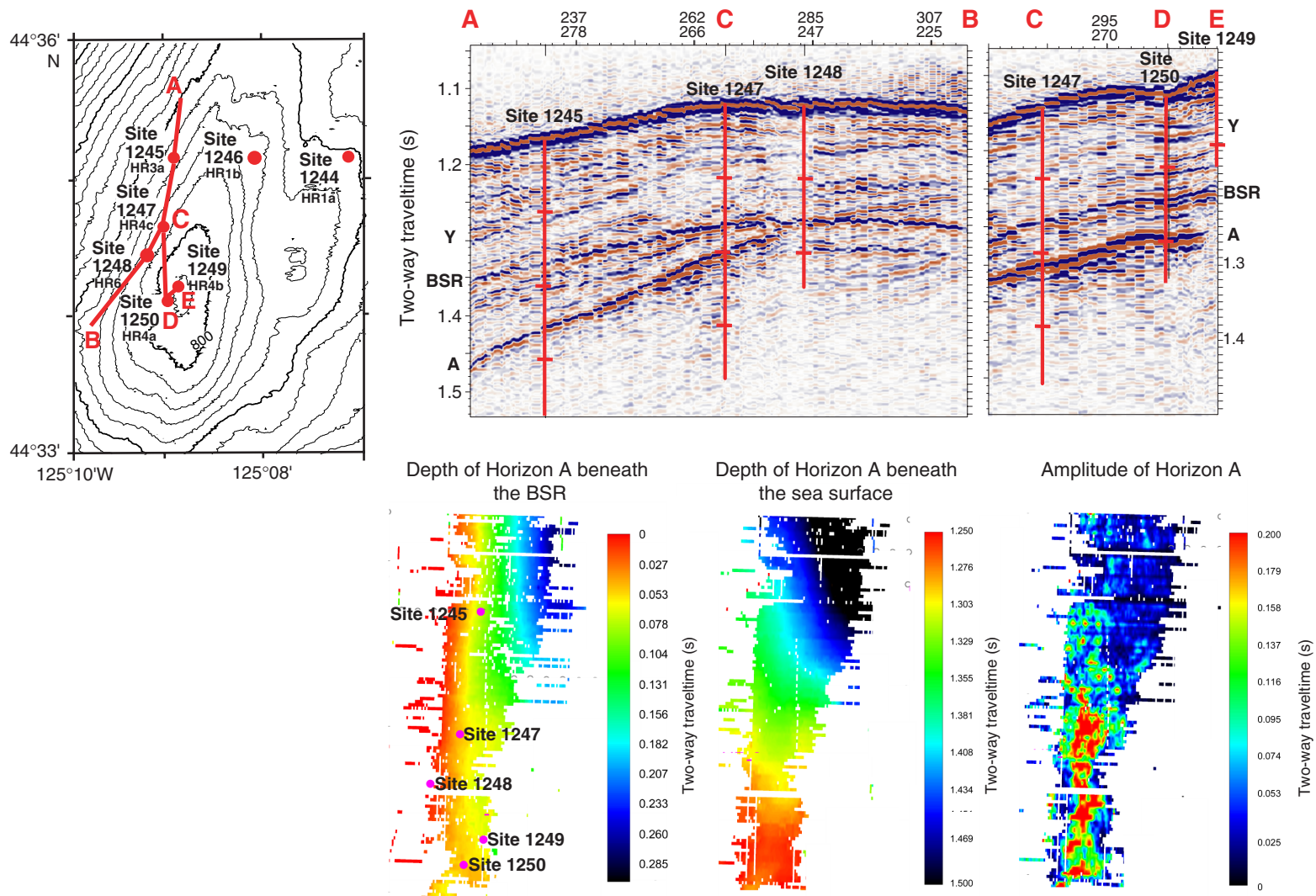


Figure F6

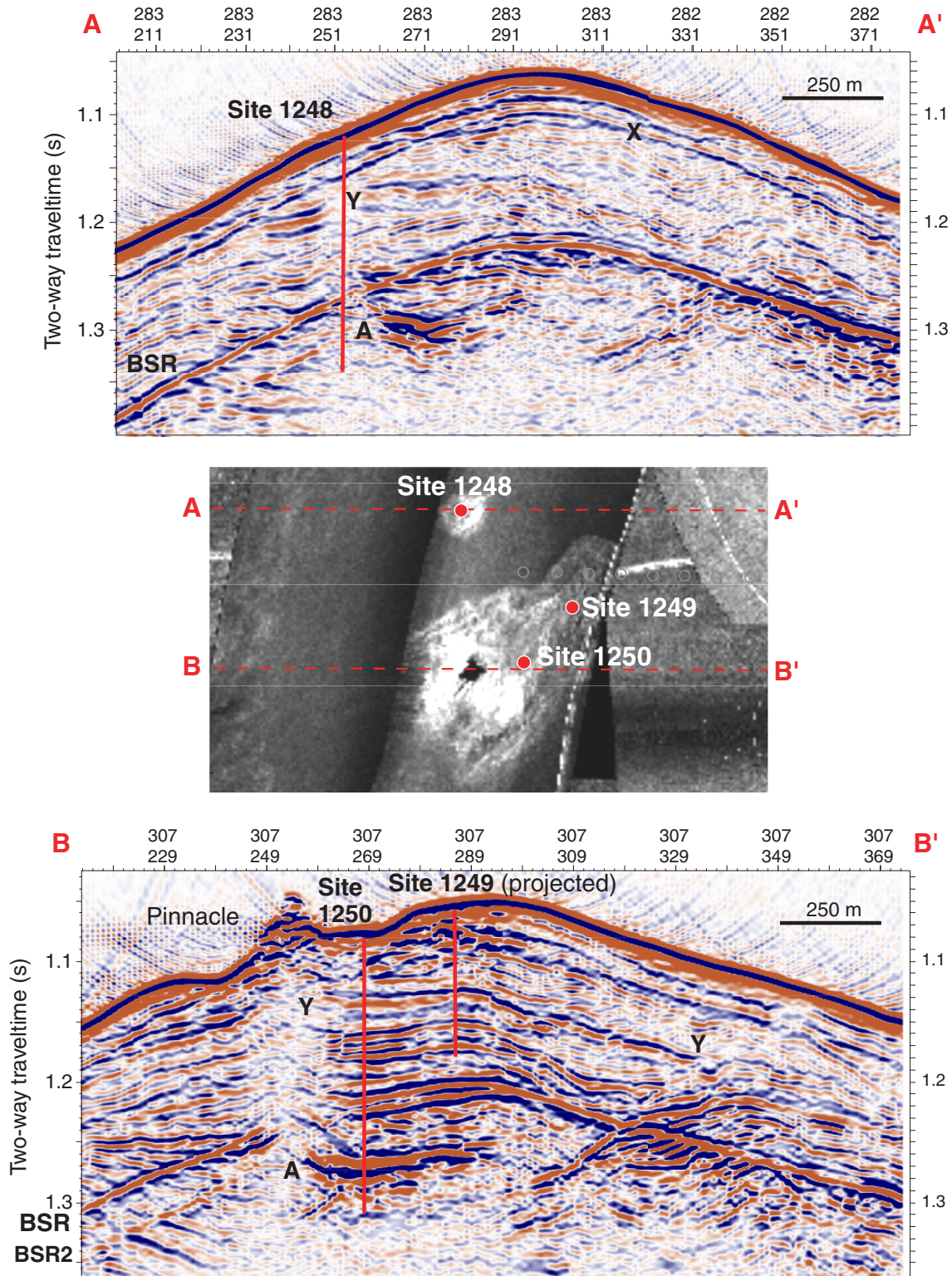


Figure F7

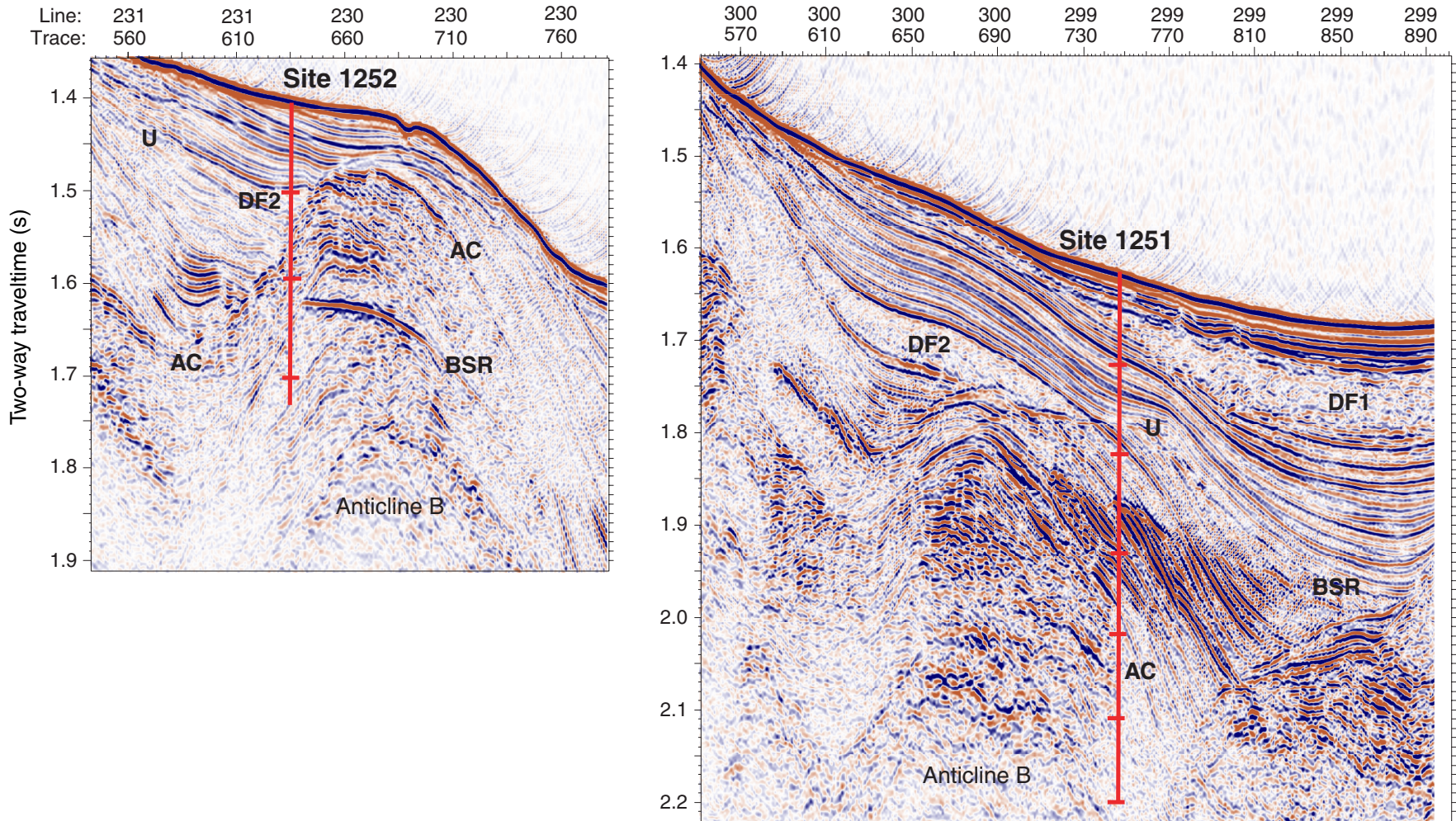


Figure F8

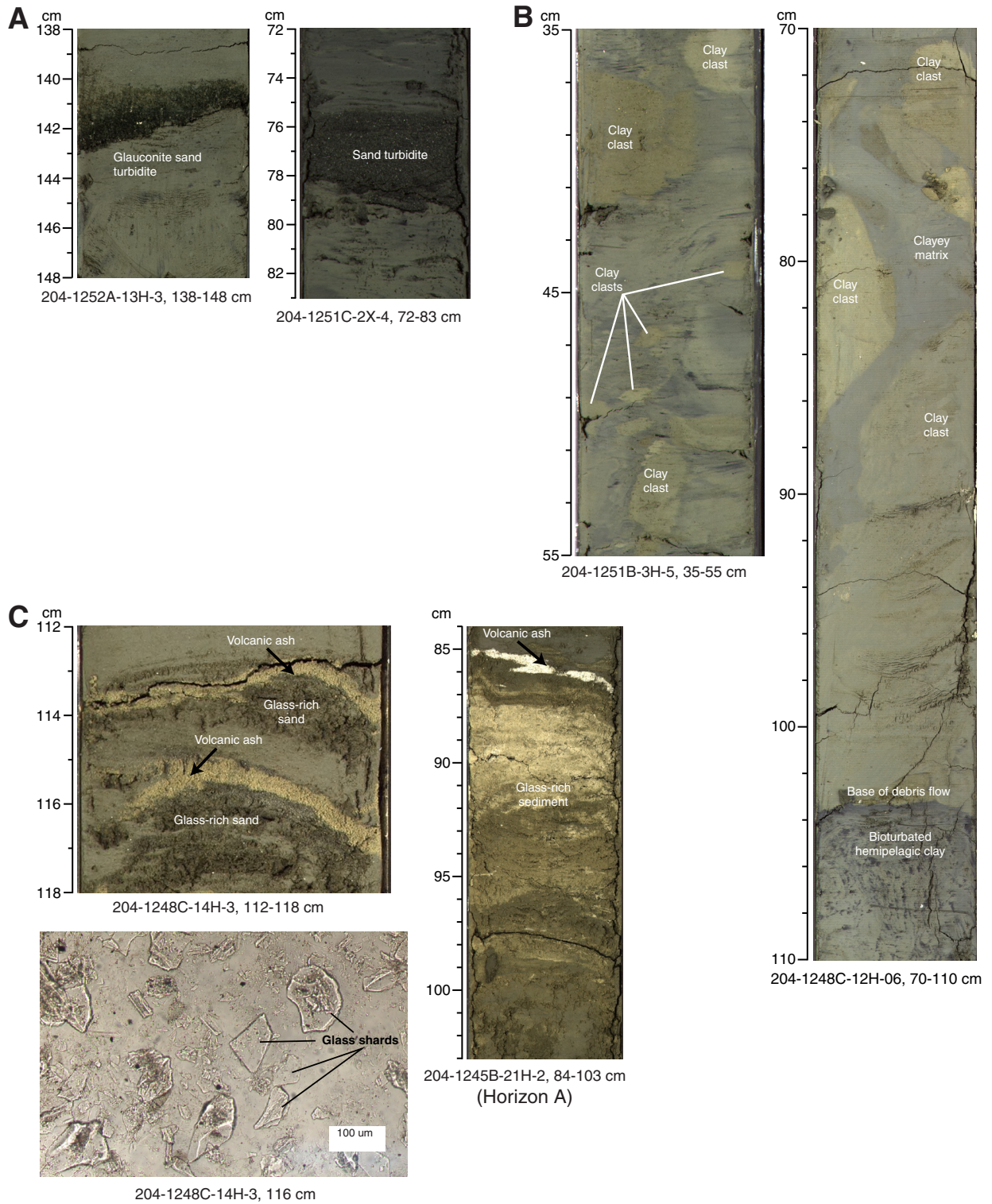


Figure F9

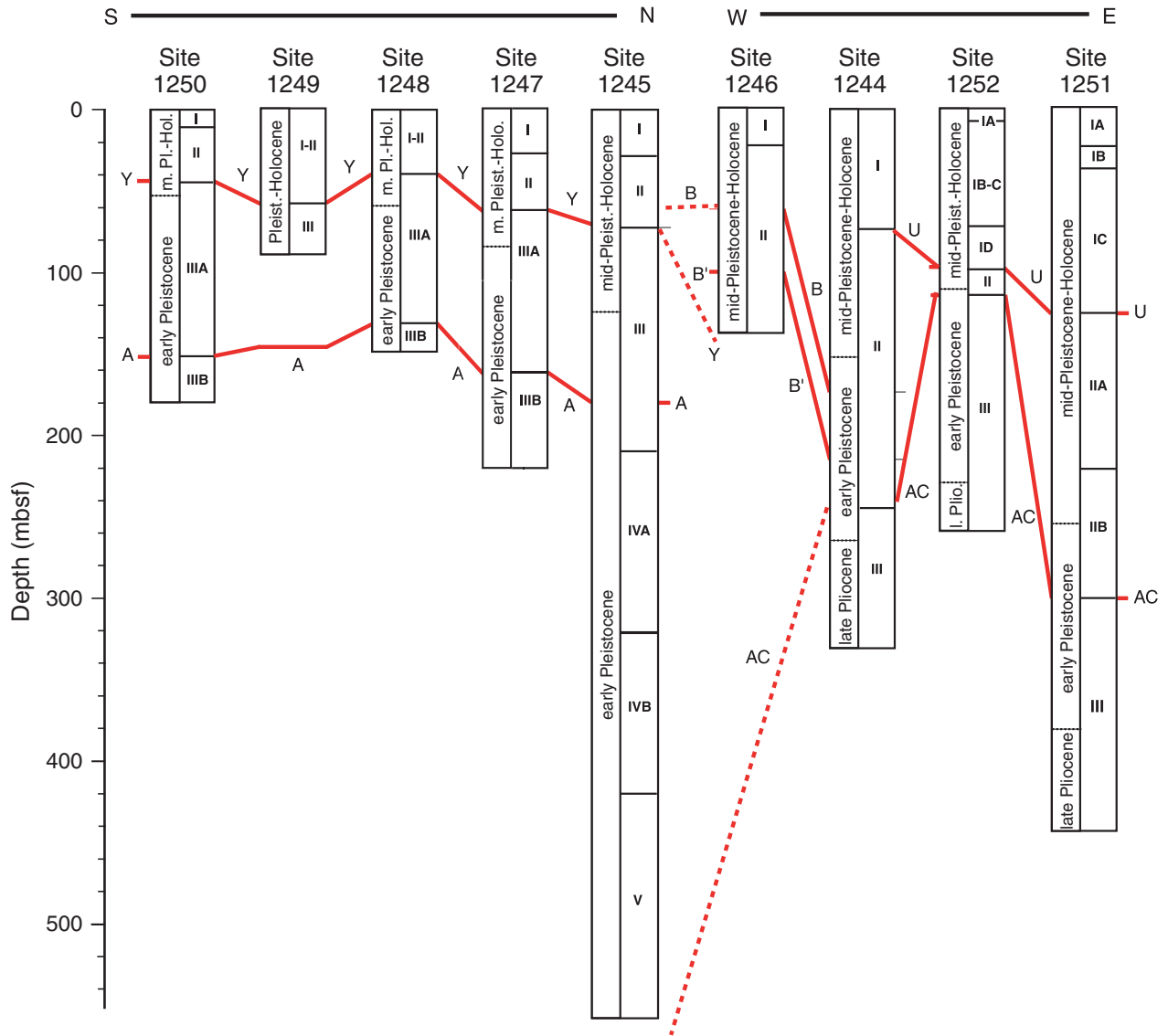


Figure F10

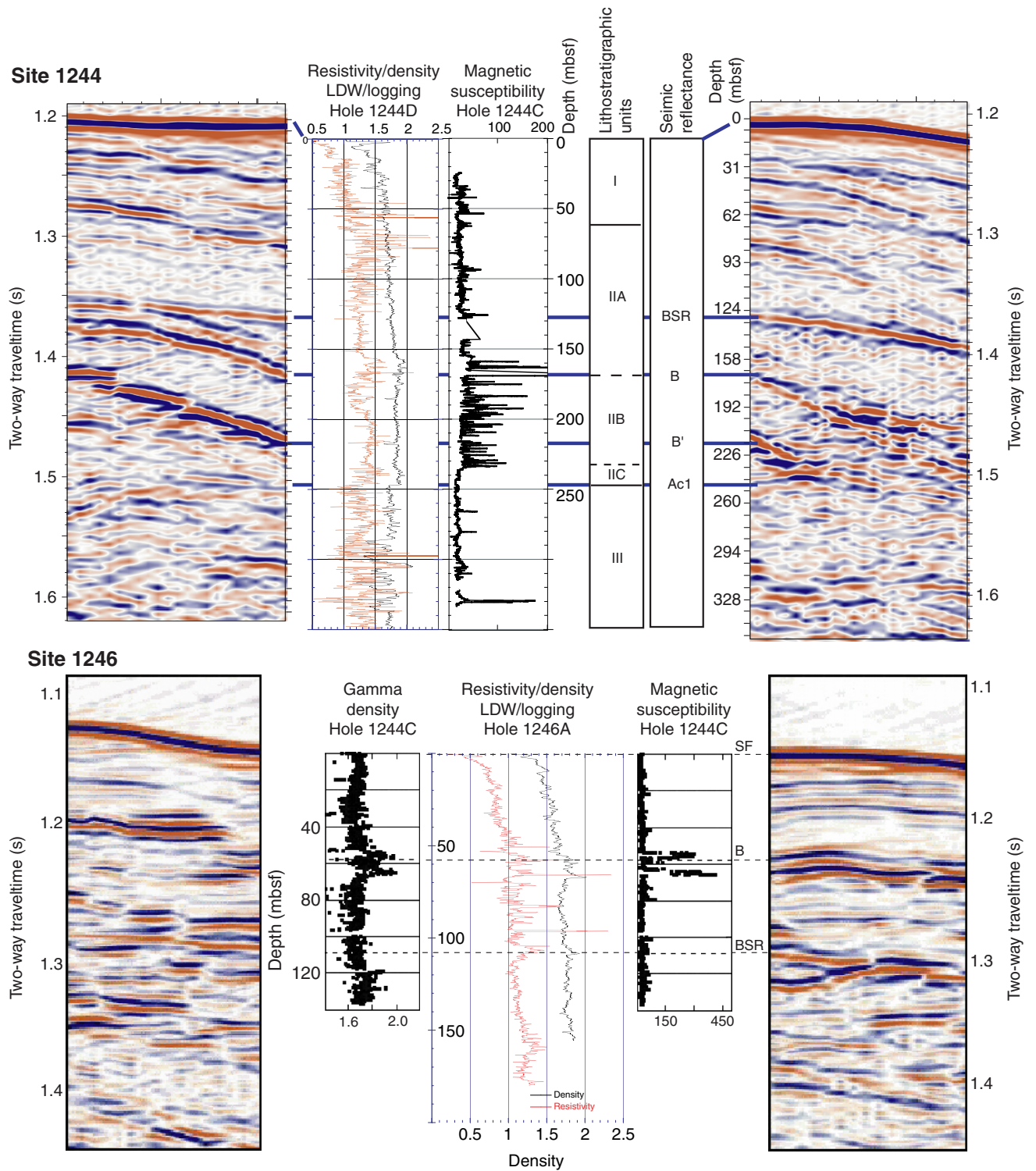
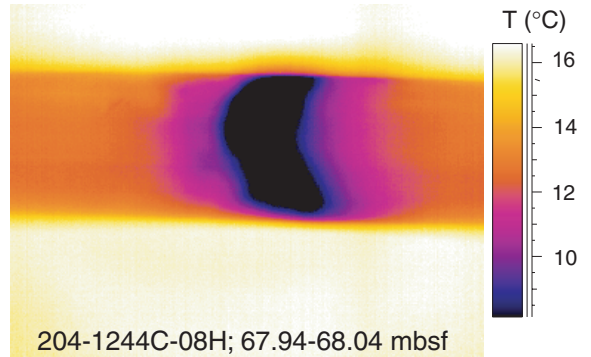
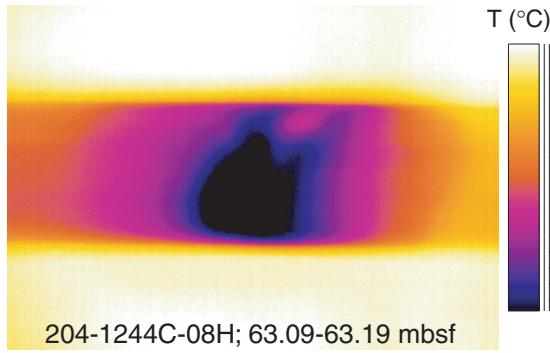


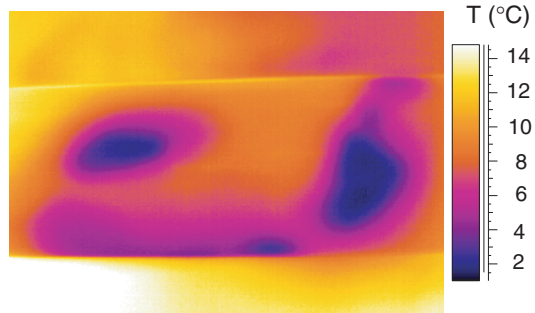
Figure F11



204-1244C-08H-1; 47-52 cm



204-1244C-08H-5; 48-80 cm



204-1244C-10H-2; 83.70-84.30 mbsf

**Figure F12**

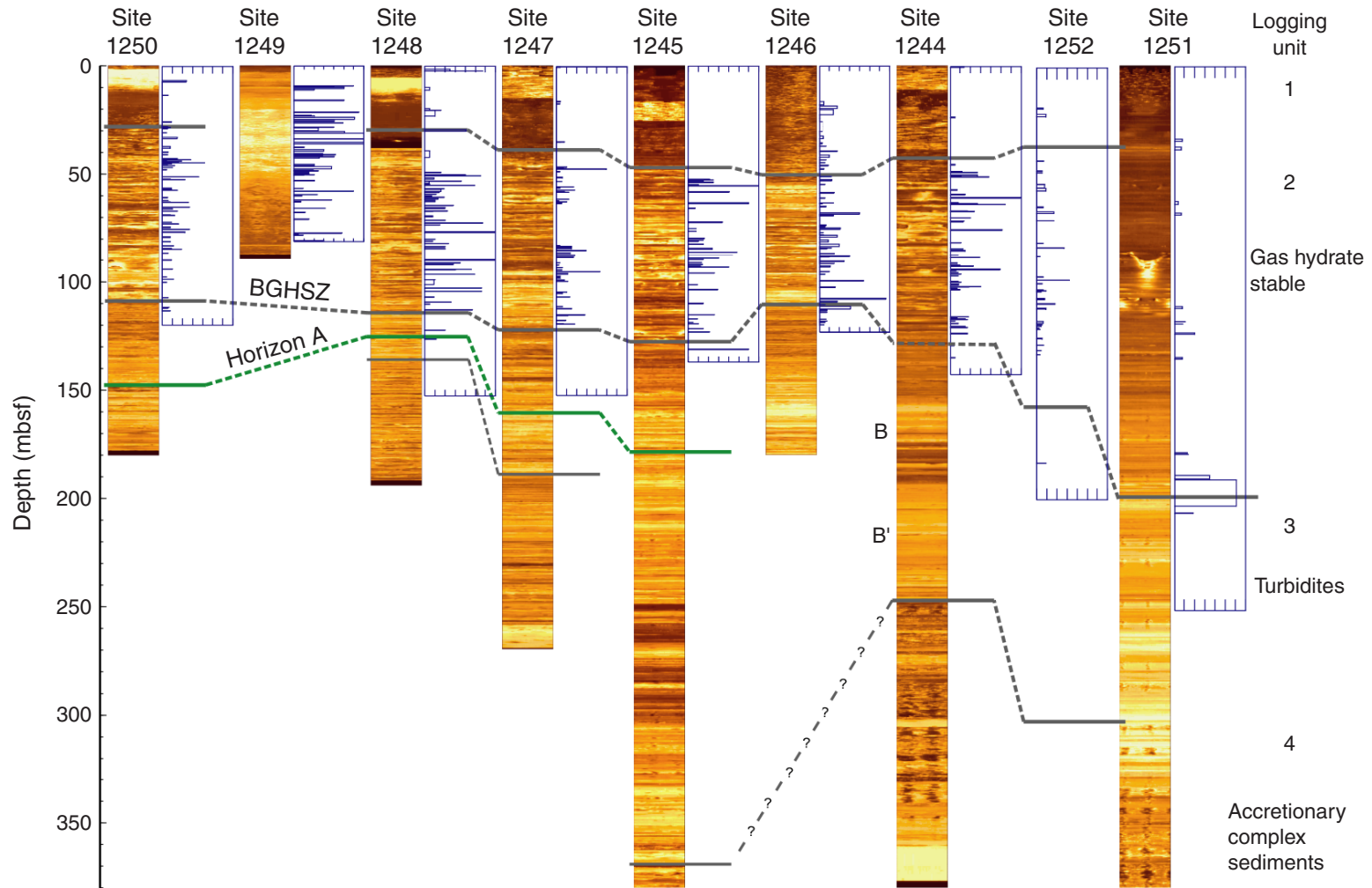


Figure F13



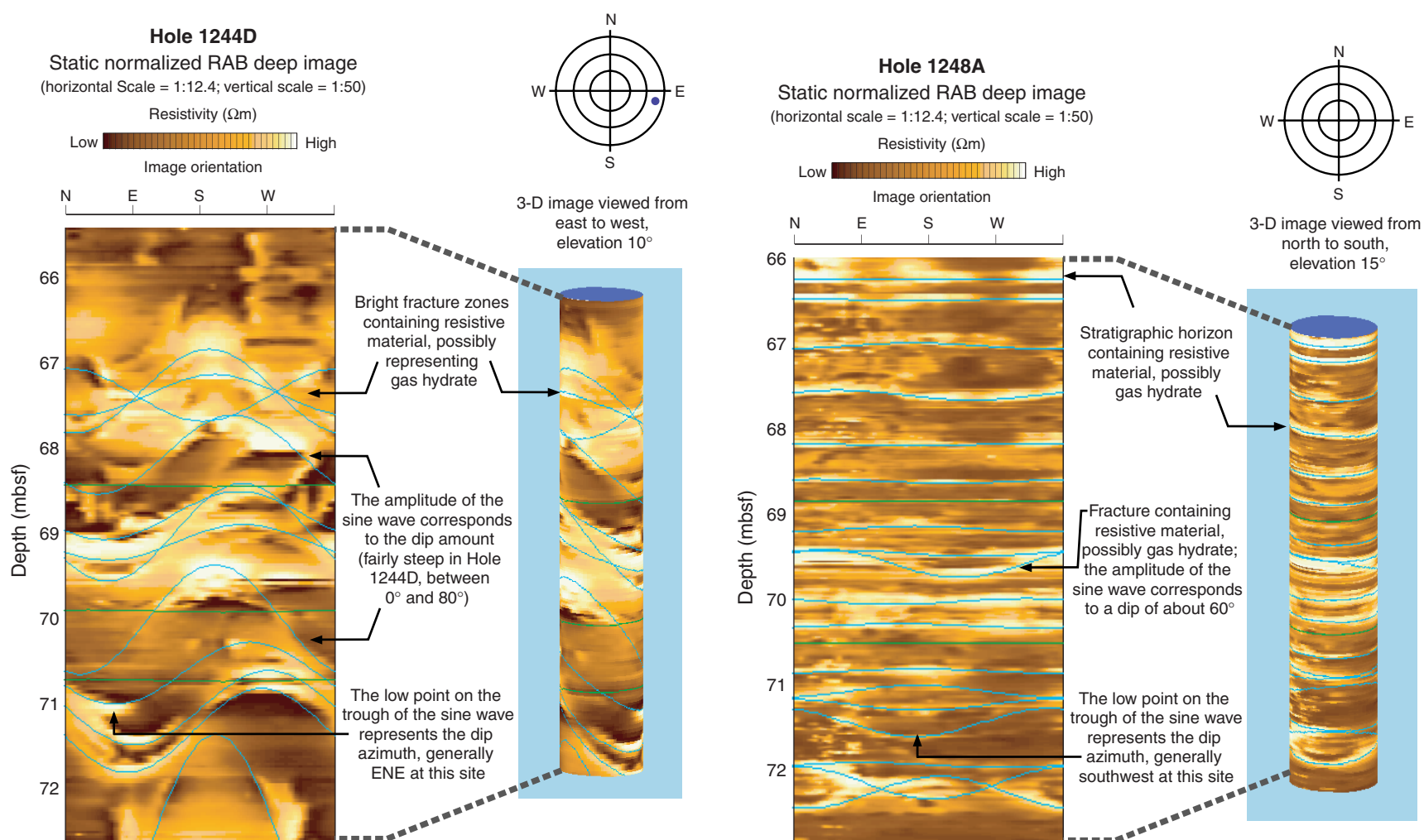


Figure F14

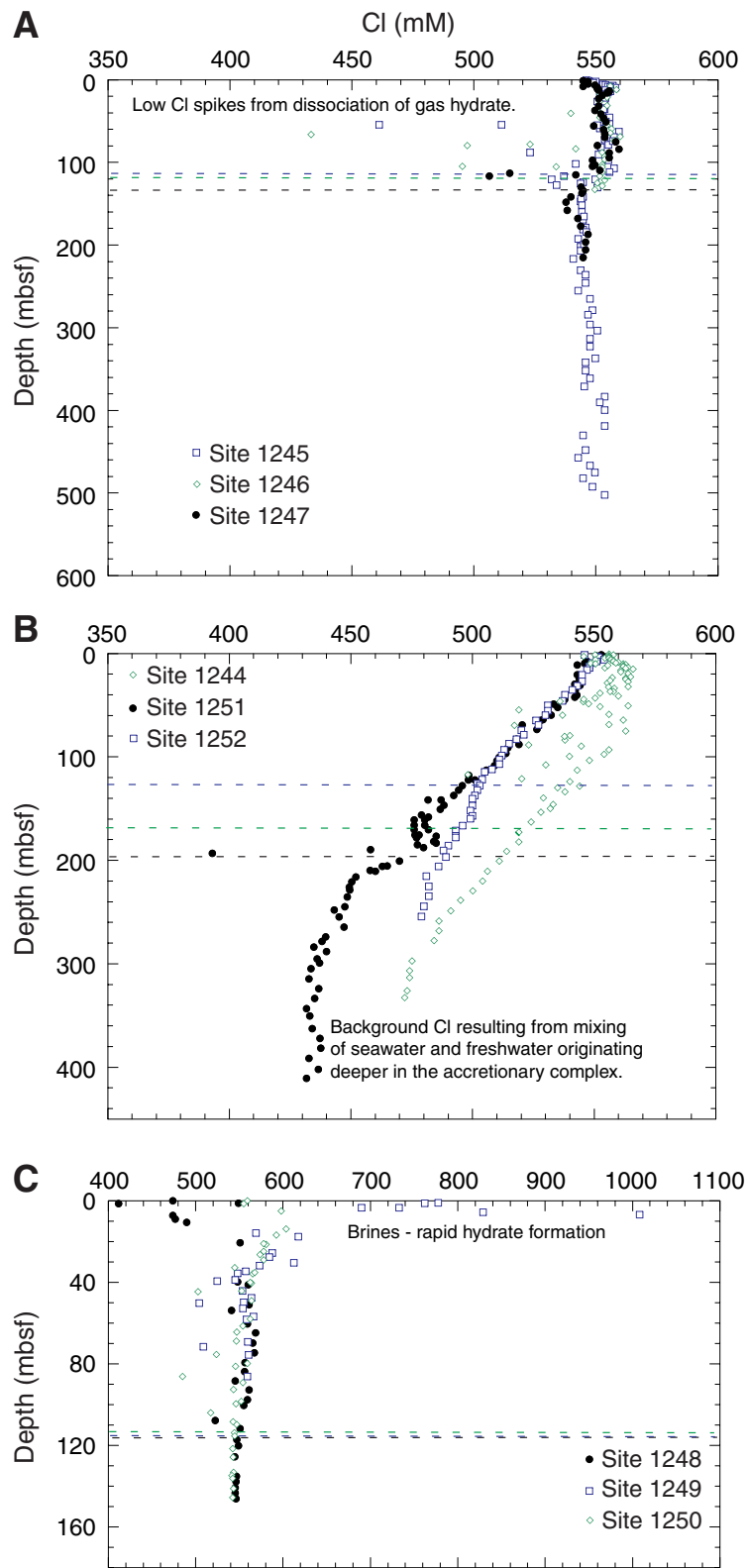


Figure F15

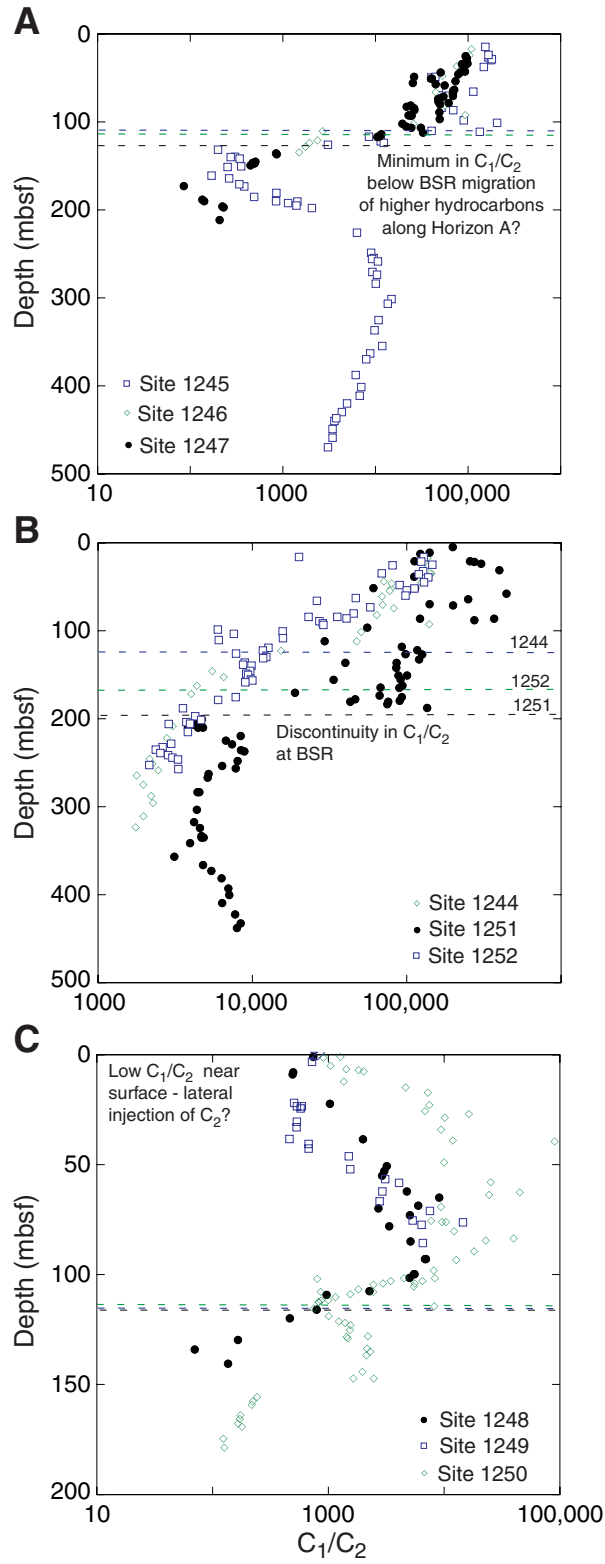


Figure F16

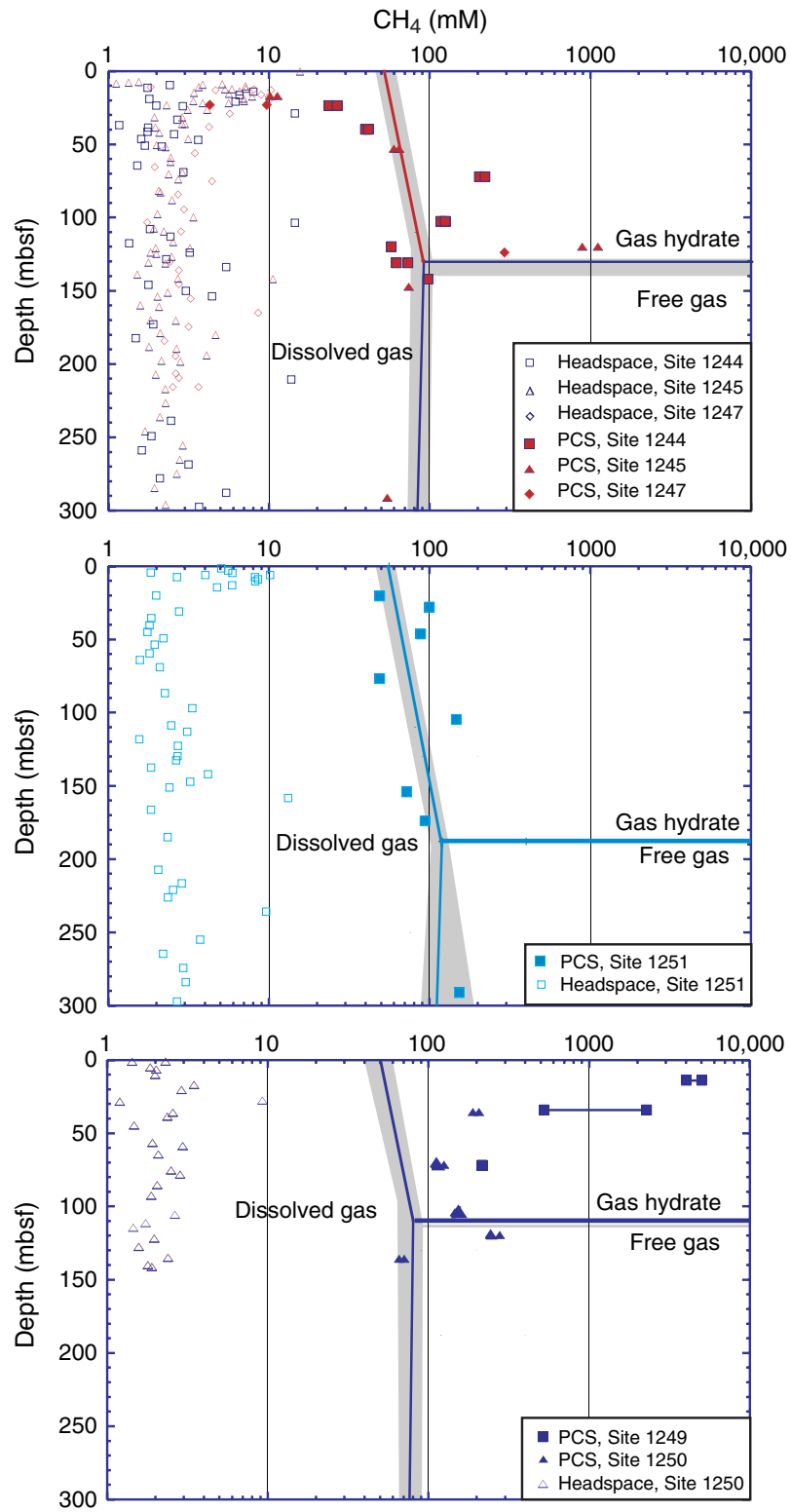
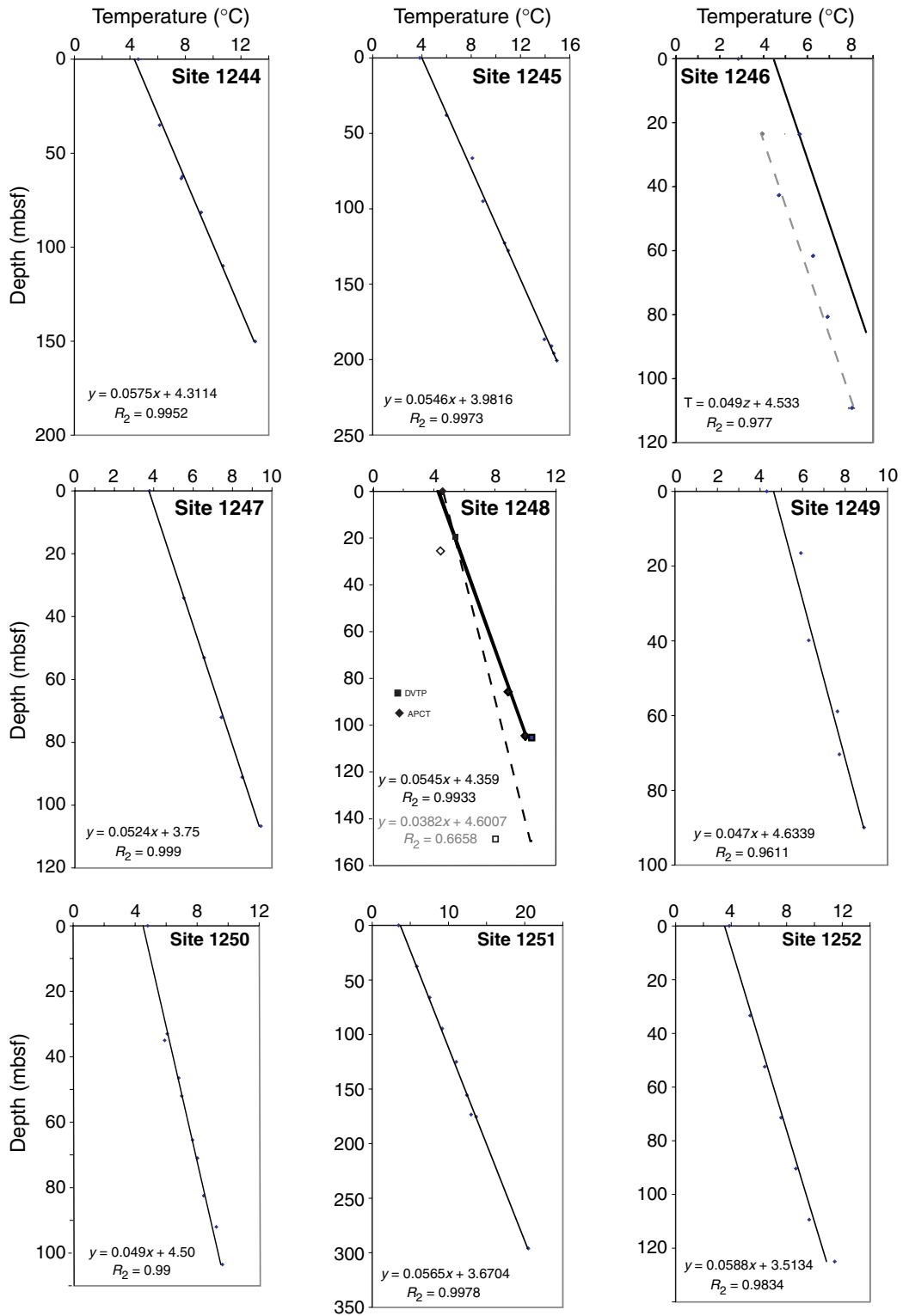


Figure F17



**Figure F18**

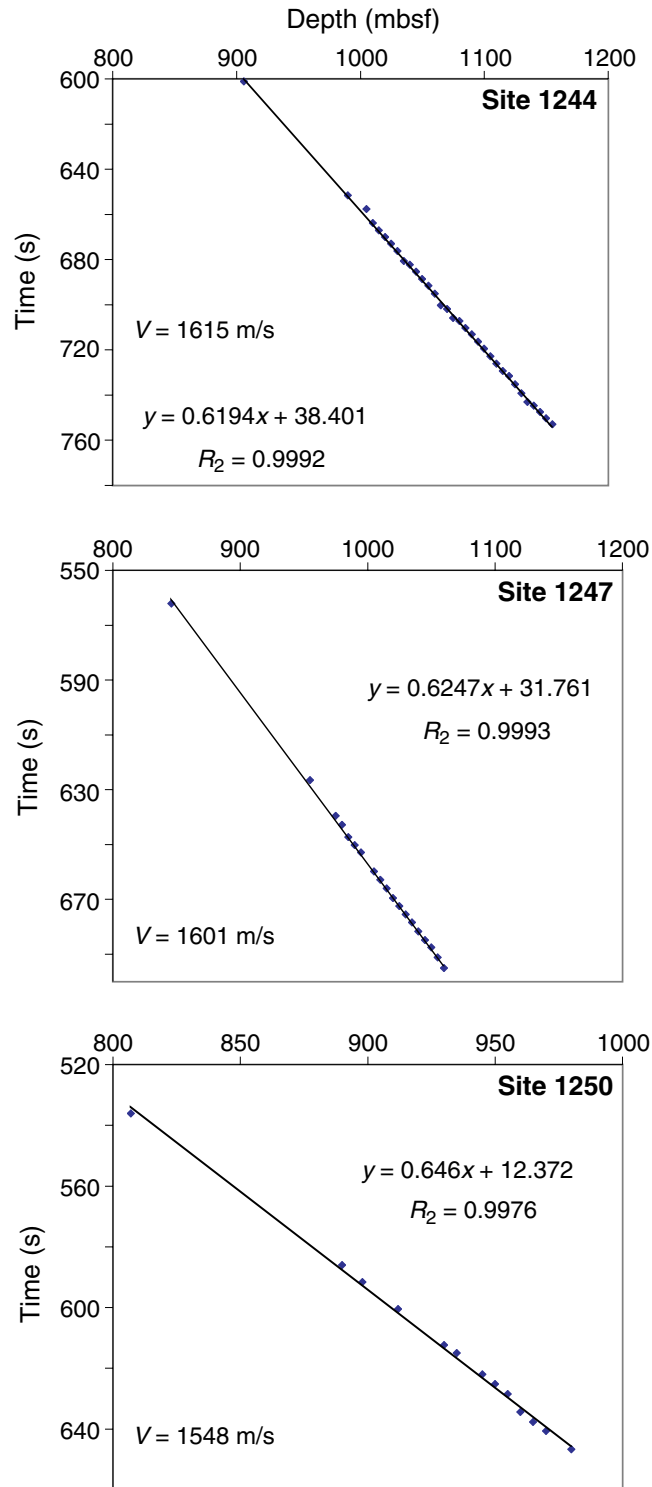


Figure F19

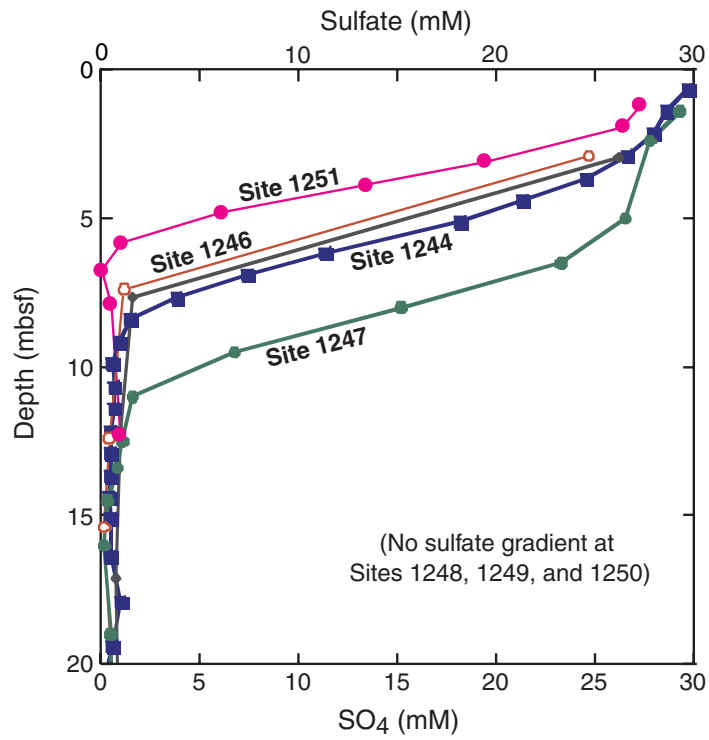
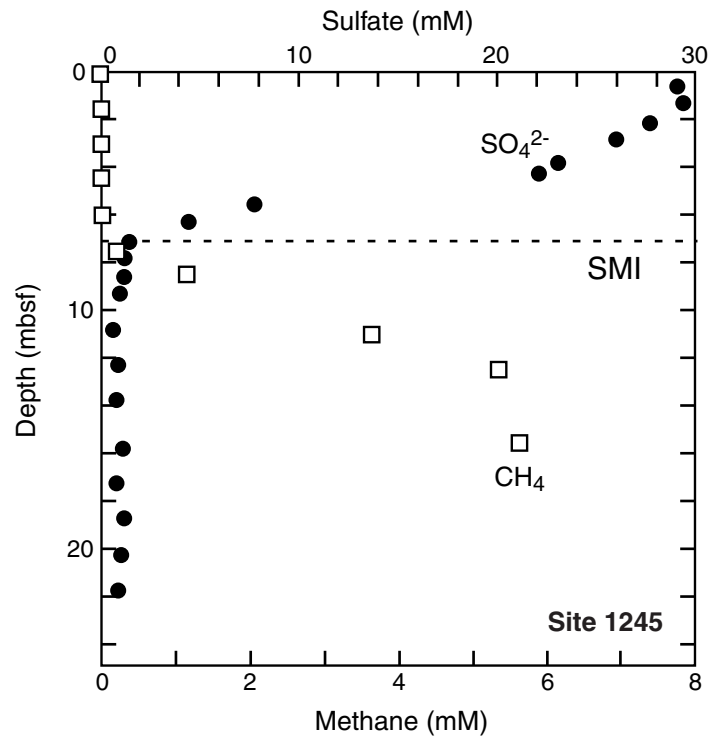


Figure F20

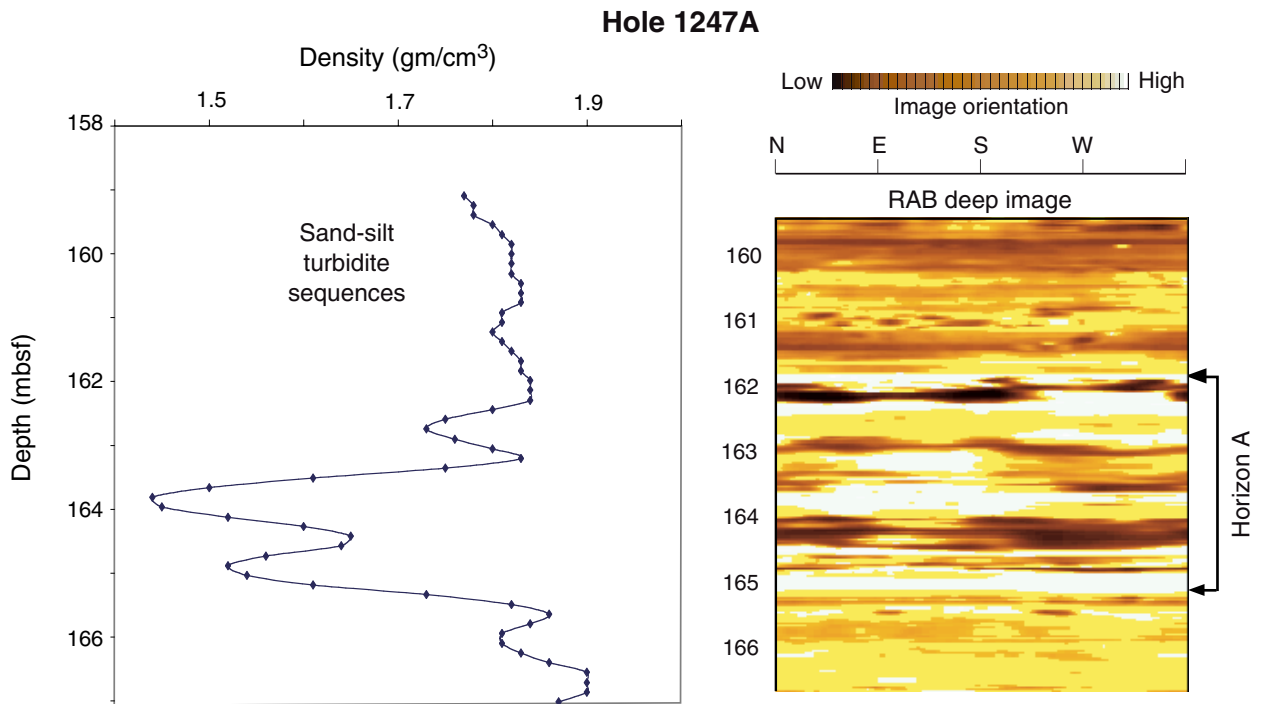
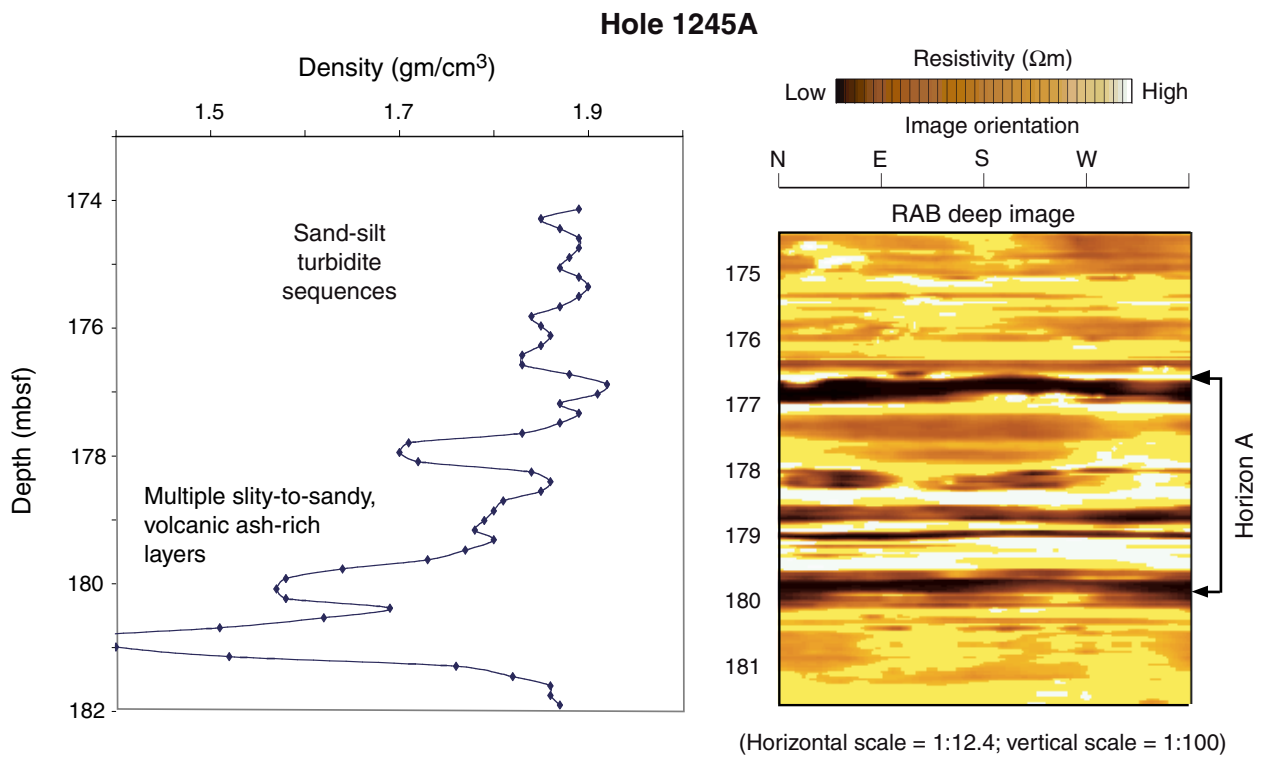


Figure F21



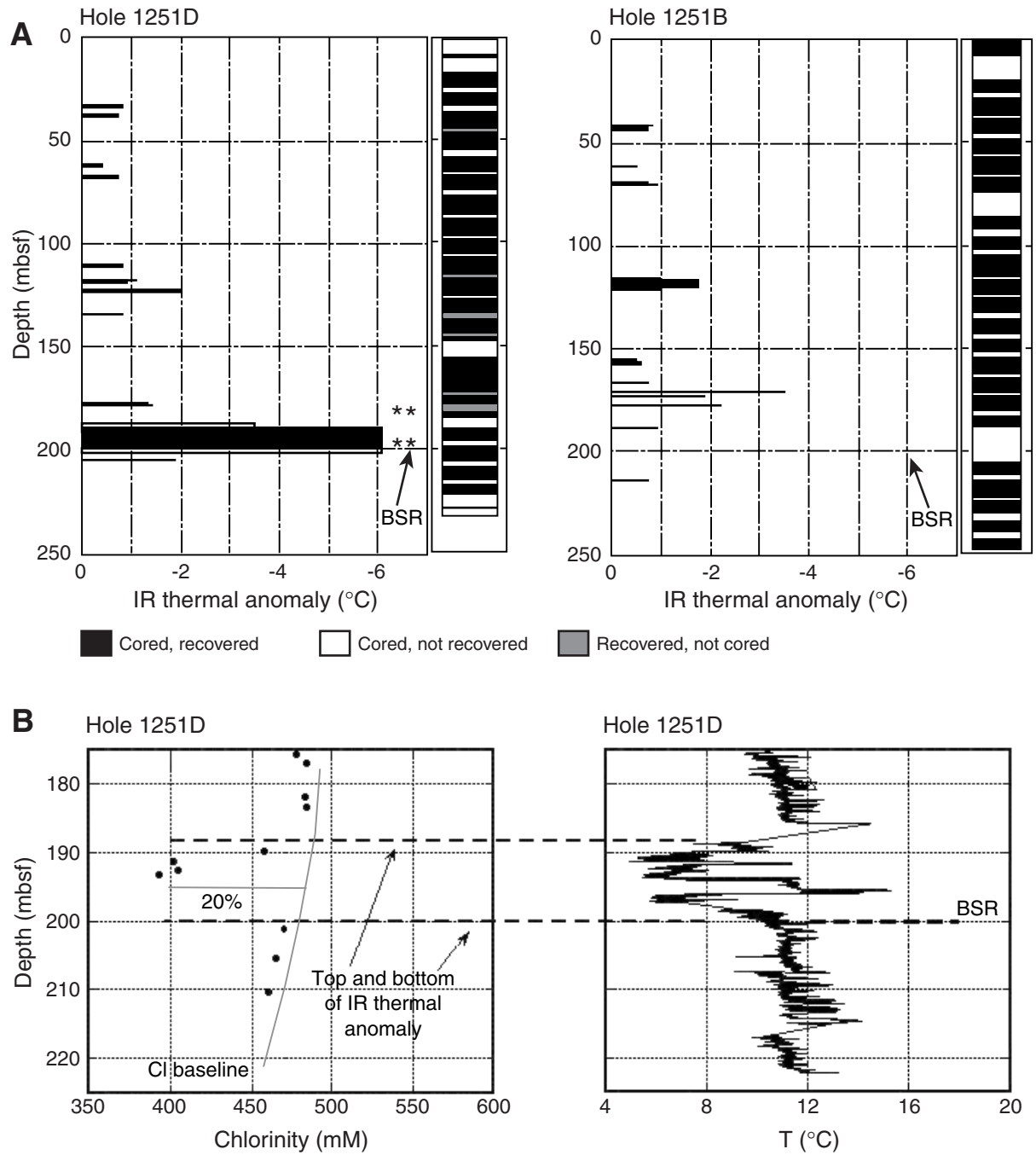


Figure F22